

Functional methods for correlation functions of integrable face and anyon models

Von der Fakultät für Mathematik und Physik
der Gottfried Wilhelm Leibniz Universität Hannover

zur Erlangung des akademischen Grades

Doktor der Naturwissenschaften

Dr. rer. nat.

genehmigte Dissertation von

Daniel Westerfeld, M.Sc.

2022

Referent: Prof. Dr. Holger Frahm,
Leibniz Universität Hannover

Korreferenten: Prof. Dr. Frank Göhmann,
Bergische Universität Wuppertal
Prof. Dr. Eric Jeckelmann,
Leibniz Universität Hannover

Vorsitz der Promotionskommission: Prof. Dr. Rolf J. Haug,
Leibniz Universität Hannover

Tag der Promotion: 05.04.2022

Abstract

The computation of correlation functions in models of statistical mechanics is the key to comparing theoretical results with actual measurements. In the context of integrable lattice models there exists a rich literature on correlators in vertex models and related quantum-spin chains. Less is known for integrable face models and their related anyon chains.

Therefore, we define generalised transfer matrices allowing for a solution of the ‘inverse problem’, i.e. we express local operators by means of objects from the Yang-Baxter algebra. This motivates the study of reduced density matrices which contain the information of all correlation functions. Instead of directly calculating them, we show that they fulfil a set of functional equations. We use these equations to study density matrices in (R)SOS models and their related anyon chains. In particular, we find integral representations for the two and three-point functions of the $r = 4$ RSOS model and calculate those quantities for the $r = 5$ model in the thermodynamic limit. In addition we observe a factorisation of the three-point functions into two-point functions and propose an efficient algorithm to factorise reduced density matrices for generic models.

In the last section we study density matrices for the $SO(5)_2$ face models. We examine the structure of the two-site reduced density matrices and simplify them for certain topological sectors. Since there exist different inequivalent sets of Boltzmann weights, the latter is done for each choice leading to sets of discrete functional equations.

Keywords: correlation functions, face models, anyons, density matrices, functional equations

Zusammenfassung

Die Berechnung von Korrelationsfunktionen für Modelle aus der statistischen Mechanik ist der Schlüssel zum Vergleich theoretischer Resultate und echter Messungen. Im Kontext integrierbarer Gittermodelle existieren zahlreiche Arbeiten zu Korrelationsfunktionen für Vertex-Modelle sowie für die mit ihnen verwandten Quantenspinnketten. Weniger ist bekannt für integrierbare Face-Modelle und die zugehörigen Anyonketten.

Deshalb definieren wir verallgemeinerte Transfermatrizen, die eine Lösung des „inversen Problems“ erlauben, d.h. wir drücken lokale Operatoren durch Objekte aus der Yang-Baxter Algebra aus. Dies motiviert das Studium reduzierter Dichtematrizen, welche die vollständige Information über alle Korrelationsfunktionen beinhalten. Anstatt diese direkt zu berechnen, zeigen wir, dass sie einen Satz von Funktionalgleichungen erfüllen, welche genutzt werden können, um die Dichtematrizen von (R)SOS-Modellen sowie den zugehörigen Anyonketten zu studieren. Insbesondere finden wir Integralausdrücke für die Zwei- und Dreipunktfunktionen des $r = 4$ RSOS-Modells und berechnen diese Größen für das $r = 5$ Modell im thermodynamischen Limes. Außerdem beobachten wir eine Faktorisierung der Dreipunktfunktionen in Zweipunktfunktionen und schlagen einen effizienten Algorithmus zur Faktorisierung reduzierter Dichtematrizen für generische Modelle vor.

Im letzten Abschnitt untersuchen wir Dichtematrizen für $SO(5)_2$ -Face-Modelle. Wir untersuchen die Struktur der zweiplatz-reduzierten Dichtematrizen und vereinfachen diese für bestimmte topologische Sektoren. Da es verschiedene inäquivalente Boltzmann-Gewichte gibt, wird letzteres für jede mögliche Wahl getan und die jeweiligen Sätze diskreter Funktionalgleichungen hergeleitet.

Schlagerworte: Korrelationsfunktionen, Face-Modelle, Anyonen, Dichtematrizen, Funktionalgleichungen

Contents

Abstract	i
Zusammenfassung	iii
Introduction	1
Part I Preliminaries	5
1 Face models and their Hamiltonian limits	7
1.1 Integrable lattice models	7
1.2 Hamiltonian limits	14
1.3 The Temperley-Lieb algebra	15
1.4 Example: The restricted solid-on-solid model	16
2 Anyon models	21
2.1 Non-Abelian anyons	21
2.2 Example: Fibonacci anyons	24
3 Solving the Inverse Problem	27
3.1 Solution for the Heisenberg model	27
3.2 Solution for the CSOS model	29
3.3 Solution for generic IRF/anyon models	32
4 The N-site reduced density matrix	37
4.1 Definition of the reduced density matrix	37
4.2 Properties of the reduced density matrix	39
Part II Applications	43
1 Models of SOS type	45
1.1 The cyclic solid-on-solid models	45
1.2 The restricted solid-on-solid models	48
1.3 Fibonacci anyons	64
2 $SO(5)_2$ anyons	71
2.1 The $SO(5)_2$ model	71
2.2 The Temperley-Lieb model	74

Contents

2.3 The BMW models	76
Conclusions	81
A Proof of Theorem 1.	84
B Proof of Theorem 2.	87
C Proof of Theorem 3.	93
D Factorisation of D_3 for the $r = 5$ RSOS model	94
References	99

Introduction

To understand the behaviour of atoms and molecules, we need to describe them quantum mechanically. For very simple systems like the harmonic oscillator or two-body systems like the hydrogen atom an exact solution of the Schrödinger equation is possible. However, as we increase the number of particles and consider realistic interactions, an exact solution is practically impossible in almost all cases and methods from statistical physics and numerics must be applied.

Alternatively, one might try to search for models which do have the property of being *exactly solvable* but only roughly resemble the considered physical system. The first and most famous example is the Heisenberg model developed by Werner Heisenberg [1] and Paul Dirac [2], which was used to describe ferromagnetism of solids. Later, Hans Bethe found the exact solution for this one-dimensional spin-1/2 chain (nowadays also known as the XXX model) by developing the coordinate Bethe ansatz [3].

In the following years more and more exactly solvable (also called *integrable*) models have been discovered. One-dimensional quantum (spin) chains were realised via transfer matrices of two-dimensional classical lattice models [4]. More advanced techniques to solve the spectral problem for these models were developed, such as the algebraic Bethe ansatz. Besides, new classes of integrable models have been found for example the so-called *interaction-round-a-face models* (IRF or, in short, face models).

Face models were introduced by Baxter in a series of papers [5–7] as an auxiliary tool for the solution of the eight-vertex model. Within this series the integrability of this new class of models was established by a face version of the Yang-Baxter equation.

Meanwhile, many more integrable face models have attracted renewed attention due to their connection to anyon models. All known elementary particles in our three-dimensional world can be classified as bosons or fermions. The wave function of bosons remains unchanged whenever two identical particles are exchanged while a fermionic wave function picks up a minus sign. In 1977 Leinaas and Myrheim realised that the restriction to bosons and fermions is a consequence of the world being three-dimensional [8]. Furthermore, in two dimensions particles with more complicated exchange statistics can exist. They were named *anyons* by Wilczek [9].

Although our world is not two-dimensional, it is possible to manufacture effectively two-dimensional lattice systems. Consider e.g. a setup where electrons are confined in a two-dimensional plane with a strong, perpendicular magnetic field. For low temperatures the resistivity of this system has been measured by Klitzing as a function of the magnetic field showing plateaus with values $\frac{2\pi\hbar}{e^2\nu}$ where ν is an integer called the filling-factor [10]. This behaviour is called the quantum-Hall-effect. For samples with less disorder also fractional values of ν appear [11]; this is called the fractional quantum-Hall-effect. A

theoretical explanation of the plateaus in the fractional case was given by Laughlin [12] who introduced quasi-particles with anyonic exchange statistics. Hence, anyons can be realised as collective excitations in two-dimensional electronic systems. The interest in anyons has recently risen due to their potential use in topological quantum computing [13].

There exists a correspondence between some anyon models and (integrable) face models. Fibonacci (or more general $su(2)_k$) anyons have been mapped to RSOS face models [14] and it was realised that this face-anyon correspondence can be extended to further models [15, 16]. Hence, the computation of correlation functions in face models gives valuable insights into anyonic systems.

Exact solutions of integrable lattice models using Bethe ansatz methods allow for a calculation of their spectrum, even in the thermodynamic limit, and unveil properties of low lying excitations. However, to compare theoretical results with possible realisations in laboratories, correlations functions need to be studied. Calculating them is much harder within this framework.

Exact expressions for correlation functions are only known for a small set of models, e.g. for the spin-1/2 Heisenberg model and generalisations thereof. In this case advanced mathematical tools such as the representation theory of quantum algebras, functional equations or the algebraic Bethe ansatz were used [17–21].

Examinations of inhomogeneous generalisations of the antiferromagnetic Heisenberg chain showed that the N -point correlation functions of the ground state can be obtained by solutions of the q -Knizhnik-Zamolodchikov (qKZ) equations. Furthermore, in Refs. [22–24] it was shown that N -point functions can be completely expressed in terms of two-point functions (the physical part) and a so-called algebraic part which is independent of the model parameters.

Although the approach via qKZ equations is limited to the thermodynamic limit, it was soon shown that the factorisation property is also true for finite lattice sizes. For instance, in [25, 26] the three-site reduced density matrices of the isotropic Heisenberg chain were expressed in terms of two-point functions.

This surprising property was established for further models, e.g. the XXZ model in an external magnetic field [27–29] where it was shown to hold for arbitrary correlation functions. Here, a hidden model-specific symmetry (the ‘fermionic basis’) was used, which makes an application for models without this symmetry challenging.

An alternative way to prove the factorisation of correlation functions has been proposed in [30] where the reduced density matrices were shown to fulfil discrete functional equations. These equations together with the known asymptotics [31] uniquely determine the density matrices. Realising that the factorised form of the density matrices indeed solves the functional equations, the factorisation property was proven. Despite

being elegant, this proof is not constructive.

Reduced density matrices have also been studied in the context of many-electron systems. In 1959 Charles Coulson conjectured that information about many-particle systems could be gained from the two-particle reduced density matrices due to interactions between electrons being dominated by two-particle terms [32]. Later, it was realised that, in fact, the spectrum of an N -electron system can be written as a functional of the two-particle density matrices [32, 33]. This resembles very much the factorisation properties of reduced density matrices of face and vertex models. In particular, we will show that the energy of the restricted solid-on-solid models can be related to the two-site reduced density matrices.

This thesis aims to develop new functional techniques and give insights into correlation functions in integrable face models. We use the results obtained for integrable face models to find explicit expressions for correlation functions in a one-dimensional chain of Fibonacci anyons.

The functional equations which are derived in this thesis only rely on physical properties of the Boltzmann weights. Hence, they are widely applicable and we do not need to restrict ourselves to face models of SOS type and are able to apply them to the non-Abelian $S0(5)_2$ face models. They are particularly interesting because they are in general not of Temperley-Lieb type and might help to answer the question whether the factorisation property of correlation functions is a general consequence of integrability or rather a special feature of Heisenberg models and their face analogs.

Thesis outline

The thesis is divided into two parts. Part I. gives a rough overview of the classes of models, mathematical techniques and objects which are needed to understand their application in Part II.

In Section I.1 we give a brief introduction to integrable lattice models with a focus on face models. Besides, we discuss their Hamiltonian limits relating them to one-dimensional quantum systems. For face models these quantum-chains often display anyonic behaviour. Hence, we discuss anyon models in Section I.2.

Correlation functions are expectation values of local operators whereas the objects of the Yang-Baxter algebra, e.g. transfer matrices, act on all lattice sites. To use integrability techniques in the context of correlation functions we show how to solve the ‘inverse problem’ for generic face models in Section I.3.

Part II. is dedicated to an application of the results to various face and anyon models. The main focus is on studies of solid-on-solid models in Section II.1. To be specific, we were able to obtain explicit results for the two- and three-sites reduced density matrices of the CSOS model in a particularly simple reference state and for the ferromagnetic

ground states of the RSOS models with $r = 4$ and $r = 5$. The latter two are also studied in the thermodynamic limit where an explicit solution of the functional equations is possible. We also provide an algorithm to factorise N -point functions into sums of two-point functions similar to the results obtained for related vertex models.

In the final Section II.2 we generalise the results to the $SO(5)_2$ face model. There exist inequivalent solutions of the Yang-Baxter equation leading to different models. Here, we establish the unitarity and generalised crossing-relations for all of them and adapt the functional equations to this case. Having characterised the two-site density matrix by a minimal number of independent functions leads to a set of functional equations.

Part I

Preliminaries

1 Face models and their Hamiltonian limits

The notion of integrability is a well defined concept in classical mechanics. A Hamiltonian system with a $2n$ -dimensional phase space M is called (*completely*) *integrable*, if there exist n independent conserved quantities I_k with $k \in \{1, \dots, n\}$ which are in involution, i.e. their Poisson brackets vanish. Furthermore, one of the conserved quantities has to be the Hamiltonian of the system. Due to Liouville's theorem a completely integrable system can always be solved by quadratures and is thus often called *solvable*. The classical inverse scattering method, a systematic approach to find and solve (classical) integrable, systems has been developed by Gardner, Green, Kruskal and Miura in 1967 [34].

A direct translation of this definition to quantum mechanics is difficult. For instance, the Hamiltonians of most quantum systems are Hermitian and yield a complete set of commuting projection operators by the spectral theorem. A precise and widely accepted definition of quantum integrability is still lacking. We will not focus too much on this problem which is discussed in more detail in [35]. For lattice models and related quantum spin chains we will follow Faddeev [36], Izergin and Korepin [37] and call two-dimensional lattice models and their equivalent quantum chains integrable if they can be solved by means of the *quantum inverse scattering method*.

In this section we will review integrable lattice models. Starting with a quick recapitulation of basic concepts we will focus on *interaction round a face* models. The following subsections discuss their *Hamiltonian limit* and apply it to an example system.

1.1 Integrable lattice models

In this section we will focus on two-dimensional classical integrable lattice models and restrict ourselves to square lattices. The most important types of models can be roughly put into three categories: *spin models*, *vertex models* and *face models*. Spin models consist of classical spins sitting on the lattice sites, the most prominent example being the Ising model. Vertex models are similar except for the dynamical variables being assigned to the links between the lattice sites. Face models are similar to spin models, however, here all four 'spins' (also called heights) around an elementary cell of the lattice interact.

Thermodynamic properties of all mentioned types of models can be computed within the *transfer matrix* formalism. The key idea is to express the partition function of the lattice model through the trace of a (possibly very large) matrix t :

$$Z = \text{tr } t^N . \tag{I.1}$$

1 Face models and their Hamiltonian limits

Here, N denotes the number of rows in the lattice. Moreover, periodic boundary conditions in vertical and horizontal direction are imposed.

In the thermodynamic limit $N, M \rightarrow \infty$ it is therefore sufficient to compute the largest eigenvalue of t which dominates the partition function. We will study this construction in more detail for face models.

As stated above, face models are classical statistical models defined on a square lattice where to each site ℓ a height a_ℓ is assigned. The heights take values from a (usually discrete) set \mathfrak{S} possibly subject to adjacency rules constraining their values on neighbouring vertices. An elegant way to encode these rules is via an adjacency graph with nodes $a \in \mathfrak{S}$ and adjacency matrix

$$A_{ab} \equiv \begin{cases} 1, & \text{spins } a \text{ and } b \text{ are allowed to be adjacent} \\ 0, & \text{spins } a \text{ and } b \text{ are not allowed to be adjacent} \end{cases} . \quad (\text{I.2})$$

The energy of the face model for a given height configuration is determined by local Boltzmann weights depending on the heights around an elementary face [38]. These weights are allowed to depend on a (spectral) parameter $u \in \mathbb{C}$. We use a graphical notation for them:

$$W \left(\begin{array}{cc|c} d & c & u \\ a & b & \end{array} \right) = \begin{array}{|c|} \hline d & c \\ \hline u \\ \hline a & b \\ \hline \end{array} = a \begin{array}{c} d \\ \diagdown \\ u \\ \diagup \\ b \end{array} c . \quad (\text{I.3})$$

We call a face model integrable if the Boltzmann weights fulfil the (face) Yang-Baxter equation (YBE):

$$\begin{aligned} \sum_{g \in \mathfrak{S}} W \left(\begin{array}{cc|c} f & g & u-v \\ a & b & \end{array} \right) W \left(\begin{array}{cc|c} f & e & v \\ g & d & \end{array} \right) W \left(\begin{array}{cc|c} g & d & u \\ b & c & \end{array} \right) \\ = \sum_{g \in \mathfrak{S}} W \left(\begin{array}{cc|c} f & e & u \\ a & g & \end{array} \right) W \left(\begin{array}{cc|c} a & g & v \\ b & c & \end{array} \right) W \left(\begin{array}{cc|c} e & d & u-v \\ g & c & \end{array} \right) . \end{aligned} \quad (\text{I.4})$$

In the graphical notation this corresponds to

$$\begin{array}{c} f \quad f \quad e \\ \diagdown \quad \diagup \quad \diagdown \quad \diagup \\ a \quad u-v \quad \bullet \quad v \\ \diagup \quad \diagdown \quad \diagup \quad \diagdown \\ b \quad b \quad c \quad d \end{array} = \begin{array}{c} f \quad e \quad e \\ \diagdown \quad \diagup \quad \diagdown \quad \diagup \\ a \quad u \quad \bullet \quad u-v \\ \diagup \quad \diagdown \quad \diagup \quad \diagdown \\ b \quad c \quad c \quad d \end{array} , \quad (\text{I.5})$$

where heights on nodes with a solid circle are summed over and heights connected by dotted lines are taken to be equal. We also assume the weights to satisfy unitarity conditions

$$\sum_{e \in \mathfrak{G}} W \left(\begin{array}{cc|c} d & e & u \\ a & b & \end{array} \right) W \left(\begin{array}{cc|c} d & c & -u \\ e & b & \end{array} \right) = a \begin{array}{c} d \quad d \\ \text{---} \text{---} \\ \diagdown \quad \diagup \\ u \quad e \\ \diagup \quad \diagdown \\ b \quad b \end{array} c = \rho(u)\rho(-u)\delta_{ac}, \quad (\text{I.6})$$

and crossing relations of the form

$$W \left(\begin{array}{cc|c} d & c & u \\ a & b & \end{array} \right) = W \left(\begin{array}{cc|c} c & b & \lambda - u \\ d & a & \end{array} \right), \quad (\text{I.7})$$

where λ is the so-called crossing parameter and ρ is a function. Both depend on the considered model.

Lastly, an initial condition for the Boltzmann weights can be expressed as:

$$W \left(\begin{array}{cc|c} d & c & 0 \\ a & b & \end{array} \right) = \begin{array}{c} d \quad c \\ \square \\ 0 \\ a \quad b \end{array} = \delta_{a,c}. \quad (\text{I.8})$$

Let us now show how to find the partition function of a face model using the transfer matrix method. To be specific we consider a lattice of L faces in horizontal and N in vertical direction. To an allowed height configuration along a row we associate a state

$$|\mathbf{a}\rangle = |a_0 a_1 \dots a_L\rangle \text{ with } A_{a_\ell, a_{\ell+1}} = 1 \text{ for } \ell = 0, \dots, L-1 \quad (\text{I.9})$$

and define \mathcal{H}^L as the span of all those states. Note that the adjacency condition couples every spin with its neighbours. Consequently, \mathcal{H}^L can in general not be decomposed into tensor products of local spaces. Here, one might already see parallels to the fusion path states of anyonic models which will be explained later.

A subspace of \mathcal{H}^L is spanned by states with periodic boundary conditions. It is denoted by $\mathcal{H}_{\text{per}}^L$ and can be visualised as closed walks of length L on the adjacency graph. It is known from graph theory that the number of walks of length L from a vertex a to a vertex b on a graph with adjacency matrix A is given by $(A^L)_{ab}$. Hence, the dimension of $\mathcal{H}_{\text{per}}^L$ is

$$\dim \mathcal{H}_{\text{per}}^L = \text{tr} A^L. \quad (\text{I.10})$$

In many cases one observes that for $L \gg 1$ the dimension of the state space behaves as $\dim(\mathcal{H}_{\text{per}}^L) \sim \alpha^L$ where α is *not* an integer number, further indicating an anyonic

1 Face models and their Hamiltonian limits

character of the models. For the rest of this section we will work with periodic boundary conditions in both vertical and horizontal direction (so effectively bending the lattice around a torus). Thermodynamic quantities can be computed by means of the transfer matrix method. In our context the (inhomogeneous) transfer matrix $t(u) : \mathcal{H}_{\text{per}}^L \rightarrow \mathcal{H}_{\text{per}}^L$ is defined by its matrix elements

$$\langle \mathbf{a} | t(u) | \mathbf{b} \rangle = \begin{array}{c} a_0 \quad a_1 \quad \dots \quad a_{L-1} \quad a_0 = a_L \\ \boxed{u - u_1 \quad \dots \quad u - u_L} \\ b_0 \quad b_1 \quad \dots \quad b_{L-1} \quad b_0 = b_L \end{array} . \quad (\text{I.11})$$

The Yang-Baxter equation and unitarity of the weights for integrable face models imply $[t(u), t(v)] = 0$ for an arbitrary set of inhomogeneities $\{u_i\}_{i=1}^L$:

$$\begin{aligned} \langle \mathbf{a} | t(u)t(v) | \mathbf{b} \rangle &= \begin{array}{c} a_0 \quad a_1 \quad \dots \quad a_{L-1} \quad a_0 = a_L \\ \begin{array}{|c|c|c|} \hline u - u_1 & & u - u_L \\ \hline v - u_1 & & v - u_L \\ \hline \end{array} \\ b_0 \quad b_1 \quad \dots \quad b_{L-1} \quad b_0 = b_L \end{array} \\ &= \frac{1}{\rho(u-v)\rho(v-u)} \times \begin{array}{c} a_0 \quad a_1 \quad \dots \quad a_{L-1} \quad a_0 = a_L \\ \begin{array}{|c|c|c|} \hline u - v & & v - u \\ \hline v - u_1 & & v - u_L \\ \hline u - u_1 & & u - u_L \\ \hline \end{array} \\ b_0 \quad b_1 \quad \dots \quad b_{L-1} \quad b_0 = b_L \end{array} \\ &= \frac{1}{\rho(u-v)\rho(v-u)} \times \begin{array}{c} a_0 \quad a_1 \quad \dots \quad a_{L-1} \quad a_0 = a_L \\ \begin{array}{|c|c|c|} \hline v - u_1 & & v - u_L \\ \hline u - u_1 & & u - u_L \\ \hline \end{array} \\ b_0 \quad b_1 \quad \dots \quad b_{L-1} \quad b_0 = b_L \end{array} \end{aligned}$$

$$\begin{aligned}
 &= \frac{1}{\rho(u-v)\rho(v-u)} \times \begin{array}{c} a_0 \quad a_1 \quad \dots \quad a_{L-1} \quad a_0 = a_L \\ \begin{array}{|c|c|c|c|} \hline v-u_1 & & & v-u_L \\ \hline u-u_1 & & & u-u_L \\ \hline \end{array} \\ b_0 \quad b_1 \quad \dots \quad b_{L-1} \quad b_0 = b_L \end{array} \begin{array}{c} \diamond \\ \diamond \end{array} \\
 &= \begin{array}{c} a_0 \quad a_1 \quad \dots \quad a_{L-1} \quad a_0 = a_L \\ \begin{array}{|c|c|c|c|} \hline v-u_1 & & & v-u_L \\ \hline u-u_1 & & & u-u_L \\ \hline \end{array} \\ b_0 \quad b_1 \quad \dots \quad b_{L-1} \quad b_0 = b_L \end{array} = \langle \mathbf{a} | t(v)t(u) | \mathbf{b} \rangle
 \end{aligned}$$

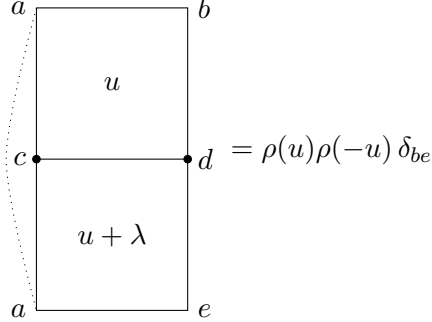
In the first step, unitarity has been used to introduce an identity. Then the Yang-Baxter equation is employed repeatedly exchanging the order of the spectral parameters. Due to periodic boundary conditions the weight on the left can be moved to the right where unitarity is used again and both weights cancel each other. Thus, we obtain $t(u)t(v) = t(v)t(u)$ as desired. Note that an essential ingredient for the introduction of inhomogeneities is that the Yang-Baxter equation is of difference form, i.e. only the differences of the spectral parameters enter. This is the case for all models considered in this thesis. We therefore do not need to discuss the general case

The partition function can be computed via $Z = \text{tr} \left\{ t(u)^N \right\}$ so it suffices to diagonalise the transfer matrix. Due to integrability the eigenvectors are independent of the spectral parameter. The inhomogeneities may physically be interpreted as a variation of the interaction in the horizontal direction. They are introduced mainly as an auxiliary tool for computations where only the homogeneous limit $u_i \rightarrow 0$ is ultimately of interest. If all $u_i = 0$ we say the model is homogeneous.

Hence, all thermodynamic properties of classical face models can be obtained from the spectrum of the transfer matrix. Let us therefore study a widely applicable method to solve the spectral problem based on functional relations. Similar methods will be frequently used in later chapters so it is worth to spend some time on it.

1 Face models and their Hamiltonian limits

First note, that unitarity (I.6) and crossing symmetry (I.7) can be combined to yield:



$$= \rho(u)\rho(-u) \delta_{be}. \quad (\text{I.12})$$

Now consider the product $t(u_i) \cdot t(u_i + \lambda)$ where u_i is any of the inhomogeneities. By means of (I.12) and the initial condition it is evident (see [39] for more details) that

$$t(u_i) \cdot t(u_i + \lambda) = \mathbb{1} \cdot \prod_{i,k=1}^L \rho(u_i - u_k) \rho(u_k - u_i) \quad \text{for every } i \in \{1, 2, \dots, L\} \quad (\text{I.13})$$

and hence the eigenvalues $\Lambda(u)$ fulfil a discrete set of *exact* inversion relations:

$$\Lambda(u_i)\Lambda(u_i + \lambda) = \prod_{k=1}^L \rho(u_i - u_k) \rho(u_k - u_i) \quad \text{for every } i \in \{1, 2, \dots, L\}. \quad (\text{I.14})$$

Repeatedly using the unitary condition one finds

$$\prod_{i=1}^L t(u_i) = \prod_{i=1}^L t(u_i + \lambda) = \mathbb{1} \prod_{k,l=1}^L \rho(u_k - u_l) \rho(u_l - u_k) \quad (\text{I.15})$$

leading to only $L - 1$ of the inversion relations being independent. Supplemented with analytic properties of the eigenvalues the inversion relations (and generalisations thereof) have been used to solve the spectral problem of various models (see e.g. [39–41]). We will show in Section I.1.4 how this is done for a concrete example. We will also need the notion of local operators. An operator \mathcal{O} is called an n -point operator, if there exist natural numbers n_1, n_2 with $n_2 - n_1 + 1 = n$ such that

$$\langle \mathbf{a} | \mathcal{O} | \mathbf{b} \rangle = \left(\prod_{i=0}^{n_1-1} \delta_{a_i b_i} \right) \mathcal{O}_{b_{n_1} \dots b_{n_2}}^{a_{n_1} \dots a_{n_2}} \left(\prod_{i=n_2}^L \delta_{a_i b_i} \right). \quad (\text{I.16})$$

The simplest local operators are elementary operators $(E_\beta^\alpha)_i : \mathcal{H}^L \rightarrow \mathcal{H}^L$ with matrix

elements

$$\begin{aligned}
 \langle \mathbf{a} | (E_{\beta}^{\alpha})_i | \mathbf{b} \rangle &= \delta_{a_i, \alpha} \delta_{b_i, \beta} \prod_{j \neq i} \delta_{a_j b_j} \\
 &= \text{---} \underset{\beta = b_i}{\overset{\alpha = a_i}{\diamond}} \text{---} \underset{a_{i-1}}{a_{i+1}} \text{---}, \tag{I.17}
 \end{aligned}$$

which change only the height a_i , but also depend on its neighbours due to the adjacency condition. They generalise to elementary multi-point operators

$$\begin{aligned}
 \langle \mathbf{a} | E_{\beta_{n_1} \dots \beta_{n_2}}^{\alpha_{n_1} \dots \alpha_{n_2}} | \mathbf{b} \rangle &= \prod_{k=n_1}^{n_2} \delta_{a_k, \alpha_k} \delta_{b_k, \beta_k} \prod_{j \notin \{n_1 \dots n_2\}} \delta_{a_j b_j} \\
 &= \text{---} \underset{\beta_{n_1} = b_{n_1} \dots \beta_{n_2} = b_{n_2}}{\overset{\alpha_{n_1} = a_{n_1} \dots \alpha_{n_2} = a_{n_2}}{\text{---}}} \underset{a_{n_1-1}}{a_{n_2+1}} \text{---}. \tag{I.18}
 \end{aligned}$$

Another important example are the so-called Yang-Baxter operators, defined as

$$\langle \mathbf{a} | W_i(u) | \mathbf{b} \rangle := W \left(\begin{array}{cc|c} a_{i-1} & b_i & u \\ a_i & a_{i+1} & \end{array} \right) \prod_{j \neq i} \delta_{a_j b_j}. \tag{I.19}$$

It is easy to see that the Yang-Baxter equation (I.4) can be expressed in terms of Yang-Baxter operators as

$$W_i(u) W_{i+1}(u+v) W_i(v) = W_{i+1}(v) W_i(u+v) W_{i+1}(u), \tag{I.20}$$

where u and v are arbitrary spectral parameters. However, we are not only interested in classical lattice models but also in their Hamiltonian (quantum) limits. While integrable vertex models are often related to quantum spin chains (e.g. the 6-vertex model yields the Heisenberg spin chain), many face models lead to anyonic models.

1.2 Hamiltonian limits

Taking $\mathcal{H}_{\text{per}}^L$ as the Hilbert space of a quantum system, we may think of $t(u)$ as a generating function for integrals of motion:

$$t(u) = \sum_k H_k u^k \quad (\text{I.21})$$

with $[H_k, H_l] = 0$. The transfer matrix is a non-local operator acting on all lattice sites simultaneously. For this reason, none of the operators H_k is a meaningful candidate for a short-range Hamiltonian. If, however, the Boltzmann weights of a homogeneous model have the property that for some value $u = u_s$

$$\begin{array}{ccc} a & & b \\ \hline & u_s & \\ \hline c & & d \end{array} = \delta_{b,c}, \quad (\text{I.22})$$

we see that $t(u_s)$ is just a shift operator. After a possible substitution $u \rightarrow u - u_s$ we may assume $u_s = 0$, i.e.

$$\langle \mathbf{a} | t(0) | \mathbf{b} \rangle = \prod_{i=0}^{L-1} \delta_{a_{i+1} b_i}. \quad (\text{I.23})$$

Note that this is a lattice version of the translation operator. Thus, we can define a momentum operator P by

$$\exp(-iP) = t(0). \quad (\text{I.24})$$

Likewise $t(0)^{-1}$ shifts in the inverse direction and by means of crossing symmetry we have $t(0)^{-1} = t(\lambda)$. As a direct consequence we see that the logarithmic derivative of $t(u)$ at $u = 0$ is a local operator

$$\begin{aligned} \langle \mathbf{a} | t^{-1}(0) t'(0) | \mathbf{b} \rangle &= \sum_i \dots \begin{array}{ccc} a_{i-1} & a_i & a_{i+1} \\ \hline & W'(0) & \\ \hline b_{i-1} & b_i & b_{i+1} \end{array} \dots \\ &= \sum_i \prod_{j \neq i} \delta_{a_j b_j} W' \left(\begin{array}{cc|c} a_{i-1} & a_i & \\ \hline b_i & b_{i+1} & 0 \end{array} \right). \end{aligned} \quad (\text{I.25})$$

We can rewrite it as

$$H = \sum_{i=0}^{L-1} h_{(i-1)i(i+1)} \quad (\text{I.26})$$

with the local Hamiltonian given by

$$\langle \mathbf{a} | h_{(i-1)i(i+1)} | \mathbf{b} \rangle = \prod_{j \neq i} \delta_{a_j b_j} W' \left(\begin{array}{cc|c} a_{i-1} & a_i & 0 \\ b_i & b_{i+1} & \end{array} \right). \quad (\text{I.27})$$

Note that it depends on three consecutive heights whilst changing only one of them.

Performing this Hamiltonian limit, we can assign a quantum system with local Hamiltonian to each integrable face model. We will see that these models often correspond to non-Abelian anyon models which will be defined in the next section. This correspondence between (some) anyon models and integrable face models has been frequently used (see for example [14–16]).

Using higher order derivatives of $\log(t(u))$ one can construct local operators acting on more than two sites.

1.3 The Temperley-Lieb algebra

Before we start examining concrete examples of IRF models, let us study the underlying algebraic structures. Many models can be constructed from representations of the so-called Temperley-Lieb algebra (or its relatives). We will not present detailed calculations but rather give a short overview.

The Temperley-Lieb algebra $TL_n(\beta)$ is an algebra (over \mathbb{C}) generated by the elements $\{\mathbf{1}, e_1, \dots, e_{n-1}\}$ subject to the relations

$$\begin{aligned} e_i^2 &= \sqrt{\beta} e_i \\ e_i e_{i \pm 1} e_i &= e_i \\ e_i e_j &= e_j e_i \quad \text{for } |i - j| \geq 2 \end{aligned} \quad (\text{I.28})$$

where β is a free parameter.

The Temperley-Lieb algebra can be related to the Hecke algebra $H_n(q)$. Its generators g_i ($1 \leq i \leq n - 1$) satisfy the relations

$$\begin{aligned} g_i g_{i+1} g_i &= g_{i+1} g_i g_{i+1}, \\ g_i g_j &= g_j g_i \quad \text{for } |i - j| \geq 2. \\ g_i^2 &= (q^2 - 1) g_i + q^2. \end{aligned} \quad (\text{I.29})$$

Note the similarity between (I.29) and the defining relation of the Yang-Baxter operators (I.20).

1 Face models and their Hamiltonian limits

An explicit map π from the Hecke to the Temperley-Lieb algebra is given by

$$\pi : H_n(q) \rightarrow TL_n(\beta), g_i \mapsto qe_i - \mathbf{1} \quad (\text{I.30})$$

where $\sqrt{\beta} = q + q^{-1}$. Taking the limit $q \rightarrow 1$ one finds that $H_n(q) \rightarrow S_n$ where S_n is the symmetric group of order n . Thus, $H_n(q)$ may be seen as a deformation or quantisation of S_N .

Now, imagine we had found a representation of $TL_n(\beta)$ on the Hilbert space of a face model. We shall simply write e_i for the image of the generators under such a representation. Regarding (I.30) we make the ansatz

$$W_i(u) = 1 + f_\beta(u)e_i. \quad (\text{I.31})$$

We introduced a spectral parameter u via the function f_β (β is the same as in the defining relations of $TL_n(\beta)$) which is usually called a *Baxterisation*.

Boltzmann-weights fulfilling the Yang-Baxter equation can now be found by plugging the ansatz into (I.20) which yields

$$f_\beta(u) + f_\beta(v) + \sqrt{\beta}f_\beta(u)f_\beta(v) + f_\beta(u)f_\beta(v)f_\beta(u+v) = f_\beta(u+v). \quad (\text{I.32})$$

One can verify that

$$f_\beta(u) = \frac{\sin(u)}{\sin(\lambda - u)} \quad (\text{I.33})$$

is a trigonometric solution for $\beta = 4 \cos^2(\lambda)$.

This leads to a systematic way to find integrable face models: First, define the Hilbert space of states by giving the adjacency conditions (I.2). Then find a representation of the Temperley-Lieb algebra on it and use (I.31) and (I.33) to find Boltzmann weights.

There are indeed powerful methods to construct such representations which are based on graph theory and towers of algebras. An explicit recipe can be found in [42]. It is worth noting that the RSOS model, which is defined in the next section, can be obtained in this way.

1.4 Example: The restricted solid-on-solid model

Let us pause with the general development of the theory and study an important example. The restricted solid-on-solid (RSOS) model is a variant of Baxter's 8-vertex solid-on-solid model [38]. Historically introduced as an auxiliary model for the solution of the 8-vertex model, solid-on-solid models and their relatives have recently attracted much interest due to their relation to anyonic models [14, 43, 44].

The heights of the RSOS model belong to the set $\mathfrak{S} = \{1, 2, \dots, r-1\}$ where $r \geq 4$ is

1.4 Example: The restricted solid-on-solid model

a natural number. The adjacency graph is the Dynkin diagram of the Lie algebra A_{r-1} :

$$\bullet \xrightarrow{1} \bullet \xrightarrow{2} \dots \xrightarrow{r-2} \bullet \xrightarrow{r-1} \bullet$$

Adjacent heights must therefore differ by ± 1 and lie between 1 and $r-1$. These models are particularly interesting because of their relations to conformal field theories (CFTs). In 1984 it was shown [38, 45–47] that all unitary minimal conformal field theories with central charge $c < 1$ are classified by their central charge

$$c = 1 - \frac{6}{l(l+1)} \quad \text{with } l = 3, 4, 5 \dots \quad (\text{I.34})$$

and conformal weights according to the Kac formula. Each of those models can be obtained as the continuous limit of the critical RSOS model with $r = l$.

The weights of the critical model are trigonometric solutions of the YBE. Explicitly they are given by:

$$W \left(\begin{array}{cc|c} a & b & u \\ c & d & \end{array} \right) = \delta_{ad} \sqrt{\frac{g_b g_c}{g_a g_d}} \rho(u + \lambda) - \delta_{bc} \rho(u) \quad (\text{I.35})$$

with

$$\rho(u) = \frac{\sin(u - \lambda)}{\sin(\lambda)}, \quad g_x = \frac{\sin(\lambda x)}{\sin(\lambda)}. \quad (\text{I.36})$$

They satisfy the unitarity relation (I.6) but crossing symmetry requires some care and acquires additional (gauge) factors:

$$W \left(\begin{array}{cc|c} a & b & u \\ c & d & \end{array} \right) = \sqrt{\frac{g_b g_c}{g_a g_d}} W \left(\begin{array}{cc|c} b & d & \lambda - u \\ a & c & \end{array} \right). \quad (\text{I.37})$$

Let us demonstrate as a concrete example the application of the inversion equations (I.14) to solve for the spectrum. First note that we can write the transfer matrix as

$$t(u) = \sum_{n=-L/2}^{L/2} t_{2n} e^{i2nu} \quad (\text{I.38})$$

and consequently the eigenvalues are given by a finite Fourier series

$$\Lambda(u) = \sum_{n=-L/2}^{L/2} \Lambda_{2n} e^{i2nu}. \quad (\text{I.39})$$

The leading Fourier coefficients can be computed from the asymptotic behaviour of $t(u)$

1 Face models and their Hamiltonian limits

and are given by

$$\Lambda_{\pm L} = \left(\prod_{\ell=1}^L \exp(\mp i(u_\ell + \lambda/2)) \right) \frac{2 \cos((2j+1)\lambda)}{(2 \sin \lambda)^L}, \quad j \in \left\{0, \frac{1}{2}, 1, \dots, \frac{r-2}{2}\right\}. \quad (\text{I.40})$$

as shown in [48].

This enables a spectral decomposition of the RSOS model into topological sectors with ‘quantum dimension’

$$d_q(j) = \frac{\sin(\pi(2j+1)/r)}{\sin(\pi/r)}, \quad (\text{I.41})$$

labelled by the quantum number j . The emergence of this topological quantum number can be traced back to symmetries of the anyon chains corresponding to the RSOS models (see Eq. (I.54) where the generators of such topological symmetries are defined). The inversion relations (I.14) become quadratic equations for the remaining $L-1$ coefficients. However, this procedure is quite inefficient for large system sizes. For the periodic RSOS model (and some related models) Bethe equations have been derived from the inversion relations [39] which can be tackled with usual methods.

Although this functional approach gives the whole spectrum, it does not yield an expression for the corresponding eigenstates. Besides, the algebraic Bethe ansatz method is not suitable for most IRF models. The computation of correlation functions $\langle \phi_0 | \mathcal{O} | \phi_0 \rangle$, where $|\phi_0\rangle$ is the ground state and \mathcal{O} a local operator, is thus a complicated task. We will develop new functional methods for the resolution of this problem which circumvent the computation of the eigenstates. In particular, we will show how to characterise and compute the correlation functions without explicit expressions for the eigenstates.

Having, at least in principle, solved the spectral problem, we study the Hamiltonian limit. Therefore, we first observe that

$$W' \left(\begin{array}{cc|c} a_{i-1} & a_i & 0 \\ b_i & a_{i+1} & \end{array} \right) = \frac{1}{\sin \lambda} W \left(\begin{array}{cc|c} a_{i-1} & a_i & \lambda \\ b_i & a_{i+1} & \end{array} \right) - \cot(\lambda) \delta_{b_i a_i} \quad (\text{I.42})$$

where W' is the derivative with respect to the spectral parameter u . We define the operators e_i to be

$$\langle \mathbf{a} | e_i | \mathbf{b} \rangle = \left(\prod_{k \neq i} \delta_{a_k b_k} \right) W \left(\begin{array}{cc|c} a_{i-1} & a_i & \lambda \\ b_i & a_{i+1} & \end{array} \right), \quad (\text{I.43})$$

1.4 Example: The restricted solid-on-solid model

which explicitly read

$$\langle \mathbf{a} | e_i | \mathbf{b} \rangle = \delta_{a_{i-1} a_{i+1}} \sqrt{\frac{g_{a_i} g_{b_i}}{g_{a_{i-1}} g_{a_{i+1}}}} \prod_{k \neq i} \delta_{a_k b_k}. \quad (\text{I.44})$$

It can be shown that they yield a representation of the Temperley-Lieb algebra.

Using Eqs. (I.25), (I.42) and (I.43) we can express the Hamiltonian as

$$H_{\text{RSOS}} = t(0) \cdot t'(0)^{-1} = \frac{1}{\sin \lambda} \sum_i e_i - L \cot(\lambda) \cdot \mathbb{1}. \quad (\text{I.45})$$

2 Anyon models

In classical mechanics the exchange of two identical particles does not change the state of the system (i.e. the point in phase space). However, in quantum systems in three spatial dimensions the exchange of two identical fermions leads to a sign change of the wave functions. In two spatial dimensions the exchange of particles is described by the braid group, which allows more complicated exchange statistics [8] and gives rise to so-called *anyons*.

Anyons are characterised by their braiding relations. Specifically the interchange of two Abelian anyons can lead to a phase factor $e^{i\theta}$ in contrast to the restriction of $\theta = 0$ for bosons and $\theta = \pi$ for fermions. For non-Abelian anyons the braiding relations are extended to include unitary transformations on degenerate subspaces of many-particle wave functions [9]. Hence, the braiding of non-Abelian anyons may also change the anyon types.

Anyons appear e.g. as quasi particles in fractional quantum Hall states [12] and have recently aroused huge interest due to their potential use in topological quantum computing [13, 49].

In this section we will briefly describe the mathematical structures underlying anyonic models. Afterwards, we discuss a simple but still powerful non-Abelian anyon model – the Fibonacci anyons. They describe the physics of the fractional quantum Hall effect at filling factor $\nu = \frac{5}{2}$ [14].

2.1 Non-Abelian anyons

The modern mathematical language to describe anyonic theories uses modular tensor categories [50, 51]. We will not go into too much detail with the definitions and therefore only give a superficial description which suffices to understand all models discussed in the thesis. For a more detailed review see for example [52].

An anyon model consists of a (finite) set \mathcal{C} of anyon types (also called topological charges). To be more precise: they are the objects of the tensor category \mathcal{C} .

Those charges obey a commutative and associative fusion algebra

$$\psi_a \otimes \psi_b = \bigoplus_c N_{ab}^c \psi_c \tag{I.46}$$

where the fusion rules N_{ab}^c are non-negative integers. They are non-zero if and only if ψ_c is a possible outcome of a fusion process involving anyons of type ψ_a and ψ_b . Associativity and commutativity lead to

$$N_{ab}^c = N_{ba}^c, \tag{I.47}$$

2 Anyon models

$$\psi_a \otimes (\psi_b \otimes \psi_c) = (\psi_a \otimes \psi_b) \otimes \psi_c \Leftrightarrow \sum_f N_{af}^d N_{bc}^f = \sum_e N_{ab}^e N_{ec}^d. \quad (\text{I.48})$$

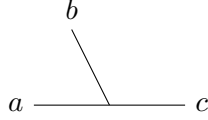
The last equivalence can be seen by employing (I.46) twice and comparing the coefficients of each anyon type.

Note that the symbols \otimes and \oplus are in general not the tensor product and direct sum but abstract structures of the tensor category. However, we will often deal with tensor categories which stem from representations of some algebra and the fusion rules correspond to the decomposition of the tensor product of two representations into irreducible representations (irreps).

In any anyon model there exists at least one charge, the vacuum charge ψ_1 , which is also called the trivial anyon. Fusion with the trivial anyon has no effect, i.e. $N_{a1}^c = \delta_{ac}$. Every anyon type $\psi_a \in \mathcal{C}$ has a unique conjugate charge $\psi_{\bar{a}}$ which fulfils $N_{ab}^1 = \delta_{b\bar{a}}$. The anyon $\psi_{\bar{a}}$ is therefore also called the antiparticle of a , since they annihilate each other to the vacuum.

An anyon model is called non-Abelian if there exist (at least) two anyon types, say a and b , such that $\sum_c N_{ab}^c > 1$. If N_{ab}^c is either 0 or 1 we call the model multiplicity free. All models studied in this thesis will be of such type.

We use a graphical notation for the fusion of anyons where a vertex



is allowed provided that $N_{ab}^c \neq 0$. The diagram can be interpreted as the worldline of anyons a and b which fuse and result in an anyon of type c . In this case time flows from top left to bottom right.

Associativity of multiple fusion processes is governed by so-called F -moves, which allow for a reordering:

$$\begin{array}{c} b \quad c \\ | \quad | \\ a \text{---} e \text{---} d \end{array} = \sum_f \left(F_d^{abc} \right)_f^e \begin{array}{c} b \quad c \\ \diagdown \quad / \\ f \text{---} d \end{array}. \quad (\text{I.49})$$

For a consistent physical model the F -Moves have to fulfil the pentagon equations. They are consistency conditions for multiple fusion events and best understood in their graphical forms.

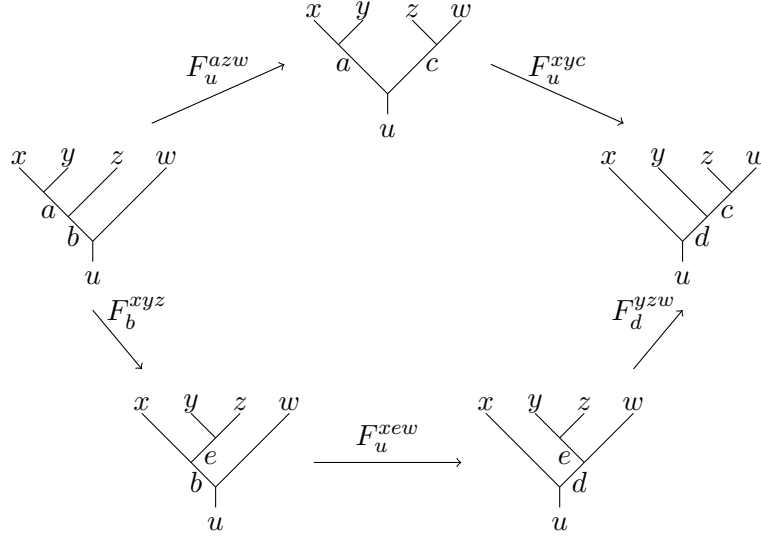


Figure 1: The pentagon equations.

Demanding the diagram in Fig. 1 to commute results in equations for the matrix elements of the F -moves:

$$(F_u^{xyc})_{da} (F_u^{azw})_{cb} = \sum_e (F_d^{yzw})_{ce} (F_u^{xew})_{db} (F_b^{xyz})_{ea}. \quad (\text{I.50})$$

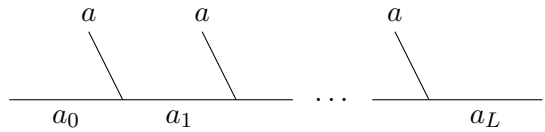
Note that this is a polynomial system of equations for the F -moves which is usually hard to solve (see e.g. [51]). For most models the solution is only unique after some gauge fixing. We will not provide more details here since for the models considered in this thesis explicit expressions for the F -moves are known.

We will now discuss the physics of interacting anyons. Consider a chain of L anyons of type ψ_a . For the moment we assume them to be at a distance from each other where interactions are negligible. In that case the degenerate ground states are spanned by *fusion paths*.

Starting with an auxiliary anyon ψ_{a_0} an orthogonal basis of fusion path states is constructed by fusing ψ_{a_ℓ} and ψ_a into $\psi_{a_{\ell+1}}$ resulting in

$$|a_0 a_1 \dots a_L\rangle \text{ with } N_{a_\ell a}^{a_{\ell+1}} = 1 \text{ for } \ell = 0 \dots L-1 \quad (\text{I.51})$$

or, graphically,



Here one can already see a connection with the previously defined face models. If the set \mathfrak{S} of heights coincides with the topological charges and the fusion rules fulfil

2 Anyon models

$N_{a_\ell a}^{a_{\ell+1}} = A_{a_\ell a_{\ell+1}}$, we can identify fusion paths with basis states of the face model.

When the anyons come closer, nearest-neighbours will fuse and we characterise the interaction by assigning different energies to the possible outcomes. For a mathematical description of this process we build local projection operators acting on the fusion path basis by means of the F -moves. They are given by

$$P_i^{(aa \rightarrow \ell)} := \sum_{a_{i-1}, a_i, a'_i, a_{i+1}} \left[(F_{a_{i+1}}^{a_{i-1}aa})_{\ell}^{a'_i} \right]^* (F_{a_{i+1}}^{a_{i-1}aa})_{\ell}^{a_i} | \cdots a_{i-1} a'_i a_{i+1} \cdots \rangle \langle \cdots a_{i-1} a_i a_{i+1} \cdots |. \quad (\text{I.52})$$

Though depending on the sites $i-1$, i and $i+1$ they leave the first and the last invariant. A straight forward generalisation allows to express local three anyon projection operators as

$$\langle \mathbf{a} | P_i^{(aaa \rightarrow \ell)} | \mathbf{b} \rangle \equiv \left(\prod_{k \notin \{i, i+1\}} \delta_{a_k b_k} \right) \sum_x \left[(F_{a_{i+1}}^{b_{i-1}aa})_x^{a_i} (F_{b_{i+2}}^{b_{i-1}xa})_{\ell}^{a_{i+1}} \right]^* (F_{b_{i+2}}^{b_{i-1}xa})_{\ell}^{b_{i+1}} (F_{b_{i+1}}^{b_{i-1}aa})_x^{b_i}. \quad (\text{I.53})$$

Restricting ourselves to periodic boundary conditions the anyon model possesses additional (topological) symmetries and the Hilbert space can be decomposed into topological sectors. To measure them we insert an auxiliary anyon of type ℓ , scatter it through the ring and finally remove it [14]. Mathematically this process corresponds to a product of F -moves:

$$\langle \mathbf{a} | Y_{\ell} | \mathbf{b} \rangle = \prod_{i=1}^L (F_{b_{i+1}}^{\ell a_i j})_{a_{i+1}}^{b_i}. \quad (\text{I.54})$$

2.2 Example: Fibonacci anyons

The Fibonacci anyons are a mathematically simple example of a non-Abelian anyon model, and yet at the same time they are just rich enough to allow for *universal* quantum computation. Since they have been shown to arise from certain lattice models [14], they are very relevant in the area of topological quantum computation. The convenient combination of simplicity and universality in the Fibonacci anyon model is likely why in most texts on the general topic it has become the standard example against which new ideas are probed.

The tensor category Fib has only two objects, the identity anyon 1 and a second anyon τ . The only non-trivial fusion rule is $\tau \otimes \tau = 1 \oplus \tau$, from which we see that the model is in fact non-Abelian. The F -moves of the Fibonacci anyons are quite simple, with the only non-trivial move being

$$(F_{\tau}^{\tau\tau\tau})_f^e = \begin{pmatrix} \phi^{-1} & \phi^{-1/2} \\ \phi^{-1/2} & -1/\phi \end{pmatrix}_{ef}, \quad (\text{I.55})$$

2.2 Example: Fibonacci anyons

where $e, f \in \{1, \tau\}$ and $\phi := \frac{1}{2}(1 + \sqrt{5})$ is the golden ratio. All other F -moves are 1 if they are allowed by the fusion rules and 0 otherwise.

We will now focus on a chain of interacting τ anyons as described in Section I.2.1. Because of $P_i^{(\tau\tau \rightarrow 1)} + P_i^{(\tau\tau \rightarrow \tau)} = \mathbb{1}$ a general nearest-neighbour Hamiltonian is given by

$$H = J \sum_{i=0}^{L-1} P_i^{(\tau\tau \rightarrow 1)}. \quad (\text{I.56})$$

The coupling constant J describes an interaction favouring fusion into 1 ($J < 0$) or τ ($J > 0$) anyons. Note that the operators $X_i := -\phi P_i^{(\tau\tau \rightarrow 1)}$ form a representation of the Temperley-Lieb algebra, cf. (I.28), which is identical to the standard representation associated with $su(2)_3$.

The anyons of an $su(2)_3$ theory can be labeled by generalised spins $j = 0, \frac{1}{2}, 1, \frac{3}{2}$. An automorphism of the corresponding fusion algebra allows us to identify $j = 0, \frac{3}{2}$ with the trivial ($x = 1$) and $j = \frac{1}{2}, 1$ with the τ -anyon of the Fibonacci chain. Starting from fusion path states $|x_0 x_1 \dots x_L\rangle$ of Fibonacci anyons with $x_n \in \{1, \tau\}$ we obtain the Hilbert space of the $r = 5$ RSOS model defined in Section II.4 by mapping

$$x_n \mapsto a_n \equiv \begin{cases} 1 & \text{for } x_n = 1, \quad n \text{ odd} \\ 2 & \text{for } x_n = \tau, \quad n \text{ even} \\ 3 & \text{for } x_n = \tau, \quad n \text{ odd} \\ 4 & \text{for } x_n = 1, \quad n \text{ even} \end{cases}. \quad (\text{I.57})$$

Note that this mapping gives only half of the basis states of the RSOS model, since a_n will be even (odd) on the even (odd) sublattice. The other half is obtained by switching odd and even in (I.57). This also provides a mapping of the anyon Hamiltonian to an operator in the RSOS model. Similarly the projection operators X_i are mapped to the local operators e_i defined in (I.44). In particular, we find for the anyon Hamiltonian

$$H = J \sum_i P_i^{(\tau\tau \rightarrow 1)} \mapsto \frac{J}{\phi} \sum_i e_i. \quad (\text{I.58})$$

3 Solving the Inverse Problem

Measurements of physical quantities are in the majority of cases related to correlation functions. To compare mathematical models with actual experiments it is therefore desirable to be able to compute them. Quite often this proves to be a hard task and even for integrable models it is still a subject of current research.

On first sight this is no surprise: The Yang-Baxter algebra yields highly non-local operators while correlations functions are expectation values of local operators. Hence, the solution of the inverse problem was a big achievement.

3.1 Solution for the Heisenberg model

A solution of the quantum inverse problem for the XXZ model has been developed by Kitanine, Maillet and Terras in 1999 [53] and was used to compute correlation functions also in the thermodynamic limit [19]. We will quickly review the procedure and see the difficulties that impede a direct generalisation to IRF models.

Let us first give a very brief introduction to the XXZ model: Recall that the (periodic) spin-1/2 XXZ model can be constructed from the $U_q(sl(2))$ - R -matrix. Defining $b(u) := \frac{\sinh(u)}{\sinh(u+\eta)}$ and $c(u) := \frac{\sinh(\eta)}{\sinh(u+\eta)}$, it explicitly reads

$$R(u) = \begin{pmatrix} 1 & 0 & 0 & 0 \\ 0 & b(u) & c(u) & 0 \\ 0 & c(u) & b(u) & 0 \\ 0 & 0 & 0 & 1 \end{pmatrix} \quad (\text{I.59})$$

and acts on the tensor product of two spaces $V_a = \mathbb{C}^2$ and $V_b = \mathbb{C}^2$. It yields a representation of the Yang-Baxter algebra on $\bigotimes_{i=1}^L V_i$ (where all $V_i = \mathbb{C}^2$) via the monodromy matrix

$$T_a(u) = R_{a1}(u - u_1) \dots R_{aL}(u - u_L) . \quad (\text{I.60})$$

The space $V_q := \bigotimes_{i=1}^L V_i$ is called the quantum space while V_a is the auxiliary space.

Here, as usual, $R_{ai}(u - u_i)$ is the action of $R(u - u_i)$ on V_a and V_i . Since $R(u)$ solves the Yang-Baxter equation, the RTT -equation

$$R_{ab}(u - v)T_a(u)T_b(v) = T_b(v)T_a(u)R_{ab}(u - v) \quad (\text{I.61})$$

holds and implies the commutativity of the transfer matrices $t(u) = \text{tr}_a T_a(u)$:

$$[t(u), t(v)] = 0 . \quad (\text{I.62})$$

3 Solving the Inverse Problem

The Hamiltonian of the periodic XXZ-spin-1/2 chain can then be constructed from the logarithmic derivative of $t(u)$.

As a matrix on V_a the monodromy matrix $T_a(u)$ takes the form

$$T_a(u) = \begin{pmatrix} A(u) & B(u) \\ C(u) & D(u) \end{pmatrix} \quad (\text{I.63})$$

where the matrix elements are operators on V_q . Their commutation relations are inferred from the *RTT* relation. This is the starting point for the algebraic Bethe ansatz solution. Starting from a so-called pseudo-vacuum $|0\rangle$, excited states are constructed as

$$|\lambda_1, \dots, \lambda_n\rangle = B(\lambda_1) \dots B(\lambda_n)|0\rangle \quad (\text{I.64})$$

where the complex numbers λ_i are a solution to the Bethe equations. Such vectors are sometimes also called *on-shell Bethe vectors* as opposed to vectors $|\lambda_1, \dots, \lambda_n\rangle$ where the parameters λ_i do not solve the Bethe equations which are then called *off-shell*. More details on the algebraic Bethe ansatz and a derivation of the Bethe equations can be found in [54].

On first sight the computation of correlation functions, i.e.

$$\langle \lambda_1, \dots, \lambda_n | \mathcal{O} | \lambda_1, \dots, \lambda_n \rangle \quad (\text{I.65})$$

seems hopeless for a local operator \mathcal{O} since it is sandwiched between states constructed by means of the non-local B operators. However, this becomes manageable by expressing local operators through elements of the Yang-Baxter algebra.

For the XXZ model local spin-1/2 operators acting on V_ℓ can be expressed (see [53] for a proof) as:

$$\sigma_\ell^- = \prod_{i=1}^{\ell-1} (A + D)(u_i) \cdot B(u_\ell) \cdot \prod_{i=\ell+1}^L (A + D)(u_i) \quad (\text{I.66})$$

$$\sigma_\ell^+ = \prod_{i=1}^{\ell-1} (A + D)(u_i) \cdot C(u_\ell) \cdot \prod_{i=\ell+1}^L (A + D)(u_i) \quad (\text{I.67})$$

$$\sigma_\ell^z = \prod_{i=1}^{\ell-1} (A + D)(u_i) \cdot (A - D)(u_\ell) \cdot \prod_{i=\ell+1}^L (A + D)(u_i). \quad (\text{I.68})$$

Now any local operator can be reconstructed in terms of elements of the monodromy matrix and transfer matrix. Hence, integrability techniques can be applied. This method has been extended to a bigger class of integrable models in [55].

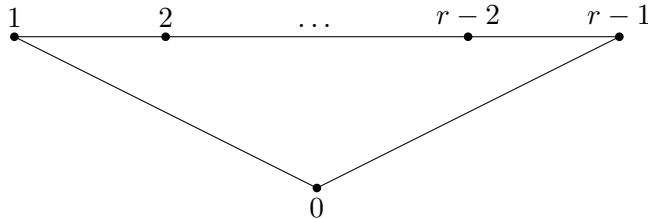
For instance we obtain

$$(E_{\beta}^{\alpha})_i = \prod_{l=1}^{i-1} t(u_l) T^{\beta\alpha}(u_i) \prod_{l=1}^i t(u_i)^{-1}.$$

However, the situation is more complicated in case of IRF models which are not constructed from a monodromy matrix and lack an auxiliary space. We will first show how this problem has been approached for a ‘hybrid’ model – the cyclic solid-on-solid model. It can be formulated as a solution to the *dynamical* Yang-Baxter equation and a solution of the inverse problem has recently been given in [56].

3.2 Solution for the CSOS model

Let us discuss in more detail the first solution of the quantum inverse problem for an IRF model. The heights of the *cyclic solid-on-solid* (CSOS) model are taken from the set $\mathfrak{S} = \{0, 1, 2, \dots, r-1\}$ and the adjacency graph is given by



It corresponds to the Dynkin diagram of the affine Lie algebra \tilde{A}_{r-1} . The origin of the CSOS model dates back until 1988 [57], when it was developed by Pearce and Seaton as a new variant of the unrestricted SOS model. Unlike the already discussed RSOS model it admits a solution by algebraic Bethe ansatz methods. This was achieved by an embedding of the Boltzmann weights into the elements of a *dynamical* R -matrix.

Felder’s work on elliptic quantum groups [58] enabled an application of methods that result into an Algebraic Bethe ansatz solution of the CSOS model [59, 60].

Given an R -matrix $R(u, s) \in \text{End}(V_1 \otimes V_2)$ which solves the *dynamical* Yang-Baxter equation (DYBE)

$$\begin{aligned} R_{1,2}(u_{12}, s + \eta h_3) R_{1,3}(u_{13}, s) R_{2,3}(u_{23}, s + \eta h_1) &= \\ &= R_{2,3}(u_{23}, s - \eta h_1) R_{1,3}(u_{13}, s + \eta h_2) R_{1,2}(u_{12}, s) \end{aligned} \tag{I.69}$$

one can build an $E_{\tau, \eta}(\mathfrak{sl}(2))$ module, i.e. a representation of the algebra generated by the RTT -relation:

$$\begin{aligned} R_{1,2}(u_{12}, s + \eta h_3) T_{1,3}(u_1, s) T_{2,3}(u_2, s + \eta h_1) &= \\ &= T_{2,3}(u_2, s) T_{1,3}(u_1, s + \eta h_2) R_{1,2}(u_{12}, s). \end{aligned} \tag{I.70}$$

3 Solving the Inverse Problem

The additional parameter s on which the operators depend is called dynamical parameter and we use the abbreviation $u_{ij} = u_i - u_j$. In the $\mathfrak{sl}(2)$ case we have $R(u, s) \in \text{End}(\mathbb{C}^2 \otimes \mathbb{C}^2)$ and $h = \sigma^z$, e.g.

$$R_{1,2}(u_{12}, s + \eta h_3)(|i\rangle \otimes |j\rangle \otimes |k\rangle) = R(u, s + \mu)(|i\rangle \otimes |j\rangle) \otimes |k\rangle \quad (\text{I.71})$$

if $h|k\rangle = \mu|k\rangle$.

From the DYBE it can be seen that the R -matrix itself solves the RTT -relation. For the CSOS model it reads

$$R(u, s) = \begin{pmatrix} 1 & 0 & 0 & 0 \\ 0 & a(u; s) & b(u; s) & 0 \\ 0 & b(u; -s) & a(u; -s) & 0 \\ 0 & 0 & 0 & 1 \end{pmatrix}. \quad (\text{I.72})$$

The entries a and b are defined in terms of the elliptic theta function $\theta(u) := \theta_1(\eta u; \tau)$ and we require $\text{Im}(\tau) > 0$. Then

$$a(u; s) = \frac{\theta(s+1)\theta(u)}{\theta(s)\theta(u+1)} \text{ and } b(u; s) = \frac{\theta(1)\theta(u+s)}{\theta(s)\theta(u+1)}. \quad (\text{I.73})$$

The entries of the R -matrix are the Boltzmann weights of a face model

$$R(u, s)_{kl}^{ij} = \begin{array}{c} \begin{array}{ccc} & k & \\ s & \square & s+k \\ & u & \\ i & \dots & l \end{array} \\ \begin{array}{ccc} s+i & j & s+k+l \\ & = s+i+j & \end{array} \end{array}. \quad (\text{I.74})$$

Using the R -matrix we obtain a representation on the Hilbert space $\mathcal{H} = \bigotimes_{i=1}^N \mathbb{C}^2$, defining $T(u, \{u_i\}, s) \in \text{End}(\mathbb{C}^2 \otimes \mathcal{H})$ by

$$T(u, \{u_i\}, s) = R_{a,N} \left(u - u_N, s + \sum_{i=1}^{N-1} h_i \right) R_{a,N-1} \left(u - u_{N-1}, s + \sum_{i=1}^{N-2} h_i \right) \dots R_{a,1}(u - u_1, s) \quad (\text{I.75})$$

$$= \begin{pmatrix} A(u) & B(u) \\ C(u) & D(u) \end{pmatrix}_{[a]} \quad (\text{I.76})$$

3.2 Solution for the CSOS model

where the matrix is represented in the canonical basis of $V_a = \mathbb{C}^2$. The inhomogeneities $\{u_i\}$ are arbitrary complex numbers, so we are actually dealing with an inhomogeneous version of the dynamical 6-vertex model. From now on we will not display them explicitly and simply write $T(u, s)$.

Note that this is analogous to the coproduct of usual quantum groups [61]. The monodromy matrix T acts on the underlying vertex labels, i.e. on an auxiliary space $V_a = \mathbb{C}^2$ and \mathcal{H} and not directly on the face heights that are parameterised by s .

Taking the trace does not directly yield an integrable model since $t(u, s) = \text{tr}_{V_a} T(u, s)$ does not define a family of commuting operators on \mathcal{H} . To fix this problem we lift all operators to the space of meromorphic $\mathcal{H}[0]$ -valued functions $\mathcal{H}_f = \text{Fun}(\mathcal{H}[0])$. Here $\mathcal{H}[0]$ is the zero weight space, i.e. the kernel of the total spin operator $h_{1,2,\dots,N} = \sum_{i=1}^N h_i$. For the special choice of $\eta = m/r$ with m and r coprime all weights are r -periodic in s and we can restrict s to the set $C_{s_0}^r := s_0 + \mathbb{Z}/r$, where $s_0 \in \mathbb{C}$ and $r \in \mathbb{N}$ are fixed constants. A state is therefore a function $f : C_{s_0}^r \rightarrow \mathcal{H}[0]$. Note that now the state space \mathcal{H}_f can be described by paths of the height variables with periodic boundary conditions modulo r :

$$|\mathbf{a}\rangle : C_{s_0}^r \rightarrow \mathcal{H}[0], s \mapsto |\mathbf{a}\rangle(s) = \delta_{s,a_0} e_{a_1-a_0} \otimes e_{a_2-a_1} \otimes \cdots \otimes e_{a_N-a_{N-1}}, \quad (\text{I.77})$$

with the canonical basis vectors $e_{\pm 1}$ of \mathbb{C}^2 . To get rid of the s dependence of T and arrive at an integrable face model, define the dynamical operators τ_s and \hat{s} , which act according to $\tau_s f(s) = f(s+1)$ and $\hat{s}f(s) = sf(s)$. The lifted monodromy matrix $\hat{T}(u) \in \text{End}(\mathbb{C}^2 \otimes \mathcal{H}_f)$ is then given by:

$$\hat{T}(u) = T(u, \hat{s}) \tau_s^{h_a} = \begin{pmatrix} A(u, \hat{s}) \tau_s & B(u, \hat{s}) \tau_s^{-1} \\ C(u, \hat{s}) \tau_s & D(u, \hat{s}) \tau_s^{-1} \end{pmatrix}. \quad (\text{I.78})$$

To illustrate the definitions we use the graphical notation which was introduced in (I.74), e.g. the matrix element $\langle \mathbf{b} | \hat{A}(u) | \mathbf{a} \rangle$ in the path basis of \mathcal{H}_f is depicted as

$$\begin{array}{c}
 \begin{array}{ccccccc}
 & a_1 - a_0 & & & a_L - a_{L-1} & & \\
 a_0 & \vdots & a_1 & \vdots & & \vdots & a_{L-1} & \vdots & a_L \\
 \hline
 & u - u_1 & & & & & u - u_L & & \\
 \hline
 b_0 & \vdots & b_1 & \vdots & & \vdots & b_{L-1} & \vdots & b_L \\
 & b_1 - b_0 & & & & & b_L - b_{L-1} & &
 \end{array}
 \end{array}
 + \delta_{b_0, a_0+1} \delta_{b_N, a_N+1} \quad (\text{I.79})$$

where the two δ are the result of the shift τ_s in the definition of $\hat{A}(u) = A(u, \hat{s}) \tau_s$.

3 Solving the Inverse Problem

We can now discuss the solution of the inverse problem. In [56] local operators

$$\langle \mathbf{b} | \left(E_{\beta}^{\alpha} \right)_{i,i+1} | \mathbf{a} \rangle = \delta_{a_{i+1}-a_i, \alpha} \delta_{b_{i+1}-b_i, \beta} \quad (\text{I.80})$$

were considered and expressed by matrix elements of the monodromy matrix. There are two important things to notice: First of all, note that they only fix differences between heights due to the fact that they actually act on the underlying vertex model. Secondly, in our graphical notation elements of the monodromy matrix are labelled on the horizontal ends. Hence, solving the inverse problem means shifting the indices α and β from the vertical to the horizontal direction.

We do not repeat the proof from [56] and just state the result:

$$\left(E_{\beta}^{\alpha} \right)_{i,i+1} = \prod_{k=1}^i \hat{t}(u_k) \hat{T}_{\alpha, \beta}(u_i + 1) \prod_{k=1}^{i+1} \hat{t}(u_k)^{-1} \hat{\tau}_s^{\beta - \alpha}. \quad (\text{I.81})$$

The proof in [56] is based on the dynamical Yang-Baxter algebra and thus it is for instance unclear how to extend it to other IRF models. We will solve this problem in subsequent sections.

3.3 Solution for generic IRF/anyon models

So far we have seen solutions of the inverse problem for spin chains related to vertex models and a special IRF model which can be cast into a very similar form. We will now proceed and present a solution for generic IRF models only relying on physical symmetries of the Boltzmann weights. Most of this section is based on [62].

Let us reconsider the Hilbert space of anyonic models. Recall that it is spanned by fusion path states. They can be decomposed into sectors $\mathcal{H}_{\alpha\beta}^L$ labelled by the auxiliary anyons $\alpha = a_0$ and $\beta = a_L$. We call them auxiliary because they are the starting and end point of a fusion process with the physical anyons forming a chain of length L .

Given a classical IRF model with L columns and N horizontal rows this identification suggests to view the left and right boundary heights as auxiliary spins. We go one step further and note that sequences $\underline{\alpha} = (\alpha_0 \alpha_1 \dots \alpha_N)$ with $N_{\alpha_n a_*}^{\alpha_{n+1}} = A_{\alpha_n \alpha_{n+1}} = 1$ of heights on vertical lines can be identified with fusion paths spanning an 'auxiliary' Hilbert space \mathcal{V}^N . We agree that from now on greek indices will be used to label auxiliary heights.

We represent the matrix elements of generic linear operators B on the space $\mathcal{V}^N \hat{\otimes} \mathcal{H}^L$

3.3 Solution for generic IRF/anyon models

as ¹

$$\begin{aligned}
 (\langle \mathbf{a} | \hat{\otimes} \langle \underline{\alpha} |) B (| \underline{\beta} \rangle \hat{\otimes} | \mathbf{b} \rangle) = & \begin{array}{c} \alpha_0 = a_0 \qquad \qquad \qquad \dots \qquad \qquad \qquad \beta_0 = a_L \\ \alpha_1 \qquad \qquad \qquad \qquad \qquad \qquad \qquad \qquad \qquad \beta_1 \\ \vdots \qquad \qquad \qquad \qquad \qquad \qquad \qquad \qquad \qquad \vdots \\ \alpha_{N-1} \qquad \qquad \qquad \qquad \qquad \qquad \qquad \qquad \qquad \beta_{N-1} \\ \alpha_N = b_0 \qquad \qquad \qquad \dots \qquad \qquad \qquad \beta_N = b_L \end{array} \cdot \\
 & \text{(I.82)}
 \end{aligned}$$

The matrix elements of B in \mathcal{V}^N are linear operators on \mathcal{H}^L and vice versa:

$$B^{\underline{\alpha}\underline{\beta}} = \langle \underline{\alpha} | B | \underline{\beta} \rangle, \quad B_{\mathbf{b}}^{\mathbf{a}} = \langle \mathbf{a} | B | \mathbf{b} \rangle. \quad \text{(I.83)}$$

A special example of such operators which will be frequently used is $T(u) : \mathcal{V}^1 \hat{\otimes} \mathcal{H}^L \rightarrow \mathcal{V}^1 \hat{\otimes} \mathcal{H}^L$, given by:

$$\begin{aligned}
 (\langle \mathbf{a} | \hat{\otimes} \langle \underline{\alpha} |) T(u) (| \underline{\beta} \rangle \hat{\otimes} | \mathbf{b} \rangle) = & \begin{array}{c} \alpha_0 = a_0 \quad a_1 \qquad \qquad \qquad a_{L-1} \quad \beta_0 = a_L \\ \boxed{u - u_1 \quad \dots \quad u - u_L} \\ \alpha_1 = b_0 \quad b_1 \qquad \qquad \qquad b_{L-1} \quad \beta_1 = b_L \end{array} \cdot \\
 & \text{(I.84)}
 \end{aligned}$$

Note that by tracing

$$\begin{aligned}
 t(u) = \text{tr}_{\mathcal{V}^1} T(u) &= \sum_{\alpha, \beta} T_{\beta\beta}^{\alpha\alpha}(u), \\
 \langle \mathbf{a} | t(u) | \mathbf{b} \rangle &= \begin{array}{c} a_0 \quad a_1 \qquad \qquad \qquad a_{L-1} \quad a_0 = a_L \\ \boxed{u - u_1 \quad \dots \quad u - u_L} \\ b_0 \quad b_1 \qquad \qquad \qquad b_{L-1} \quad b_0 = b_L \end{array} \quad \text{(I.85)}
 \end{aligned}$$

we recover the transfer matrix. We will also need the mappings

$$T_{\alpha\beta}(u) = \sum_{\gamma\delta} T_{\alpha\beta}^{\gamma\delta}(u), \quad T^{\alpha\beta}(u) = \sum_{\gamma\delta} T_{\gamma\delta}^{\alpha\beta}(u), \quad \text{(I.86)}$$

which send $\mathcal{H}_{\alpha\beta}^L \rightarrow \mathcal{H}^L$ and vice versa. Note that $T_{\alpha\beta}(u)T^{\alpha\beta}(v)$ is a linear operator

¹The symbol $\hat{\otimes}$ indicates that the index of the joint vertex of the two factors coincides.

3 Solving the Inverse Problem

on \mathcal{H}^L which leaves $\mathcal{H}_{\text{per}}^L$ invariant and thus defines a unique operator $\mathcal{H}_{\text{per}}^L \rightarrow \mathcal{H}_{\text{per}}^L$ by restriction. Strictly speaking one should write $\left(T_{\alpha\beta}(u)T^{\alpha\beta}(v)\right)\Big|_{\mathcal{H}_{\text{per}}^L}$ which we omit to not overload the notation. Domain and image space should anyway always be clear from context.

Also recall the definition of elementary operators $(E_\beta^\alpha)_i$ from Eq. (I.17). We can now formulate one of the main results of this thesis.

Theorem 1. *The local operator $(E_\beta^\alpha)_i$ can be expressed as²*

$$\left(E_\beta^\alpha\right)_i = \prod_{k,\ell=1}^L \frac{1}{\rho(u_k - u_\ell)} \left(\prod_{k=1}^{i-1} t(u_k)\right) T_{\alpha\beta}(u_i) T^{\alpha\beta}(u_{i+1}) \left(\prod_{k=i+2}^L t(u_k)\right). \quad (\text{I.87})$$

The function ρ is the same as in the unitarity relation (I.6).

Proof. Let us first prove the statement for an easy example where the chain length is $L = 2$, i.e. two faces per row. For $|\mathbf{a}\rangle, |\mathbf{b}\rangle \in \mathcal{H}_{\text{per}}^2$ we use the unitarity relation (I.6) and find:

$$\begin{aligned} \langle \mathbf{a} | T_{\alpha\beta}(u_1) T^{\alpha\beta}(u_2) | \mathbf{b} \rangle &= \alpha \begin{array}{ccc} a_0 & a_1 & a_0 \\ \hline u_1 - u_1 & u_1 - u_2 & \\ \hline u_2 - u_1 & u_2 - u_2 & \\ \hline b_0 & b_1 & b_0 \end{array} \beta = \alpha \begin{array}{ccc} a_0 & a_1 & a_0 \\ & \diagup & \diagdown \\ & u_1 - u_2 & \\ & \diagdown & \diagup \\ & u_2 - u_1 & \\ & \diagup & \diagdown \\ b_0 & b_1 & b_0 \end{array} \beta \\ &= \prod_{k,\ell=1}^2 \rho(u_k - u_\ell) \delta_{a_0 b_0} \delta_{a_1 \alpha} \delta_{b_1 \beta} = \prod_{k,\ell=1}^2 \rho(u_k - u_\ell) \langle \mathbf{a} | \left(E_\beta^\alpha\right)_1 | \mathbf{b} \rangle. \end{aligned}$$

For $L > 2$ the procedure works similarly. First use the initial condition in every row. Then use unitarity until all Boltzmann weights are turned into Kronecker δ 's. Whenever unitarity is used we produce two ρ -functions and find the correct prefactor. A detailed demonstration can be found in Appendix A. \square

Note that this proof only requires unitarity (I.6) and the initial condition of the Boltzmann weights. The theorem is therefore widely applicable.

We have thus provided an expression of local 1-point operators by means of operators from the Yang-Baxter algebra. A generalisation to n -point operators is straightforward.

²To avoid more lengthy expressions we use the convention, that empty products evaluate to 1 and all operators which contain the non-existing parameter u_0 are omitted.

3.3 Solution for generic IRF/anyon models

An elementary operator acting on several neighbouring sites $1 \leq n_1 \leq n_2 \leq L$ can be expressed as

$$\begin{aligned}
E_{\beta_{n_1} \dots \beta_{n_2}}^{\alpha_{n_1} \dots \alpha_{n_2}} &= \prod_{k, \ell=1}^L \frac{1}{\rho(u_k - u_\ell)} \left(\prod_{k=1}^{n_1-1} t(u_k) \right) \times \\
&\quad \times T_{\alpha_{n_1} \beta_{n_1}}(u_{n_1}) \left(\prod_{k=n_1+1}^{n_2} T_{\alpha_k \beta_k}^{\alpha_{k-1} \beta_{k-1}}(u_k) \right) T^{\alpha_{n_2} \beta_{n_2}}(u_{n_2+1}) \left(\prod_{k=n_2+2}^L t(u_k) \right) \\
&= \left(\prod_{k=1}^{n_1-1} t(u_k) \right) T_{\alpha_{n_1} \beta_{n_1}}(u_{n_1}) \times \\
&\quad \times \left(\prod_{k=n_1+1}^{n_2} T_{\alpha_k \beta_k}^{\alpha_{k-1} \beta_{k-1}}(u_k) \right) T^{\alpha_{n_2} \beta_{n_2}}(u_{n_2+1}) \left(\prod_{k=1}^{n_2+1} t^{-1}(u_k) \right).
\end{aligned} \tag{I.88}$$

We emphasise that this construction and its proof is valid for all face models whose Boltzmann weights satisfy the unitarity conditions. This is the starting point for the definition of the *reduced density matrix*, which will be discussed in the next section.

4 The N -site reduced density matrix

Having solved the inverse problem the Yang-Baxter algebra can be used as a tool to compute correlation functions. Let us briefly review the case of the spin-1/2 Heisenberg chain and why the situation is more complicated for IRF models (and their corresponding anyon chains).

Recall from Section I.3 that for the Heisenberg spin chain one can construct the eigenvectors of the transfer matrix as Bethe vectors $|\lambda_1, \dots, \lambda_n\rangle$. If now $|\lambda_1, \dots, \lambda_n\rangle$ is an on-shell Bethe vector and \mathcal{O} a local operator, one can use the inverse problem and express \mathcal{O} through elements of the Yang-Baxter algebra such that $\mathcal{O}|\lambda_1, \dots, \lambda_n\rangle$ can be written as a linear combination of off-shell Bethe vectors. Correlation functions may thus be reduced to the computation of scalar products of an on-shell and an off-shell Bethe vector.

This has been achieved by Slavnov in 1989 in terms of determinant expressions for the scalar product of an on-shell and an off-shell Bethe vector [63]. However, for higher rank spin chains a determinant formula for scalar products of on- and off-shell Bethe vectors is still unknown.

The dependence on the Algebraic Bethe ansatz can be circumvented using functional relations. For the XXX and related models many results have been obtained this way (see e.g. [23, 25, 64, 65] and [66] for a generalisation to higher rank models).

Most IRF models cannot be solved via algebraic Bethe ansatz methods. We will therefore follow the second route by defining reduced density matrices and deriving functional equations fulfilled by them. The content of this section is largely based on [62].

4.1 Definition of the reduced density matrix

Recall that we can decompose any local N -point operator into a sum of elementary operators (I.17). Hence, a complete characterisation of the introduced models requires reduced density matrices, i.e operators of the form

$$\frac{1}{\langle \phi_0 | \phi_0 \rangle} \langle \phi_0 | E_{\beta_{n_1} \dots \beta_{n_2}}^{\alpha_{n_1} \dots \alpha_{n_2}} | \phi_0 \rangle. \quad (\text{I.89})$$

which act only on a subpart of the lattice. Here $|\phi_0\rangle \in \mathcal{H}^L$ is the ground state of the model. More generally one may consider the general right (left) eigenvectors $|\phi\rangle$ ($\langle\phi|$) of the transfer matrix corresponding to a particular eigenvalue $\Lambda(u)$, i.e. $t(u)|\phi\rangle = \Lambda(u)|\phi\rangle$ ($\langle\phi|t(u) = \langle\phi|\Lambda(u)$).

Let us introduce the operators $\tilde{T}_N : \mathcal{H}^L \rightarrow \mathcal{H}^L$, corresponding to $N = n_2 - n_1 + 2$ consecutive rows of the face model with fixed sequences $\alpha = (\alpha_\ell)_{\ell=n_1-1}^{n_2+1}$ and $\beta =$

4 The N -site reduced density matrix

$(\beta_\ell)_{\ell=n_1-1}^{n_2+1}$ of auxiliary indices (although not written explicitly the index N is to be understood as the combination (n_1, n_2))

$$\tilde{T}_N(\lambda_{n_1}, \dots, \lambda_{n_2+1})^{\underline{\alpha}\underline{\beta}} = \prod_{k=n_1}^{n_2+1} T_{\alpha_k \beta_k}^{\alpha_{k-1} \beta_{k-1}}(\lambda_k). \quad (\text{I.90})$$

Now define

$$D_N(\lambda_{n_1}, \dots, \lambda_{n_2+1})^{\underline{\alpha}\underline{\beta}} = \frac{\langle \phi | \tilde{T}_N(\lambda_{n_1}, \dots, \lambda_{n_2+1})^{\underline{\alpha}\underline{\beta}} | \phi \rangle}{\langle \phi | \phi \rangle \prod_{k=n_1}^{n_2+1} \Lambda(\lambda_k)}. \quad (\text{I.91})$$

By construction D_N is a matrix on the auxiliary space $\simeq \mathcal{V}^N$. Note that $D_N^{\underline{\alpha}\underline{\beta}} = 0$ for $\alpha_{n_1-1} \neq \beta_{n_1-1}$, $\alpha_{n_2+1} \neq \beta_{n_2+1}$ as a consequence of $|\phi\rangle \in \mathcal{H}_{\text{per}}^L$.

Graphically this operator can be depicted as (here shown for $N = 2$ with $n_1 = 1$, $n_2 = 1$):

$$\begin{aligned}
 D_2(\lambda_1, \lambda_2)^{\{\underline{\alpha}\}\{\underline{\beta}\}} &= \begin{array}{c} \text{---} \Phi \text{---} \\ \alpha_0 \quad \beta_0 \\ \alpha_1 \quad \tilde{T}_2(\lambda_1, \lambda_2) \quad \beta_1 \\ \alpha_2 \quad \beta_2 \\ \text{---} \Phi \text{---} \end{array} \cdot \frac{1}{\langle \Phi | \Phi \rangle \Lambda(\lambda_1) \Lambda(\lambda_2)} \\
 &= \begin{array}{c} \text{---} \Phi \text{---} \\ \alpha_0 \quad \beta_0 \\ \lambda_1 - u_1 \quad \dots \quad \lambda_1 - u_L \\ \alpha_1 \quad \beta_1 \\ \lambda_2 - u_1 \quad \dots \quad \lambda_2 - u_L \\ \alpha_2 \quad \beta_2 \\ \text{---} \Phi \text{---} \end{array} \cdot \frac{1}{\langle \Phi | \Phi \rangle \Lambda(\lambda_1) \Lambda(\lambda_2)}
 \end{aligned} \quad (\text{I.92})$$

where the projection onto the eigenstate $|\Phi\rangle$ is indicated by sandwiching of \tilde{T}_N . Note that $D_N^{\{\underline{\alpha}\}\{\underline{\beta}\}} = 0$ for $\alpha_{n_1-1} \neq \beta_{n_1-1}$, $\alpha_{n_2+1} \neq \beta_{n_2+1}$ for states $|\Phi\rangle \in \mathcal{H}_{\text{per}}^L$. This allows to decompose D_N into blocks labeled by α_{n_1-1} and α_{n_2+1} , i.e.

$$D_2(\lambda_1, \lambda_2)^{\{\underline{\alpha}\}\{\underline{\beta}\}} = \left(D_2^{[\alpha_0, \alpha_2]}(\lambda_1, \lambda_2) \right)_{\beta_1}^{\alpha_1} \quad (\text{I.93})$$

for the example $N = 2$ displayed above.

Comparing with (I.88) we observe that the reduced density matrix of the face model

4.2 Properties of the reduced density matrix

for N consecutive edges (or segments of the fusion path) in an eigenstate $|\Phi\rangle$ of the transfer matrix is obtained from D_N by proper choice of the arguments λ_k :

$$D_N(\lambda_{n_1}, \dots, \lambda_{n_2+1})^{\{\underline{\alpha}\}\{\underline{\beta}\}} \Big|_{\lambda_k=u_k, k=n_1, \dots, n_2+1} = \frac{1}{\langle \Phi | \Phi \rangle} \langle \Phi | E_{\beta_{n_1} \dots \beta_{n_2}}^{\alpha_{n_1} \dots \alpha_{n_2}} | \Phi \rangle, \quad (\text{I.94})$$

In a slight misuse of notation we shall denote D_N as N -site density matrix below. D_N is normalised such that $\text{tr}_{\mathcal{V}^N} D_N(\lambda_{n_1}, \dots, \lambda_{n_2+1}) = 1$, which constrains the diagonal elements of D_N . Taking partial traces, i.e. summing over pairs $(\alpha_\ell, \beta_\ell)$ of auxiliary indices, any n -point function with $n \leq N$ can be computed from D_N . Hence, instead of the reduced density matrices as defined in (I.89) we can try to compute D_N as a function of the spectral parameters. This gives us additional freedom to generate functional equations which will be shown in the next section.

4.2 Properties of the reduced density matrix

We start our investigation with some general properties which result directly from symmetries of the local Boltzmann weights and are therefore quite general. Model specific peculiarities will be investigated later.

Recall the definition of Yang-Baxter operators in Eq. (I.19):

$$\langle \underline{\alpha} | W_i(u) | \underline{\beta} \rangle := W \left(\begin{array}{cc|c} \alpha_{i-1} & \beta_i & u \\ \alpha_i & \alpha_{i+1} & \end{array} \right) \prod_{j \neq i} \delta_{a_j b_j}. \quad (\text{I.95})$$

It follows immediately from the Yang-Baxter equation (I.4) that

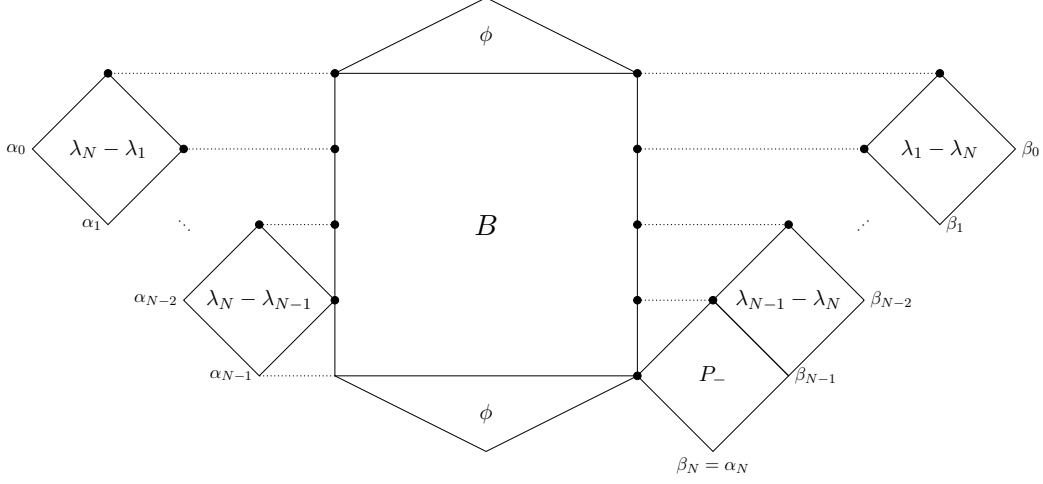
$$W_i(\lambda_{i+1} - \lambda_i) \cdot D_N(\lambda_1, \dots, \lambda_i, \lambda_{i+1}, \dots, \lambda_N) = D_N(\lambda_1, \dots, \lambda_{i+1}, \lambda_i, \dots, \lambda_N) \cdot W_i(\lambda_{i+1} - \lambda_i), \quad (\text{I.96})$$

where we assume that $1 \leq i < N$. This equation is particularly useful since it allows for a reordering of the spectral parameters. Note that due to the initial condition (I.8) and crossing symmetry (I.7) $W_i(\lambda)$ degenerates to a Kronecker δ which will later be used to find a reduction relation relating D_N and D_{N-2} .

Apart from these quite obvious relations, the reduced density matrix is subject to a further functional equation, which is one of the main results of this thesis. To formulate this we introduce an operator $A_N(\lambda_1, \dots, \lambda_N) : \text{End}(\mathcal{V}^N) \rightarrow \text{End}(\mathcal{V}^N)$. Given an arbitrary operator B acting on \mathcal{V}^N as defined in (I.83), the action of A_N on B graphically defined as

$$(A_N(\lambda_1, \dots, \lambda_N)[B])^{\underline{\alpha}\underline{\beta}} = \frac{\delta_{\alpha_0 \beta_0} \delta_{\alpha_N \beta_N}}{\prod_{i=1}^N \rho(\lambda_i - \lambda_N) \rho(\lambda_N - \lambda_i)} \times$$

4 The N -site reduced density matrix



For models with crossing symmetry as in (I.7) the operator $P_- \in \text{End}(\mathcal{V}^1)$ is obtained by evaluation of the Boltzmann weight (I.3) at $u = \lambda$. For more complicated cases P_- needs to be modified, see (II.16) below. Note that the extra Kronecker δ 's ensure that the image of B has elements acting on $\mathcal{H}_{\text{per}}^L$ only.

As an example consider the action of A_2 on the reduced density operator D_2 , here shown for a system of length $L = 2$:

$$A_2(\lambda_1, \lambda_2)[D_2(\lambda_1, \lambda_2)]^{\alpha\beta} = \frac{\delta_{\alpha_0\beta_0}}{\rho(\lambda_1-\lambda_2)\rho(\lambda_2-\lambda_1)\Lambda(\lambda_1)\Lambda(\lambda_2)} \times$$

$$\times \alpha_0 \quad \beta_0 \quad \beta_1 \quad \alpha_2 = \beta_2 \quad (I.97)$$

We can now formulate the main theorem of this chapter.

Theorem 2. *The density operator $D_N(\lambda_1, \dots, \lambda_N)$ is a solution of the functional equation*

$$A_N(\lambda_1, \dots, \lambda_N)[D_N(\lambda_1, \dots, \lambda_N)] = D_N(\lambda_1, \dots, \lambda_N + \lambda) \quad (I.98)$$

if λ_N is equal to one of the inhomogeneities, i.e. $\lambda_N \in \{u_i\}_{i=1}^L$.

Proof. The proof can be found in Appendix B. □

4.2 Properties of the reduced density matrix

Some comments regarding the homogeneous limit are in order. For distinct inhomogeneities (I.98) consists of L independent equations, one for each inhomogeneity. Taking the homogeneous limit $u_i \rightarrow 0$ it seems as if those equations degenerate to a single one. However, let us assume $u_1 = 0$ and consider the difference of the functional equations at $\lambda_N = u_2$ and $\lambda_N = 0$. To increase readability we suppress the spectral parameters λ_1 to λ_{N-1} . After a division by u_2 one obtains:

$$\frac{A_N(u_2)[D_N(u_2)] - A_N(0)[D_N(0)]}{u_2} = \frac{D_N(u_2 + \lambda) - D_N(0 + \lambda)}{u_2}. \quad (\text{I.99})$$

Taking the limit $u_2 \rightarrow 0$ yields the derivative of the functional equation (I.98) with respect to the last argument. Repeating this procedure with all inhomogeneities that are still left we find that the equation is also valid for its first $L - 1$ derivatives.

Another very useful relation follows immediately from Eq. (I.12). Notice, that the operator $W_i(\lambda)$ degenerates to a Kronecker δ due to the initial condition (I.8) and crossing symmetry (I.7).

Theorem 3. *The density operator $D_N(\lambda_1, \dots, \lambda_N)$ fulfils the reduction relation*

$$\begin{aligned} \langle \boldsymbol{\alpha} | W_N(\lambda) \cdot D_N(\lambda_1, \dots, u, u + \lambda) | \boldsymbol{\beta} \rangle &= \delta_{\alpha_N \alpha_{N-2}} \delta_{\beta_N \beta_{N-2}} \times \\ &\times \langle \alpha_0 \dots \alpha_{N-2} | D_{N-2}(\lambda_1, \dots, \lambda_{N-2}) | \beta_0 \dots \beta_{N-2} \rangle \frac{\prod_{i=1}^L \rho(u - u_i) \rho(u_i - u)}{\Lambda(u) \Lambda(u + \lambda)} \end{aligned} \quad (\text{I.100})$$

for arbitrary values of u . Although not explicitly written, it is understood that the right-hand side is zero whenever the sequence $(\alpha_{N-2} \alpha_{N-1} \alpha_N)$ or $(\beta_{N-2} \beta_{N-1} \beta_N)$ is not allowed by the adjacency condition.

Proof. The proof is shown in Appendix C. □

Clearly for $u = u_j$ the scalar factor on the right cancels due to the inversion relation (I.14). However, this equation is valid for any value of u and will be prove to be very useful in the following section. A similar reduction relation was found in [67] relating two polynomial solutions of the level-one qKZ equations.

Part II

Applications

1 Models of SOS type

In this section we will use the functional equation (I.98) to compute the density matrices of face models of solid-on-solid (SOS) type and the related anyon chains. In particular, we will present results for the two- and three-point functions of Fibonacci anyons. We will closely follow the presentation in [62].

This class of face models has been introduced by Andrews, Baxter and Forrester as an auxiliary tool to solve the 8-vertex model [5–7, 38]. Based on this, *face-vertex correspondence* has been formalised [68] and been applied to a variety of models.

Here we shall not go deeper into this subject but apply our results to two critical models with a finite set \mathfrak{S} of height variables that have already been studied in earlier sections, i.e. the cyclic solid-on-solid (CSOS) model [57] and the restricted solid-on solid (RSOS) model [38].

1.1 The cyclic solid-on-solid models

As discussed in Section I.3.2 the height variables of the CSOS model take integer values $0 \leq a \leq r - 1$ for a positive integer r . Heights on adjacent sites are required to differ by ± 1 modulo r . As shown in Section I.3.2 the weights of the model can be embedded in a dynamical R -matrix. Here we will not assume this additional algebraic structure and start directly from the Boltzmann weights. Note that the weights appearing in the (critical limit of the) dynamical R -matrix (I.72) differ from those given below by a dynamical gauge transformation. The Boltzmann weights of the critical CSOS model are (heights in the arguments of W are taken modulo r)

$$\begin{aligned}
 \alpha_a &= W \left(\begin{array}{cc|c} a-1 & a & u \\ a & a+1 & \end{array} \right) = W \left(\begin{array}{cc|c} a+1 & a & u \\ a & a-1 & \end{array} \right) = \frac{\sin(\lambda - u)}{\sin \lambda}, \\
 \beta_a^\pm &= W \left(\begin{array}{cc|c} a & a \pm 1 & u \\ a \mp 1 & a & \end{array} \right) = \frac{\sin u}{\sin \lambda}, \\
 \gamma_a &= W \left(\begin{array}{cc|c} a & a+1 & u \\ a+1 & a & \end{array} \right) = 1, \\
 \delta_a &= W \left(\begin{array}{cc|c} a & a-1 & u \\ a-1 & a & \end{array} \right) = 1.
 \end{aligned} \tag{II.1}$$

Here the crossing parameter is $\lambda = \pi m/r$ where $1 \leq m \leq r - 1$ is coprime to r . In the general (non-critical) case the Boltzmann weights are given by elliptic functions and also explicitly depend on the height variable a . Interestingly the weights (II.1) coincide with the non-zero vertex weights in the R -matrix of the six-vertex model. In fact, this relation has been used extensively, e.g. to identify the operator content of the low energy

1 Models of SOS type

effective theory of the lattice model in the thermodynamic limit [69]. Furthermore, and unlike most other face models, the transfer matrix of the CSOS model has a simple eigenstate which enables a solution by means of the algebraic Bethe ansatz method based on the R -matrix (I.72) depending on a dynamical parameter related to the height variables. This property has already been used to compute form factors in the basis of Bethe eigenstates of this model [56].

Here we will utilise the existence of a particularly simple eigenstate of the CSOS transfer matrix to illustrate the approach to compute correlation functions based on the functional equation (I.98). To be specific we choose the CSOS model with $r = 3$ and crossing parameter $\lambda = 2\pi/3$. Considering a lattice of length $L = 3k$ with integer k it is easy to verify that

$$|\Omega\rangle \equiv \frac{1}{\sqrt{3}} (|012\ 012\ \dots\ 0\rangle + |120\ 120\ \dots\ 1\rangle + |201\ 201\ \dots\ 2\rangle) \in \mathcal{H}_{\text{per}}^L \quad (\text{II.2})$$

is an eigenstate of the transfer matrix with eigenvalue

$$\Lambda_0(u) = a(u) + d(u) \quad (\text{II.3})$$

where

$$a(u) \equiv \prod_{i=1}^L \frac{\sin(\lambda - (u - u_i))}{\sin \lambda}, \quad d(u) \equiv \prod_{i=1}^L \frac{\sin(u - u_i)}{\sin \lambda}. \quad (\text{II.4})$$

The definition of the Boltzmann weights immediately yields the action of the single row operators (I.84) on this state:

$$\begin{aligned} T_{\alpha+1\alpha+1}^{\alpha\alpha}(u)|\Omega\rangle &= \frac{a(u)}{\sqrt{3}} |\alpha\ \alpha + 1\ \alpha + 2\ \alpha \dots \alpha\rangle, \\ T_{\alpha-1\alpha-1}^{\alpha\alpha}(u)|\Omega\rangle &= \frac{d(u)}{\sqrt{3}} |\alpha\ \alpha - 1\ \alpha - 2\ \alpha \dots \alpha\rangle. \end{aligned} \quad (\text{II.5})$$

This allows to analyse the density matrices D_N in the state (II.2). The simplest case is $N = 1$ where periodic boundary conditions imply that $\alpha_0 = \beta_0$ and $\alpha_1 = \beta_1$. As a consequence, $D_1(\lambda)$ is a diagonal operator on \mathcal{V}^1 whose diagonal elements can be read off directly from Eqs. (II.5), e.g.

$$\langle 01|D_1^{(\Omega)}(\lambda)|01\rangle = \frac{1}{\sqrt{3}} \tilde{a}(\lambda), \quad \langle 02|D_1^{(\Omega)}(\lambda)|02\rangle = \frac{1}{\sqrt{3}} \tilde{d}(\lambda), \quad (\text{II.6})$$

where $\tilde{a}(u) = a(u)/(\sqrt{3} \Lambda_0(u))$ and analogously for \tilde{d} . Note that the trace condition $\text{tr}_{\mathcal{V}^1} D_1(\lambda) = 1$ implies $\tilde{d}(\lambda) = 1/\sqrt{3} - \tilde{a}(\lambda)$.

Similarly, the diagonal elements of the two-site density matrix $D_2(\lambda_1, \lambda_2)$ in the

reference state are obtained from (II.5). The functional equation (I.98) allows for the direct computation of all off-diagonal elements: choosing

$$\{|010\rangle, |012\rangle, |020\rangle, |021\rangle\} \cup \{|121\rangle, |120\rangle, |101\rangle, |102\rangle\} \cup \{|202\rangle, |201\rangle, |212\rangle, |210\rangle\} \quad (\text{II.7})$$

as a basis for the auxiliary space \mathcal{V}^2 and using the fact that the Boltzmann weights are invariant under the shift of all heights by an integer, we find that the density matrix has a structure of three identical 4×4 blocks $D_2^{(\Omega)}(\lambda_1, \lambda_2)$. Restricting ourselves to the first of these blocks we find for the reference state (II.2)

$$D_2^{(\Omega)}(\lambda_1, \lambda_2) = \begin{pmatrix} \tilde{a}(\lambda_1)\tilde{d}(\lambda_2) & 0 & g(\lambda_1, \lambda_2) & 0 \\ 0 & \tilde{a}(\lambda_1)\tilde{a}(\lambda_2) & 0 & 0 \\ 0 & 0 & \tilde{a}(\lambda_2)\tilde{d}(\lambda_1) & 0 \\ 0 & 0 & 0 & \tilde{d}(\lambda_1)\tilde{d}(\lambda_2) \end{pmatrix} \quad (\text{II.8})$$

or, using the notation introduced in Eq. (I.93),

$$\begin{aligned} D_2^{(\Omega)[0,0]}(\lambda_1, \lambda_2) &= \begin{pmatrix} \tilde{a}(\lambda_1)\tilde{d}(\lambda_2) & g(\lambda_1, \lambda_2) \\ 0 & \tilde{a}(\lambda_2)\tilde{d}(\lambda_1) \end{pmatrix}, \\ D_2^{(\Omega)[0,1]}(\lambda_1, \lambda_2) &= \tilde{d}(\lambda_1)\tilde{d}(\lambda_2), \quad D_2^{(\Omega)[0,2]}(\lambda_1, \lambda_2) = \tilde{a}(\lambda_1)\tilde{a}(\lambda_2). \end{aligned} \quad (\text{II.9})$$

With this ansatz we obtain from the functional equations (I.98) and (I.96) after some algebra an explicit expression for the off-diagonal element ($\lambda_{k\ell} \equiv \lambda_k - \lambda_\ell$)

$$g(\lambda_1, \lambda_2) = -\frac{\sqrt{3}}{2 \sin(\lambda_{12})} \left(\tilde{d}(\lambda_1)\tilde{a}(\lambda_2) - \tilde{a}(\lambda_1)\tilde{d}(\lambda_2) \right). \quad (\text{II.10})$$

Hence, as a consequence of the simple form of the reference state (II.2) of the $r = 3$ CSOS model, the two-site density matrix is completely determined by the one-point function $\tilde{a}(\lambda)$. This is also true for the three-site density matrix $D_3^{(\Omega)}(\{\lambda_1, \lambda_2, \lambda_3\})$. Choosing the bases

$$[0, 0] : |0120\rangle, |0210\rangle, \quad [0, 1] : |0101\rangle, |0121\rangle, |0201\rangle, \quad [0, 2] : |0102\rangle, |0202\rangle, |0212\rangle$$

1 Models of SOS type

for the $[0, a]$ -blocks in the auxiliary space \mathcal{V}^3 we find:³

$$\begin{aligned}
D_3^{(\Omega)[0,0]}(\{\lambda_j\}) &= \sqrt{3} \begin{pmatrix} \tilde{a}(\lambda_1)\tilde{a}(\lambda_2)\tilde{a}(\lambda_3) & 0 \\ 0 & \tilde{d}(\lambda_1)\tilde{d}(\lambda_2)\tilde{d}(\lambda_3) \end{pmatrix}, \\
D_3^{(\Omega)[0,1]}(\{\lambda_j\}) &= \sqrt{3} \begin{pmatrix} \tilde{a}(\lambda_1)\tilde{d}(\lambda_2)\tilde{a}(\lambda_3) & 0 & -\tilde{a}(\lambda_3)g(\lambda_1, \lambda_2) \\ -\tilde{a}(\lambda_1)g(\lambda_2, \lambda_3) & \tilde{a}(\lambda_1)\tilde{a}(\lambda_2)\tilde{d}(\lambda_3) & \star \\ 0 & 0 & \tilde{a}(\lambda_1)\tilde{a}(\lambda_2)\tilde{a}(\lambda_3) \end{pmatrix}, \\
D_3^{(\Omega)[0,2]}(\{\lambda_j\}) &= \sqrt{3} \begin{pmatrix} \tilde{a}(\lambda_1)\tilde{d}(\lambda_2)\tilde{d}(\lambda_3) & -\tilde{d}(\lambda_1)g(\lambda_1, \lambda_2) & \star\star \\ 0 & \tilde{d}(\lambda_1)\tilde{a}(\lambda_2)\tilde{d}(\lambda_3) & -\tilde{d}(\lambda_1)g(\lambda_2, \lambda_3) \\ 0 & 0 & \tilde{d}(\lambda_1)\tilde{d}(\lambda_2)\tilde{a}(\lambda_3) \end{pmatrix},
\end{aligned} \tag{II.11}$$

with

$$\begin{aligned}
\star &= -\frac{\cos(\frac{\pi}{6} - \lambda_{12})\tilde{a}(\lambda_2)g(\lambda_1, \lambda_3)}{\sin \lambda_{12}} - \frac{\sqrt{3}\tilde{a}(\lambda_1)g(\lambda_2, \lambda_3)}{2 \sin \lambda_{12}}, \\
\star\star &= \frac{\cos(\frac{\pi}{6} - \lambda_{12})\tilde{d}(\lambda_2)g(\lambda_1, \lambda_3)}{\sin \lambda_{12}} - \frac{\sqrt{3}\tilde{d}(\lambda_1)g(\lambda_2, \lambda_3)}{2 \sin \lambda_{12}}.
\end{aligned}$$

This suffices for the calculation of the nearest and next-nearest neighbour correlation functions in the reference state (II.2). In the homogeneous limit (i.e. all inhomogeneities $u_k = 0$) we have $\tilde{a}(0) = 1/\sqrt{3}$, $\tilde{d}(0) = 0$, and $g(0, 0) = 0$. Therefore, the two and three-site density matrices for $\lambda_i = 0$ are diagonal with non-zero elements

$$\begin{aligned}
\langle 012 | D_2^{(\Omega)}(0, 0) | 012 \rangle &= \langle 120 | D_2^{(\Omega)}(0, 0) | 120 \rangle = \langle 201 | D_2^{(\Omega)}(0, 0) | 201 \rangle = \frac{1}{3}, \\
\langle 0120 | D_3^{(\Omega)}(0, 0, 0) | 0120 \rangle &= \langle 1201 | D_3^{(\Omega)}(0, 0, 0) | 1201 \rangle = \langle 2012 | D_3^{(\Omega)}(0, 0, 0) | 2012 \rangle = \frac{1}{3}.
\end{aligned} \tag{II.12}$$

With Eq. (I.94) this yields the expected results for the two- and three-point functions in the reference state $|\Omega\rangle$ of the $r = 3$ CSOS model.

1.2 The restricted solid-on-solid models

The RSOS model introduced in Section I.1.4 can be treated in a similar way. Note that the state space is obtained by removing 0 from the set of heights allowed in the CSOS model. To increase readability, we repeat here the Boltzmann weights of the critical RSOS model:

$$W \left(\begin{array}{cc|c} a & b & u \\ c & d & \end{array} \right) = \delta_{ad} \sqrt{\frac{g_b g_c}{g_a g_d}} \rho(u + \lambda) - \delta_{bc} \rho(u) \tag{II.13}$$

³The coefficients in (II.11) are obtained using a combination of the functional equations (I.98) and (I.96) and the algorithm for the calculation of the structure functions in the factorised form of the N -site density matrices described below.

with

$$\rho(u) = \frac{\sin(u - \lambda)}{\sin \lambda}, \quad g_x = \frac{\sin(\lambda x)}{\sin \lambda} \quad (\text{II.14})$$

and a crossing parameter $\lambda = \pi/r$. Recall that the crossing relation (I.7) is modified to

$$W \left(\begin{array}{cc|c} a & b & u \\ c & d & \end{array} \right) = \sqrt{\frac{g_b g_c}{g_a g_d}} W \left(\begin{array}{cc|c} b & d & \lambda - u \\ a & c & \end{array} \right). \quad (\text{II.15})$$

This modification has to be taken into account whenever crossing symmetry is used, in particular in the definition of the A -operator in (I.97). To cancel the additional factors from the Boltzmann weight evaluated at $u = \lambda$ we have to rescale the corresponding weight giving the operator $P_- \in \text{End}(\mathcal{V}^1)$:

$$\langle \alpha_0 \alpha_1 \alpha_2 | P_- | \beta_0 \beta_1 \beta_2 \rangle = \alpha_1 \begin{array}{c} \alpha_0 = \beta_0 \\ \diamond \\ P_- \\ \alpha_2 = \beta_2 \end{array} \beta_1 \equiv \delta_{\alpha_0 \beta_0} \delta_{\alpha_2 \beta_2} \sqrt{\frac{g_{\alpha_0} g_{\alpha_2}}{g_{\alpha_1} g_{\beta_1}}} \alpha_1 \begin{array}{c} \alpha_0 \\ \diamond \\ \lambda \\ \alpha_2 \end{array} \beta_1. \quad (\text{II.16})$$

In addition, the third step of the proof in Appendix B needs to be reconsidered. Keeping track of the gauge factors we find that the A -operator needs to be multiplied by an additional factor of $\sqrt{g_{\beta_{N-1}}/g_{\alpha_{N-1}}}$.

As seen in Section I.1.4 the spectrum of the transfer matrix can be decomposed into topological sectors characterised by the topological quantum number j (see Eq. (I.40)). In addition, there is a discrete symmetry due to the invariance of the Boltzmann weights under a reflection of all heights, i.e. $a \rightarrow r - a$.⁴ This symmetry is passed on to the transfer matrix and the reduced density operators.

Starting with the single-site density matrix $D_1(\lambda_1)$ we observe that only its diagonal elements are allowed to be non-zero. We will now prove that $D_1(\lambda_1)$ is independent of the spectral parameter λ_1 in any eigenstate $|\Phi\rangle$ of the transfer matrix (although the matrix elements may still depend on the choice of inhomogeneities $\{u_i\}_{i=1}^L$): to compute $D_1^{[1,2]}(\lambda_1)$ we note that due to the adjacency condition

$$D_1^{[1,2]}(\lambda) = \langle 12 | D_1(\lambda) | 12 \rangle = \sum_{\alpha_1} \langle 1\alpha_1 | D_1(\lambda) | 1\alpha_1 \rangle = \frac{\langle \Phi | P_1^{(1)} t(\lambda) | \Phi \rangle}{\langle \Phi | \Phi \rangle \Lambda(\lambda)} = \frac{\langle \Phi | P_1^{(1)} | \Phi \rangle}{\langle \Phi | \Phi \rangle}, \quad (\text{II.17})$$

where we have used the definition of D_1 . Note that the one-site projection operators,

⁴Note that this reflection is an automorphism of the underlying fusion algebra $su(2)_{r-2}$ for odd r , see the discussion for $r = 5$ in Section I.2. This allows to restrict the possible topological quantum numbers in (I.40) to take integer values $j \in \{0, 1, \dots, (r-3)/2\}$.

1 Models of SOS type

defined as

$$\langle \mathbf{a} | P_\ell^{(\bar{a})} | \mathbf{b} \rangle = \delta_{a_\ell \bar{a}} \prod \delta_{a_j b_j}, \quad |\mathbf{a}\rangle, |\mathbf{b}\rangle \in \mathcal{H}^L, \quad (\text{II.18})$$

are independent of the spectral parameter. Hence, the 1-point function (II.17) is the local height probability for finding a spin $a = 1$ if $|\Phi\rangle = (\langle\Phi|)^\dagger$. With the same reasoning one concludes that $D_1^{[2,1]}(\lambda_1)$ and the reflected matrix elements are equal to (II.17). Following the same route we calculate

$$D_1^{[2,1]}(\lambda_1) + D_1^{[2,3]}(\lambda_1) = \sum_{\alpha_1} D_1^{[2,\alpha_1]}(\lambda_1) = \frac{\langle \Phi | P_1^{(2)} | \Phi \rangle}{\langle \Phi | \Phi \rangle}. \quad (\text{II.19})$$

Given that $D_1^{[2,1]}(\lambda_1)$ is constant we find that $D_1^{[2,3]}(\lambda_1)$ is also independent of λ_1 . Repeating this procedure we find that in fact all matrix elements are independent of the spectral parameter and given as sums of the local height probabilities. Generically, the latter depend on the state $|\Phi\rangle$ and the inhomogeneities. For the critical RSOS models considered here we find, however, that they are functions only of r and the local spin in the topological sectors with quantum dimension $d_q = 1$. Using the known values for the local height probabilities in the thermodynamic ground state of the homogeneous system [38] we find

$$D_1^{[a,a+1]}(\lambda) = \frac{\sin(\pi a/r) \sin(\pi(a+1)/r)}{r \cos(\pi/r)} \quad (\text{II.20})$$

for the non-zero elements of the single-site density matrix in these sectors. Note that the independence of the spectral parameter is a particular feature of the RSOS Hilbert space, cf. the λ_1 -dependent expressions for the CSOS case.

The $r = 4$ RSOS model. For the simplest nontrivial case, $r = 4$, the height variables take the values $1 \leq a \leq 3$. This model is equivalent to the Ising model via the mapping $a \rightarrow a - 2$ which results into height variables from $\{-1, 0, 1\}$. If we have $a_\ell = \pm 1$ at any site ℓ the adjacency condition enforces $a_{\ell'} = 0$ for any neighbouring site ℓ' . Hence, the lattice decomposes into two sublattices. On one of them all heights are 0 whereas on the second they are either 1 or -1 . Each elementary face of the lattice has two diagonally opposite corners with height 0 such that the interaction is effectively reduced to that of two Ising spins along the other diagonal.

From the considerations above we immediately get $D_1^{[\alpha,\beta]}(\lambda_1) = \langle \Phi | P_1^{(1)} | \Phi \rangle / \langle \Phi | \Phi \rangle$ for all states $|\alpha\beta\rangle \in \mathcal{V}^1$. Using the trace condition with $\dim \mathcal{V}^1 = 4$ it follows that

$$D_1(\lambda_1) = \frac{1}{4} \mathbb{1}, \quad (\text{II.21})$$

independent of the choice of inhomogeneities in agreement with Eq. (II.20).

For the two-site density matrix we consider the auxiliary space \mathcal{V}^2 with dimension six and we choose

$$\{|121\rangle, |123\rangle, |212\rangle, |232\rangle, |321\rangle, |323\rangle\} \quad (\text{II.22})$$

as a basis. Analogously to previous calculations we find

$$\langle 212 | D_2(\lambda_1, \lambda_2) | 212 \rangle = \sum_{\alpha_2} \langle 21\alpha_2 | D_2(\lambda_1, \lambda_2) | 21\alpha_2 \rangle = D_1^{[2,1]}(\lambda_1) = \frac{1}{4} \quad (\text{II.23})$$

and also, due to reflection symmetry, $\langle 232 | D_2(\lambda_1, \lambda_2) | 232 \rangle = 1/4$. Additionally, we have that

$$\sum_{\alpha_2} \langle 12\alpha_2 | D_2(\lambda_1, \lambda_2) | 12\alpha_2 \rangle = D_1^{[1,2]}(\lambda_1) = \frac{1}{4}. \quad (\text{II.24})$$

Hence, we find that the non-zero blocks in $D_2(\lambda_1, \lambda_2)$ are

$$\begin{aligned} D_2^{[1,1]}(\lambda_1, \lambda_2) &= \frac{1}{8} + \frac{1}{2}f(\lambda_1, \lambda_2), & D_2^{[1,3]}(\lambda_1, \lambda_2) &= \frac{1}{8} - \frac{1}{2}f(\lambda_1, \lambda_2), \\ D_2^{[2,2]}(\lambda_1, \lambda_2) &= \begin{pmatrix} \frac{1}{4} & g(\lambda_1, \lambda_2) \\ g(\lambda_1, \lambda_2) & \frac{1}{4} \end{pmatrix}, \end{aligned} \quad (\text{II.25})$$

$D_2^{[3,1]}$ and $D_2^{[3,3]}$ follow from height reflection $a_i \rightarrow r - a_i$. In general, the two functions f and g are independent. Evaluating equation (I.96) yields $f(u, v) = f(v, u)$ and $g(u, v) = g(v, u)$, i.e. the two site density operator for $r = 4$ is symmetric under exchange of the spectral parameters.

Taking (II.25) as an ansatz in the functional equation (I.98) we obtain $2L$ linear relations for the unknown functions f and g at $\lambda_2 \in \{u_1, u_2, \dots, u_L\}$:

$$\begin{aligned} \cos(2\lambda_{12}) f(\lambda_1, \lambda_2 + \lambda) + \sin(2\lambda_{12}) g(\lambda_1, \lambda_2) &= \frac{1}{4}, \\ \cos(2\lambda_{12}) g(\lambda_1, \lambda_2 + \lambda) + \sin(2\lambda_{12}) f(\lambda_1, \lambda_2) &= \frac{1}{4}. \end{aligned} \quad (\text{II.26})$$

For the actual computation of the density matrices we note that, as a consequence of (I.91,) the elements of $D_N(\lambda_1, \dots, \lambda_N) \prod_{k=1}^N \Lambda(\lambda_k)$ are Fourier polynomials in the spectral parameters λ_k . We have checked that, for small N and system sizes, the $(L+1)^N$ unknown Fourier coefficients can be determined uniquely for a given transfer matrix eigenvalue $\Lambda(u)$ using the discrete functional equations (II.26) for $N = 2$ and similarly (I.98) for general N once D_{N-1} is known (cf. the appearance of D_1 in the sum rules (II.23) and (II.24) for D_2).

This procedure is simplified if we consider density operators for eigenstates in sectors with quantum dimension $d_q(j) = 1$, i.e. topological quantum numbers $j \in \{0, 1\}$: Here we find that D_2 is determined by a single function of the spectral parameters

1 Models of SOS type

$f(\lambda_1, \lambda_2) \equiv g(\lambda_1, \lambda_2)$ such that the equations (II.26) for the elements of the two-site density matrix degenerate to a set of L equations. Another simplification in these sectors is found for spectral parameter $\lambda_2 \rightarrow i\infty$: In this limit the functions f and g vanish and $D_2(\lambda_1, \lambda_2)$ becomes the single-site density matrix $D_1(\lambda_1)$, written as an operator on \mathcal{V}^2 using the basis (II.22). In fact, we find that a similar reduction relating D_N for large λ_N to D_{N-1} for $N \geq 2$ holds in the topological sectors with quantum dimension $d_q = 1$ of the RSOS models where (recall that D_1 is independent of the spectral parameter and diagonal):⁵

$$\begin{aligned} & \lim_{\lambda_N \rightarrow i\infty} [D_N(\lambda_1, \dots, \lambda_N)]^{\alpha_0 \dots \alpha_N, \beta_0 \dots \beta_N} \\ &= [D_{N-1}(\lambda_1, \dots, \lambda_{N-1})]^{\alpha_0 \dots \alpha_{N-1}, \beta_0 \dots \beta_{N-1}} \frac{[D_1]^{\alpha_{N-1} \alpha_N, \beta_{N-1} \beta_N}}{\sum_{\alpha} [D_1]^{\alpha_{N-1} \alpha, \beta_{N-1} \alpha}}. \end{aligned} \quad (\text{II.27})$$

Using (I.96) one obtains expressions for D_N in the limit of large λ_k , $k < N$.

Hence, the asymptotics of the N -site density matrix is determined by the $(N-1)$ -site one, e.g. (recall that $f = g$ in these sectors)

$$\lim_{\lambda_3 \rightarrow i\infty} D_3(\lambda_1, \lambda_2, \lambda_3) = \frac{1}{8} \mathbb{1} + \frac{f(\lambda_1, \lambda_2)}{2} \begin{pmatrix} 1 & 0 & 0 & 0 & 0 & 0 & 0 & 0 \\ 0 & -1 & 0 & 0 & 0 & 0 & 0 & 0 \\ 0 & 0 & 0 & 1 & 0 & 0 & 0 & 0 \\ 0 & 0 & 1 & 0 & 0 & 0 & 0 & 0 \\ 0 & 0 & 0 & 0 & 0 & 1 & 0 & 0 \\ 0 & 0 & 0 & 0 & 1 & 0 & 0 & 0 \\ 0 & 0 & 0 & 0 & 0 & 0 & -1 & 0 \\ 0 & 0 & 0 & 0 & 0 & 0 & 0 & 1 \end{pmatrix} \quad (\text{II.28})$$

for the three-site density matrix of the $r = 4$ model in the basis

$$\{|1212\rangle, |1232\rangle\} \cup \{|2121\rangle, |2321\rangle\} \cup \{|2123\rangle, |2323\rangle\} \cup \{|3212\rangle, |3232\rangle\}$$

of \mathcal{V}^3 .

Remarkably, it has been shown that the density matrices of the Heisenberg spin chain can be written as

$$D_N(\lambda_1, \dots, \lambda_N) = \sum_{m=0}^{[N/2]} \sum_{I, J} \left(\prod_{p=1}^m \omega(\lambda_{i_p}, \lambda_{j_p}) \right) f_{N; I, J}(\lambda_1, \dots, \lambda_N) \quad (\text{II.29})$$

in terms of a nearest neighbour two-point function ω and a set of recursively defined

⁵A similar reduction has been found to be satisfied by the density matrices of the Heisenberg spin chain [30].

elementary functions $f_{N;I,J}$ of the spectral parameters λ_j , so-called ‘structure functions’ [23]. Here $I = (i_1, \dots, i_m)$ and $J = (j_1, \dots, j_m)$ such that $I \cap J = \emptyset$, $1 \leq i_p < j_p \leq N$ and $i_1 < \dots < i_m$.

For the density matrices in eigenstates from the topological sectors with quantum dimension $d_q(j) = 1$ ($j \in \{0, 1\}$ for the $r = 4$ RSOS model) we observe a similar behaviour: Looking for instance at the three-point density matrix and taking into account Eq. (II.29) we assume that the matrix elements of $D_3(\lambda_1, \lambda_2, \lambda_3)$ can be written as

$$\begin{aligned} f_0(\lambda_1, \lambda_2, \lambda_3) + f_{1,2}(\lambda_1, \lambda_2, \lambda_3) f(\lambda_1, \lambda_2) \\ + f_{2,3}(\lambda_1, \lambda_2, \lambda_3) f(\lambda_2, \lambda_3) + f_{1,3}(\lambda_1, \lambda_2, \lambda_3) f(\lambda_1, \lambda_3), \end{aligned} \quad (\text{II.30})$$

where f_0 and the $f_{I,J}$ are rational functions of $e^{2i\lambda_{12}}$ and $e^{2i\lambda_{23}}$ ($\lambda_{k\ell} \equiv \lambda_k - \lambda_\ell$), and $f(u, v)$ is the single function from (II.25) which determines the two-site density matrix in these topological sectors.

Most importantly, the model parameters such as the system size L and the inhomogeneities $\{u_k\}$ enter the expressions (II.29) only via the two-point function ω (or f in (II.30)). This fact can be used to implement an efficient algorithm⁶ for the numerical calculation of f_0 and $f_{I,J}$ in the ansatz (II.30) for the 3-site density matrix of the $r = 4$ RSOS model (or the structure functions $f_{N;I,J}$ appearing in an ansatz such as (II.29) for elements of the N -site density matrix D_N):

1. choose a set of spectral parameters $\Lambda = \{\lambda_1, \dots, \lambda_N\}$,
2. diagonalise the transfer matrix of a sufficiently small system with randomly chosen inhomogeneities,
3. pick an eigenstate of the transfer matrix (from the topological sector considered) and compute the generalised N -site density matrix $D_N(\lambda_1, \dots, \lambda_N)$ and the two-site density matrix $D_2(\lambda_j, \lambda_k)$ for pairs (λ_j, λ_k) from Λ using their definition (I.91),
4. compare D_2 to (II.25) to obtain numerical values for the corresponding two-point functions $f(\lambda_j, \lambda_k)$,
5. insert the data from steps 3 and 4 into (II.30) (resp. (II.29)) to get a linear equation relating the structure functions,
6. repeat steps 2 to 5 to build a system of linear equations which can be solved for the structure functions $f_{N;I,J}(\lambda_1, \dots, \lambda_N)$.

⁶A similar method has been used to compute expectation values of local operators for the spin-1/2 Heisenberg chain in a particular basis [70–72].

1 Models of SOS type

Once these functions are known for a range of spectral parameters it is straightforward to find analytical expressions, e.g. by Fourier analysis, which can be checked using (I.98). In practice it is helpful to keep one spectral parameter fixed and vary the differences λ_{ij} . Often one can guess the functional dependence on λ_{ij} by visually inspecting plots of the structure functions.

A slight complication in the present case of the $r = 4$ RSOS model is that the decomposition (II.30) is not unique. Evaluating the diagonal element $\underline{\alpha} = \underline{\beta} = (1, 2, 1, 2)$ of the functional equation (I.98) for $D_3(x, y, z)$ we find an additional relation satisfied by the two-point function f :

$$\sin(2\lambda_{12}) f(\lambda_1, \lambda_2) + \sin(2\lambda_{23}) f(\lambda_2, \lambda_3) - \sin(2\lambda_{13}) f(\lambda_1, \lambda_3) = 0. \quad (\text{II.31})$$

This identity holds for arbitrary values of λ_j , $j = 1, 2, 3$, as a consequence of $\alpha_2 = 1$ being a leaf node on the adjacency graph (c.f. the remark in Appendix B).

Hence, following the procedure outlined above we found the factorised form of the three-point density matrix $D_{N=3}$ of the $r = 4$ RSOS model. Remarkably, it turns out to be sufficient to compute the initial data for a system of length $L = 2 < N$. Moreover, we find that the structure functions are the same for all eigenstates $|\Phi\rangle$ of the transfer matrix in the topological sectors considered here. As a result we obtain

$$\begin{aligned} D_3^{[12]}(\lambda_1, \lambda_2, \lambda_3) &= \frac{1}{8} \mathbf{1} + \frac{1}{2 \sin(2\lambda_{23})} \begin{pmatrix} \sin(2\lambda_{23}) & -1 \\ 1 & -\sin(2\lambda_{23}) \end{pmatrix} f(\lambda_1, \lambda_2) \\ &\quad + \frac{\cos(2\lambda_{23})}{2 \sin(2\lambda_{23})} \begin{pmatrix} 0 & 1 \\ -1 & 0 \end{pmatrix} f(\lambda_1, \lambda_3) + \frac{1}{2} \begin{pmatrix} 0 & 1 \\ 1 & 0 \end{pmatrix} f(\lambda_2, \lambda_3), \\ D_3^{[21]}(\lambda_1, \lambda_2, \lambda_3) &= \frac{1}{8} \mathbf{1} + \frac{1}{2} \begin{pmatrix} 0 & 1 \\ 1 & 0 \end{pmatrix} f(\lambda_1, \lambda_2) + \frac{\cos(2\lambda_{12})}{2 \sin(2\lambda_{12})} \begin{pmatrix} 0 & 1 \\ -1 & 0 \end{pmatrix} f(\lambda_1, \lambda_3) \\ &\quad + \frac{1}{2 \sin(2\lambda_{12})} \begin{pmatrix} \sin(2\lambda_{12}) & -1 \\ 1 & -\sin(2\lambda_{12}) \end{pmatrix} f(\lambda_2, \lambda_3). \end{aligned} \quad (\text{II.32})$$

As before the other non-zero blocks follow from the height reflection symmetry of the density matrix. These expressions are unique up to transformations based on Eq. (II.31).

Again, we can consider the homogeneous limit $u_k \equiv 0$ for $k = 1, \dots, L$, where the expectation values of N -point functions can be obtained from the density matrix

$$D_N(\lambda_1, \dots, \lambda_N)|_{\lambda_k \equiv 0} \quad (\text{II.33})$$

according to Eq. (I.94). In this case the one-point function $D_1(0)$ is already given by (II.21). In addition, $D_2(0, 0)$ is completely fixed by the two-point function $f(0, 0)$.

For the computation of $D_3(0, 0, 0)$ the singularities for $\lambda_1 = \lambda_2$ and $\lambda_2 = \lambda_3$ in

Eq. (II.32) have to be taken care of. We expand the two-point function as

$$f(\lambda_1, \lambda_2) \simeq (0, 0) + (1, 0)\lambda_1 + (0, 1)\lambda_2 + \frac{1}{2} \left((2, 0)\lambda_1^2 + 2(1, 1)\lambda_1\lambda_2 + (0, 2)\lambda_2^2 \right) + \dots \quad (\text{II.34})$$

with $(k, \ell) \equiv \partial_1^k \partial_2^\ell f(\lambda_1, \lambda_2)|_{\lambda_1=\lambda_2=0}$. Note that $(k, \ell) = (\ell, k)$ due to the symmetry of $f(\lambda_1, \lambda_2)$. Additional relations between the coefficients of the $r = 4$ two-point function follow from the identity (II.31), e.g. $(2, 0) - 2(1, 1) = 4(0, 0)$. As a result, the singularities are removed and the homogeneous limit of D_3 is found to be

$$\begin{aligned} D_3^{[12]}(0, 0, 0) &= \frac{1}{8} \mathbf{1} + \frac{1}{2} \begin{pmatrix} (0, 0) & (0, 0) - \frac{(1, 0)}{2} \\ (0, 0) + \frac{(1, 0)}{2} & -(0, 0) \end{pmatrix} \\ D_3^{[21]}(0, 0, 0) &= \frac{1}{8} \mathbf{1} + \frac{1}{2} \begin{pmatrix} (0, 0) & (0, 0) + \frac{(1, 0)}{2} \\ (0, 0) - \frac{(1, 0)}{2} & -(0, 0) \end{pmatrix}. \end{aligned} \quad (\text{II.35})$$

Note that all other matrix elements can be obtained by height reflection symmetry. As a consequence the two- and three-point correlations in a transfer matrix eigenstate $|\Phi\rangle$ from the topological sectors with $d_q = 1$ of the homogeneous $r = 4$ RSOS model are given in terms of $(0, 0)$, i.e. the numerical value of the two-point function at spectral parameters $\lambda_1 = \lambda_2 = 0$, alone. The latter is directly related to the corresponding eigenvalue of the RSOS Hamiltonian $H = J \partial_u \ln t(u)|_{u=0}$, i.e.

$$E_\Phi = 4J L f(0, 0). \quad (\text{II.36})$$

Hence, explicit expressions for two- and three-point functions in the ground states of the infinite system can be obtained from Eqs. (II.25) and (II.35) using the known results for the energy density of the RSOS model in the thermodynamic limit [73]. We find

$$f(0, 0) = \pm \frac{1}{2\pi} \quad (\text{II.37})$$

for the ground state of the RSOS Hamiltonian with $J = -1$ (+1).

Until now the reduction relation (I.100) has not been used. Keeping in mind the additional gauge factors appearing in the crossing relation (II.15) we can use the factorised form of D_3 from (II.32) and plug it into (I.100).

In general, the product $\Lambda(u)\Lambda(u + \lambda)$ is difficult to compute. However, for $r = 4$ it can be computed explicitly using results for the Ising model [74] (to which the $r = 4$ RSOS model can be mapped):

$$\Lambda(u)\Lambda(u + \lambda) = \prod_{i=1}^L \rho(u - u_i)\rho(u_i - u) + y \prod_{i=1}^L \rho(u + \lambda - u_i)\rho(u_i - u - \lambda), \quad (\text{II.38})$$

1 Models of SOS type

where $y \in \{\pm 1\}$ is the eigenvalue of the height reflection operator Y which maps all heights $a \rightarrow r - a$. As discussed earlier, the transfer matrix commutes with Y such that to each eigenstate a unique value of y is assigned. Numerical investigations for small system sizes lead to the conjecture that for chain lengths $L = 4k$ the ground state has $y = 1$, while for $L = 4k - 2$ we find $y = -1$. In the following we will only discuss $y = 1$, the $y = -1$ case can be handled analogously.

Using the factorised form of $D_3(x, u, u + \lambda)$ (II.32) the reduction relation (I.100) yields equations for the function $f(x, u)$ valid for arbitrary spectral parameters. Since $D_1(u) = \frac{1}{4}\mathbb{1}$ is explicitly known, we can use (II.38) to find an explicit expression for the right-hand side. In particular this yields the difference equation:

$$\sin(2(x - u))f(x, u) + \cos(2(x - u))f(x, u + \lambda) = r(u), \quad (\text{II.39})$$

where the right-hand side reads

$$r(u) = \frac{1}{2 + 2y \prod_{i=1}^L \frac{\rho(u+\lambda-u_i)\rho(u_i-u-\lambda)}{\rho(u-u_i)\rho(u_i-u)}} - \frac{1}{4}. \quad (\text{II.40})$$

From now on we will work in the homogeneous limit $u_i \rightarrow 0$. In this case the expression simplifies to

$$r(u) = \frac{1}{2(1 + y \tan(2u)^L)} - \frac{1}{4}. \quad (\text{II.41})$$

In addition, Eq. (I.100) yields an explicit expression for $f(u, u + \lambda)$:

$$f(u, u + \lambda) = \frac{1}{2(1 + y \tan(2u)^L)} - \frac{1}{4}. \quad (\text{II.42})$$

Note that in contrast to the discrete functional equations (II.26) which are valid only at a finite set of points, Eq. (II.39) holds for arbitrary spectral parameters x and u . This functional equation for $r = 4$ case is special compared to the $r = 5$ case. For $r = 4$ the two-point function f fulfils an additional identity (II.31) which can also be deduced from the reduction relation (I.100). This information is the key to generate the continuous functional equation. Besides, for other values of r an explicit expression for $\Lambda(u)\Lambda(u + \lambda)$ is not known. We will now use these equations to explicitly calculate f for arbitrary chain lengths.

To solve (II.39) we define $h(x, u) = \sin(2(x - u))f(x, u)$ and often suppress x in the argument, i.e simply write $h(u)$. Since $\lambda = \pi/4$, we arrive at

$$h(u) - h(u + \lambda) = r(u). \quad (\text{II.43})$$

Before we start with the solution of this equation, let us look at the function $h(x, u)$ with

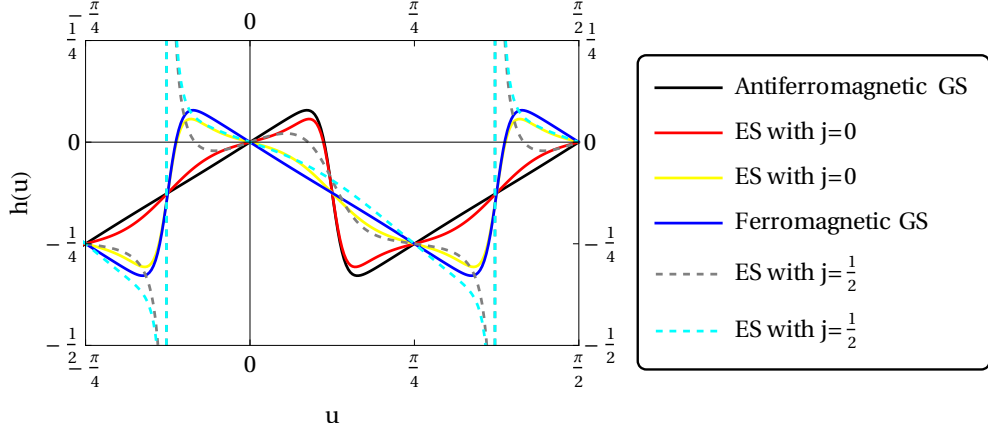


Figure 2: The function $h(u)$ is plotted for different states at chain length $L = 8$. One can see that the (anti-)ferromagnetic ground state (GS) resembles periodically repeating straight lines while the excited states (ES) from the $j = 0$ sector are periodically varying around them. Excited states from the $j = \frac{1}{2}$ sector (the dashed lines) display poles.

$x = 0$ in the homogeneous limit. From Fig. 2 we expect $h(u)$ in the (anti-)ferromagnetic ground state in the thermodynamic limit to consist of periodically repeated straight lines. We shall later show that this is indeed the case.

Note that in the thermodynamic limit $L \rightarrow \infty$

$$r(u) = \begin{cases} \frac{1}{4} & \text{for } u \in \left(-\frac{\pi}{8} + k\pi, \frac{\pi}{8} + k\pi\right) \text{ with } k \in \mathbb{Z}, \\ -\frac{1}{4} & \text{for } u \in \left(\frac{\pi}{8} + n\pi, \frac{3\pi}{8} + n\pi\right] \text{ with } n \in \mathbb{Z}. \end{cases} \quad (\text{II.44})$$

Furthermore, from (II.42) we deduce $h(0, \lambda) = -\frac{1}{4}$ and employing the periodicity of h we get $h(0, \lambda + n\pi) = -\frac{1}{4}$, which serves as a boundary condition for the solution of the functional equation. Also note that $r(u)$ agrees with the right-hand side of the discrete functional equation (II.26) in a finite range around $u = 0$. This is expected since for a chain length L Eq. (I.98) also holds for the first $L - 1$ derivatives. Performing the thermodynamic limit $L \rightarrow \infty$ we conclude that the functional equation fixes all derivatives at the origin and assuming h to be analytic at $(0, 0)$ therefore also in a (small) neighbourhood.

It is easy to see that one solution of (II.43) in the thermodynamic limit is given by

$$h(x, u) = \frac{x - u}{\pi} \text{ for } (x - u) \in \left(-\frac{\pi}{8}, \frac{3\pi}{8}\right). \quad (\text{II.45})$$

Note that it is a function of $(x - u)$ and it suffices to fix its values in the given interval since it is π -periodic. Hence, we can calculate $f(0, 0) = \frac{1}{2\pi}$ in agreement with the result for the ferromagnetic ground state in Eq. (II.37).

1 Models of SOS type

Another simple solution is

$$h(x, u) = \frac{u - x}{\pi} \text{ for } (x - u) \in \left(-\frac{3\pi}{8}, \frac{\pi}{8}\right). \quad (\text{II.46})$$

This solution corresponds to the antiferromagnetic ground state yielding $f(0, 0) = -\frac{1}{2\pi}$.

Let us compare the result for the thermodynamic limit with the finite size results. Therefore we plot the function $h(0, u)$ computed from the exact finite size density operators together with the result from (II.45)

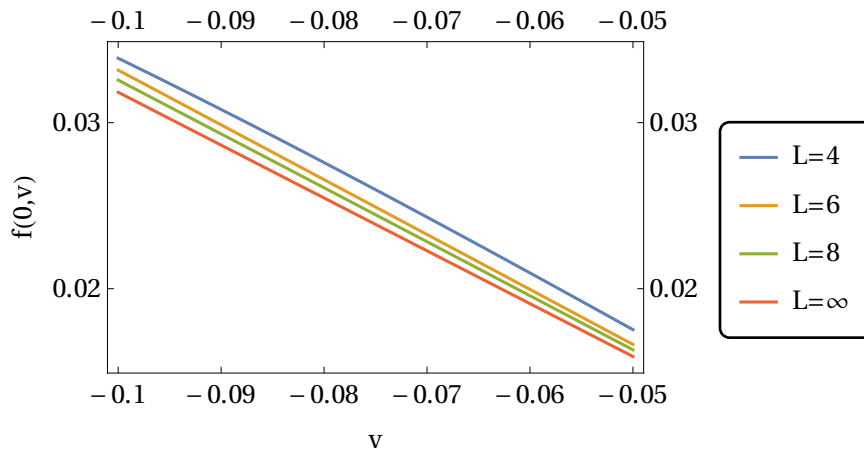


Figure 3: Plots of the function $h(0, u)$ for chain lengths of $L = 4, 6$ and $L = 8$ as well as the result obtained in the thermodynamic limit for the ferromagnetic ground state. Even for small system sizes we see a quick convergence. We chose a very small interval for v to resolve the small differences between the functions.

Now let us solve the functional equation for finite chain lengths L . Defining $a(z) = h(iz + \frac{\lambda}{2})$ and $b(z) = r(iz)$ the functional equation is transformed to

$$a\left(z + i\frac{\lambda}{2}\right) - a\left(z - i\frac{\lambda}{2}\right) = b(z) \quad (\text{II.47})$$

and can be solved by Fourier methods. Numerical investigations for small L reveal that $a(z)$ tends to a non-zero constant for $z \rightarrow \pm\infty$ such that we have to differentiate in order to calculate the Fourier transform.

We define the Fourier transforms

$$\begin{aligned} A(k + i\epsilon) &= \frac{1}{2\pi} \int_{-\infty}^{\infty} dz a'(z) e^{-iz(k+i\epsilon)}, \\ B(k + i\epsilon) &= \frac{1}{2\pi} \int_{-\infty}^{\infty} dz b'(z) e^{-iz(k+i\epsilon)}, \end{aligned} \quad (\text{II.48})$$

where we introduced a small parameter $\epsilon > 0$ which will remove poles from the integration

contour. The inverse transformation yields

$$\begin{aligned} a'(z) &= \int_{-\infty}^{\infty} dk A(k+i\epsilon) e^{iz(k+i\epsilon)} \\ b'(z) &= \int_{-\infty}^{\infty} dk B(k+i\epsilon) e^{iz(k+i\epsilon)} \end{aligned} \quad (\text{II.49})$$

Here we assumed that $a(z)$ does not have poles in the strip $-\lambda/2 \leq \text{Im}(z) \leq \lambda/2$, which is true for the ferromagnetic ground state [48]. To find solutions for other states the integration contour needs to be changed appropriately.

Taking the Fourier transform of the derivative of Eq. (II.39) we obtain

$$A(k+i\epsilon) = -\frac{B(k+i\epsilon)}{2 \sinh\left(\frac{1}{8}\pi(k+i\epsilon)\right)}. \quad (\text{II.50})$$

Note that the shift by $i\epsilon$ will allow us to take the inverse Fourier transformation. Hence, we calculate

$$\begin{aligned} a'(z) &= -\int_{-\infty}^{\infty} dk e^{i(k+i\epsilon)z} \frac{B(k+i\epsilon)}{2 \sinh\left(\frac{\pi(k+i\epsilon)}{8}\right)} \\ &= -\int_{-\infty}^{\infty} dk \frac{e^{i(k+i\epsilon)z}}{2 \sinh\left(\frac{\pi(k+i\epsilon)}{8}\right)} \frac{1}{2\pi} \int_{-\infty}^{\infty} dy b'(y) e^{-i(k+i\epsilon)y} \\ &= -\int_{-\infty}^{\infty} dy b'(y) \int_{-\infty+i\epsilon}^{\infty+i\epsilon} dk' \frac{e^{ik'(z-y)}}{4\pi \sinh\left(\frac{\pi k'}{8}\right)} \text{ with } k' = k+i\epsilon, \end{aligned} \quad (\text{II.51})$$

where we exchanged the order of integration in the last step. Defining the kernel

$$K(z) := -\int_{-\infty+i\epsilon}^{\infty+i\epsilon} dk \frac{e^{ikz}}{4\pi \sinh\left(\frac{\pi k}{8}\right)} \quad (\text{II.52})$$

we find

$$a'(z) = \int_{-\infty}^{\infty} dy b'(y) K(z-y) = (b' * K)(z). \quad (\text{II.53})$$

where $*$ denotes the convolution.

Fortunately the kernel can be calculated exactly. First, observe that $\sinh\left(\frac{\pi(k-8i)}{8}\right) = -\sinh\left(\frac{\pi k}{8}\right)$ leading to

$$K(z) + \int_{\infty+i\epsilon-8i}^{-\infty+i\epsilon-8i} dk \frac{e^{ikz}}{4\pi \sinh\left(\frac{\pi k}{8}\right)} = K(z)(1 + e^{8z}). \quad (\text{II.54})$$

On the other hand, the left-hand side of the previous equation is simply a closed contour

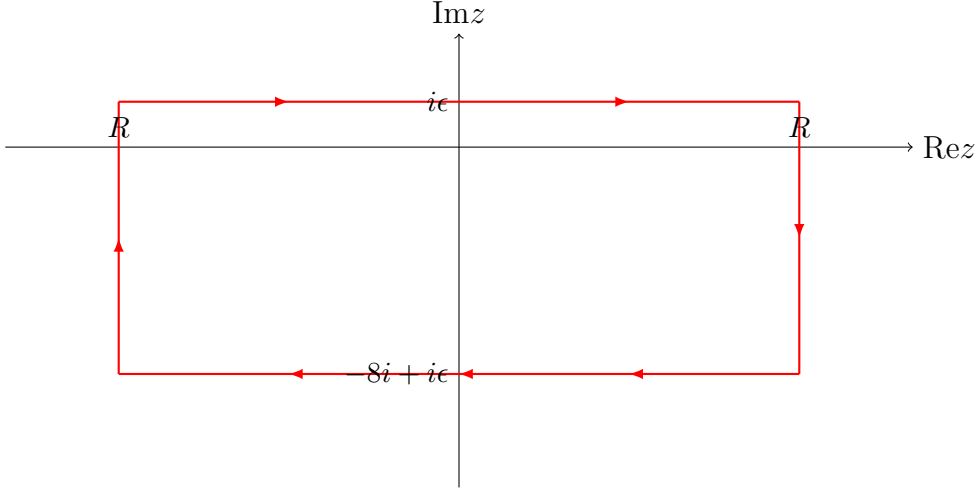


Figure 4: Graphical description of the contour \mathcal{C} .

integral along the contour \mathcal{C} from Fig. 4 enclosing the origin

$$\lim_{R \rightarrow \infty} \oint_{\mathcal{C}} dk \frac{e^{ikz}}{4\pi \sinh\left(\frac{\pi k}{8}\right)} = \left(\int_{-\infty+i\epsilon}^{\infty+i\epsilon} + \int_{\infty+i\epsilon-8i}^{-\infty+i\epsilon-8i} \right) dk \frac{e^{ikz}}{4\pi \sinh\left(\frac{\pi k}{8}\right)}, \quad (\text{II.55})$$

where we used that for $R \rightarrow \infty$ the two paths on the sides do not contribute.

Hence, we use the residue theorem to find

$$K(z)(1 + e^{8z}) = -i \text{Res}_{k=0} \frac{e^{ikz}}{2 \sinh\left(\frac{\pi k}{8}\right)} = -\frac{4i}{\pi} \quad (\text{II.56})$$

and solve for $K(z)$

$$K(z) = -\frac{4i}{\pi} \frac{1}{1 + e^{8z}}. \quad (\text{II.57})$$

To find $a(z)$ up to an x dependent constant $\psi(x)$ we use partial integration to shift the derivative to the kernel

$$\begin{aligned} a'(z) &= - \int_{-\infty}^{\infty} dy b(y) \frac{\partial}{\partial y} K(z-y) + \tilde{\psi}(x) \\ &= \int_{-\infty}^{\infty} dy b(y) \frac{\partial}{\partial z} K(z-y) + \tilde{\psi}(x) \end{aligned} \quad (\text{II.58})$$

resulting in

$$a(z) = \int_{-\infty}^{\infty} dy b(y) K(z-y) + \psi(x). \quad (\text{II.59})$$

Here x is the first spectral parameter of the function $h(x, z)$. Up to now we ignored the x dependence, since $b(z)$ is independent of it. Hence, the integration ‘constant’ $\psi(x)$, into which we absorbed the boundary term $\tilde{\psi}(x)$ from the partial integration, can

depend on x and will be determined below. Going back to the original functions we can use Eq. (II.42) to find $\psi(x)$. After simplifications we arrive at

$$h(x, u) = \frac{2}{\pi} \int_{-\infty}^{\infty} dy b(y) \frac{\sin(4(u-x))}{\sinh(4(y+iu)) \sinh(4(y+ix))}. \quad (\text{II.60})$$

Comparing this function with the numerical values from the exact D_2 operator for small system sizes, we find perfect agreement for $u \in (0, \lambda)$. In fact, the solution (II.60) is discontinuous at $u = 0, \lambda$ and one has to employ analytical continuation. Shifting the integration contour in (II.60) by $i\delta$ gives the solution on the interval $(-\delta, \lambda - \delta)$, i.e.

$$h(x, u) = \frac{2}{\pi} \int_{-\infty+i\delta}^{\infty+i\delta} dy b(y) \frac{\sin(4(u-x))}{\sinh(4(y+iu)) \sinh(4(y+ix))} \quad (\text{II.61})$$

for $u \in (-\delta, \lambda - \delta)$. We now prove that this defines indeed a solution to the original equation. Let $\delta > 0$ as well as $-\delta < u < 0$ and calculate

$$h(x, u) - h(x, u + \lambda) = \frac{2}{\pi} \left(\int_{-\infty+i\delta}^{\infty+i\delta} - \int_{-\infty}^{\infty} \right) dy b(y) \frac{\sin(4(u-x))}{\sinh(4(y+iu)) \sinh(4(y+ix))}. \quad (\text{II.62})$$

Similar as seen before this expression is a contour integral encircling a simple pole at $y = -iu$ (the left and right borders are pushed to infinity and do not contribute). By means of the residue theorem one shows that the right-hand side evaluates to $b(-iu) = r(u)$ which finishes the proof.

The solution (II.60) is very useful since it allows for a computation of correlation functions for an arbitrary system size L which enters only as a parameter in the integral. As an application, we show the deviation of $h(0, u)$ from the thermodynamic limit (II.45) for chain lengths $L = 40, 80$ and $L = 120$ in Fig. 5. Also note that the solution (II.60)

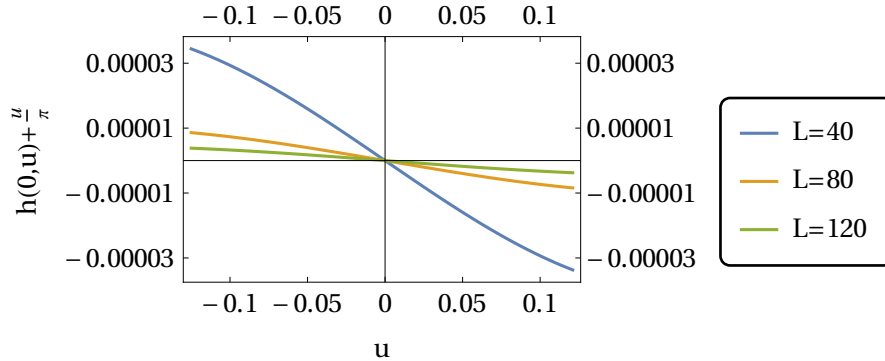


Figure 5: The differences between the finite size results for $h(0, u)$ and the thermodynamic limit $-\frac{u}{\pi}$ from Eq. (II.45)

together with (II.36) allows to calculate the finite size ground state energy for arbitrary

1 Models of SOS type

system sizes.

The $r = 5$ RSOS model. As a second example we consider the $r = 5$ RSOS model with local heights $1 \leq a \leq 4$. Analogously to the $r = 4$ RSOS model, we can compute the single site density matrix. In states from the sector with topological quantum number $j = 0$ (recall that the topological sectors in the odd r RSOS models are labelled by integers $0 \leq j \leq (r - 3)/2 = 1$) we find that the matrix elements are independent of the system size and the inhomogeneities $\{u_k\}$:

$$D_1^{[\alpha, \beta]}(\lambda) = \begin{cases} 1/(5 + \sqrt{5}) & \text{for } (\alpha\beta) \in \{(12), (21), (34), (43)\}, \\ \sqrt{5}/10 & \text{for } (\alpha\beta) \in \{(23), (32)\}, \end{cases} \quad (\text{II.63})$$

as given by Eq. (II.20).

The auxiliary space \mathcal{V}^2 for the two-site density matrix of the $r = 5$ model has dimension ten. Due to the adjacency condition the Hilbert space of states splits into two subspaces spanned by fusion paths with a_0 even and odd, respectively. The transfer matrix is a map between these two subspaces and hence, products of an even number of transfer matrices (or more general single row operators) will be block diagonal and may be written as the sum of an even and an odd part. According to this decomposition of the Hilbert space we choose the following basis for \mathcal{V}^2 :

$$\{|121\rangle, |123\rangle, |321\rangle, |323\rangle, |343\rangle\} \cup \{|212\rangle, |232\rangle, |234\rangle, |432\rangle, |434\rangle\}. \quad (\text{II.64})$$

The two sets are related by reflection $a_i \rightarrow r - a_i$ and hence, we may restrict ourselves to the subspace generated by the first. Again the structure of the density operator $D_2(\lambda_1, \lambda_2)$ is constrained by sum rules such as (II.23) and (II.24). We find the non-zero blocks of D_2 in the first subspace with odd a_0 to be (b is a constant)

$$\begin{aligned} D_2^{[1,1]}(\lambda_1, \lambda_2) &= -\frac{1}{2} + 4D_1^{[2,1]} + f(\lambda_1, \lambda_2), \\ D_2^{[1,3]}(\lambda_1, \lambda_2) &= D_2^{[3,1]}(\lambda_1, \lambda_2) = e(\lambda_1, \lambda_2), \\ D_2^{[3,3]}(\lambda_1, \lambda_2) &= \begin{pmatrix} d(\lambda_1, \lambda_2) & c_1(\lambda_1, \lambda_2) \\ c_2(\lambda_1, \lambda_2) & b \end{pmatrix}. \end{aligned} \quad (\text{II.65})$$

The sum rules immediately imply

$$e(\lambda_1, \lambda_2) = \frac{1}{2} - 3D_1^{[2,1]} - f(\lambda_1, \lambda_2), \quad b = D_1^{[2,1]}. \quad (\text{II.66})$$

Furthermore, the trace condition $\text{tr}_{\mathcal{V}^2} D_2(\lambda_1, \lambda_2) = 1$ yields

$$d(\lambda_1, \lambda_2) = f(\lambda_1, \lambda_2) + D_1^{[2,1]}. \quad (\text{II.67})$$

Using the relations (I.96) we find that the off-diagonal functions are related via

$$c_1(\lambda_1, \lambda_2) = c_2(\lambda_2, \lambda_1) \equiv (\sqrt{5} + 2)^{\frac{1}{2}} g(\lambda_1, \lambda_2) \quad (\text{II.68})$$

and

$$f(\lambda_1, \lambda_2) = \frac{g(\lambda_1, \lambda_2) + g(\lambda_2, \lambda_1)}{2} + \left(5 + 2\sqrt{5}\right)^{\frac{1}{2}} \cot \lambda_{12} \frac{g(\lambda_1, \lambda_2) - g(\lambda_2, \lambda_1)}{2}. \quad (\text{II.69})$$

Moreover, further simplifications are found for eigenstates of the transfer matrix in the $j = 0$ topological sector (where $b = 1/(5 + \sqrt{5})$ according to Eq. (II.63)): in this sector the off-diagonal elements of D_2 coincide, i.e. $g(\lambda_1, \lambda_2) = g(\lambda_2, \lambda_1)$, and therefore $g(\lambda_1, \lambda_2) = f(\lambda_1, \lambda_2)$. As a consequence D_2 can again be expressed in terms of a single scalar function $f(\lambda_1, \lambda_2)$ satisfying the functional equation

$$f(\lambda_1, \lambda_2 + \lambda) = \frac{\sqrt{5} - 2}{4(\cos(2\lambda_{12}) - \cos(2\lambda))} - \frac{\cos(2(\lambda_{12} - \lambda)) - \cos(2\lambda)}{\cos(2\lambda_{12}) - \cos(2\lambda)} f(\lambda_1, \lambda_2) \quad (\text{II.70})$$

for $\lambda_2 \in \{u_1, \dots, u_L\}$. Defining $\varphi(x) \equiv \cos(2x) - \cos(2\lambda)$ and setting $\chi(\lambda_1, \lambda_2) \equiv f(\lambda_1, \lambda_2)/\varphi(\lambda_{12})$ we can rewrite this equation as

$$\chi(\lambda_1, \lambda_2) + \chi(\lambda_1, \lambda_2 + \lambda) = \frac{\sqrt{5} - 2}{4\varphi(\lambda_{12})\varphi(\lambda_{12} - \lambda)}. \quad (\text{II.71})$$

As in the $r = 4$ RSOS model the density matrices D_N can be computed recursively for any given transfer matrix eigenvalue using their analytical properties and the functional equations. In particular, we find that the asymptotic behaviour of the N -site density matrices is related to the $N - 1$ -site one as given by (II.27), e.g.

$$\lim_{\lambda_2 \rightarrow i\infty} D_2^{(\text{odd}, \text{odd})}(\lambda_1, \lambda_2) = \frac{1}{2(\sqrt{5} + 5)} \begin{pmatrix} 3 - \sqrt{5} & 0 & 0 & 0 & 0 \\ 0 & \sqrt{5} - 1 & 0 & 0 & 0 \\ 0 & 0 & \sqrt{5} - 1 & 0 & 0 \\ 0 & 0 & 0 & 2 & 0 \\ 0 & 0 & 0 & 0 & 2 \end{pmatrix} \quad (\text{II.72})$$

in the topological sector with quantum dimension $d_q = 1$, i.e. $j = 0$ for the $r = 5$ RSOS model.

Similar as in (II.32) for $r = 4$ we were able to express the three-point density matrix of the $r = 5$ RSOS model in this topological sector as a sum of terms factorising into

1 Models of SOS type

spectral parameter dependent elementary functions and the two-point function $f(\lambda_1, \lambda_2)$ solving the functional equation (II.70). Proceeding as for $r = 4$ we find the factorisation of D_3 in the one-dimensional block corresponding to the sequence $\underline{\alpha} = (1234)$ of heights to be

$$\begin{aligned} D_3^{[14]}(\lambda_1, \lambda_2, \lambda_3) = & \frac{7}{4\sqrt{5}} - \frac{3}{4} - \frac{1}{4} \left(\sqrt{5} + 1 + (3\sqrt{5} - 5) \cot \lambda_{13} \cot \lambda_{23} \right) f(\lambda_1, \lambda_2) \\ & - \frac{1}{4} \left(\sqrt{5} + 1 + (3\sqrt{5} - 5) \cot \lambda_{12} \cot \lambda_{13} \right) f(\lambda_2, \lambda_3) \\ & - \frac{1}{4} \left(\sqrt{5} + 1 - (3\sqrt{5} - 5) \cot \lambda_{12} \cot \lambda_{23} \right) f(\lambda_1, \lambda_3). \end{aligned} \quad (\text{II.73})$$

We present the complete list of non-zero matrix elements of D_3 in Appendix D.

Now it is straightforward to calculate D_3 in the homogeneous limit. Expanding the two-point function as in Eq. (II.34) for the case $r = 4$ we find for the one-dimensional block considered above

$$D_3^{[14]}(0, 0, 0) = \frac{7}{4\sqrt{5}} - \frac{3}{4} - 2(0, 0) + \frac{1}{8} (3\sqrt{5} - 5) (2(1, 1) - (2, 0)). \quad (\text{II.74})$$

All other matrix elements may be computed using Appendix D.

1.3 Fibonacci anyons

As discussed in Section I.2 we can relate face models to one-dimensional quantum chains with anyonic degrees of freedom on each lattice site. Considering the Hamiltonian limit of the homogeneous RSOS model with $r = 5$, i.e. $u_i \equiv 0$ in (I.84), one obtains a model of Fibonacci anyons [14, 43]. Here we will use the functional equation (I.98) to compute the two-site density matrix for the chain of τ -anyons.

The Hilbert space of fusion paths for these anyons was shown to be isomorphic to the a_0 odd part of the RSOS Hilbert space $\mathcal{H}_{\text{per}}^L$ for $r = 5$ and we saw in Section I.2 that the Hamiltonian of the anyon chain

$$H = J \sum_{n=0}^{L-1} P_n^{(\tau\tau \rightarrow 1)} \quad (\text{II.75})$$

belongs the family of conserved quantities generated by the transfer matrix of the RSOS model (I.85) by means of the mapping from Eq. (I.57).

We will now use the solution of the inverse problem to relate the energies of the anyon model to the density operator of the homogeneous model. Note that in this case $t(0)$ is the translation operator with eigenvalues $\Lambda(0) = \exp(2\pi ik/L)$ for some integer k . Furthermore, we have $\rho(0) = -1$ for the RSOS model. Assuming that the eigenstates of the transfer matrix are normalised, that is $\langle \Phi | \Phi \rangle = 1$, the two-point function (I.94) is

given by

$$\langle \Phi | E_{\beta_0 \beta_1 \beta_2}^{\alpha_0 \alpha_1 \alpha_2} | \Phi \rangle = D_2(0, 0)^{\{\underline{\alpha}\}\{\underline{\beta}\}}. \quad (\text{II.76})$$

Translation invariance, i.e $[H, t(0)] = 0$, implies that the energy of an eigenstate $|\Phi\rangle$ is $E_\Phi = L J \langle \Phi | P_1^{(\tau\tau\rightarrow 1)} | \Phi \rangle$. As $P_1^{(\tau\tau\rightarrow 1)}$ depends only on the first three heights of the chain, we can directly apply (II.76) to obtain

$$E_\Phi = L J \text{tr}_{\mathcal{V}^2} \left(P_1^{(\tau\tau\rightarrow 1)} D_2(0, 0) \right), \quad (\text{II.77})$$

which relates the energy density of the anyon chain to certain correlators of the RSOS model.

Plugging the explicit expression of $P_1^{(\tau\tau\rightarrow 1)}$ into (II.77) and using the simplified form of the two-site density matrix (II.65) for eigenstates $|\Phi\rangle$ in the topological sector $j = 0$ of the $r = 5$ RSOS model⁷ we finally find

$$\frac{E_\Phi}{L} = \frac{J}{2} \left(\sqrt{5} + 5 \right) (0, 0) + \frac{J}{2} \left(3 - \sqrt{5} \right). \quad (\text{II.78})$$

For the $r = 4$ RSOS model the ground state energies of the anyon model in the thermodynamic limit are known [73] giving

$$(0, 0) = \begin{cases} -2 + \sqrt{5} + \frac{1}{3} \sqrt{\frac{5}{6}(25 - 11\sqrt{5})} & \text{for } J > 0 \\ \frac{1}{2} - \frac{1}{\sqrt{5}} & \text{for } J < 0 \end{cases} \quad (\text{II.79})$$

for the corresponding two-point functions $f(0, 0)$. Finally, we show how our results can be used for the computation of three-point functions. Therefore, we consider the operator $P^{(\tau\tau\tau\rightarrow 1)}$ (see Eq. (I.53)) which projects the fusion product of three consecutive τ -anyons to an anyon of type 1

$$\langle \mathbf{a} | P_i^{(\tau\tau\tau\rightarrow \ell)} | \mathbf{b} \rangle \equiv \left(\prod_{k \notin \{i, i+1\}} \delta_{a_k b_k} \right) \sum_x \left[\left(F_{a_{i+1}}^{b_{i-1}\tau\tau} \right)_x^{a_i} \left(F_{b_{i+2}}^{b_{i-1}x\tau} \right)_\ell^{a_{i+1}} \right]^* \left(F_{b_{i+2}}^{b_{i-1}x\tau} \right)_\ell^{b_{i+1}} \left(F_{b_{i+1}}^{b_{i-1}\tau\tau} \right)_x^{b_i} \quad (\text{II.80})$$

and find

$$\langle \Phi | P_1^{(\tau\tau\tau\rightarrow 1)} | \Phi \rangle = \sqrt{5} - 2 - 2 \left(\sqrt{5} + 5 \right) (0, 0) - \frac{5}{4} \left(\sqrt{5} - 1 \right) \left(2(1, 1) - (2, 0) \right). \quad (\text{II.81})$$

Thermodynamic limit of the $r = 5$ RSOS model Taking the thermodynamic limit, the discrete functional equation (II.71) of the homogeneous model is again valid in some non-empty neighbourhood around the origin. Hence, we can solve it for the

⁷This condition holds in particular for the ground states of the antiferromagnetic anyon chain ($J > 0$) with $L \bmod 3 = 0$ and the ferromagnetic model ($J < 0$).

1 Models of SOS type

ferromagnetic ground state (belonging to the $j = 0$ topological sector). From (II.72) we deduce $\lim_{\chi \rightarrow i\infty} g(u, v) = 0$. Having in mind the analytic properties of the eigenvalue [48], we set $a(u, z) := \chi(u, iz + \frac{\lambda}{2})$ and $b(u, z) := r(u, iz)$, $r(\lambda_1, \lambda_2)$ being the function on the right-hand side of Eq. (II.71). Note that $b(u, z)$ does not have poles for $z \in \mathbb{R}$ if $0 \neq u \in \mathbb{R}$. Moreover, one finds $\lim_{z \rightarrow \pm\infty} b(u, z) = 0$. This allows to take the Fourier transform of both sides of Eq. (II.71).

For the ferromagnetic groundstate $a(u, z)$ does not have any poles in the strip $-i\lambda/2 \leq \text{Im}(z) \leq i\lambda/2$. Therefore, the Fourier transforms

$$\begin{aligned} A(u, k) &= \frac{1}{2\pi} \int_{-\infty}^{\infty} dz a(u, z) e^{-ikz} \\ B(u, k) &= \frac{1}{2\pi} \int_{-\infty}^{\infty} dz b(u, z) e^{-ikz} \end{aligned} \quad (\text{II.82})$$

can be carried out similar to the $r = 4$ case leading to

$$A(u, k) = \frac{B(u, k)}{2 \cosh\left(\frac{\lambda}{2}k\right)}. \quad (\text{II.83})$$

Proceeding as in (II.51) we see that

$$a(u, z) = \int_{-\infty}^{\infty} dy b(u, y) K(z - y) \quad (\text{II.84})$$

with

$$K(z) = \int_{-\infty}^{\infty} dk \frac{e^{ikz}}{4\pi \cosh\left(\frac{\pi k}{10}\right)} \quad (\text{II.85})$$

The kernel K can be evaluated exactly. Note that it has a simple pole at $z = -5i$. Since $\cosh\left(\frac{\pi k}{10}\right) = -\cosh\left(\frac{\pi(k-10i)}{10}\right)$ we can proceed similar to Eqs. (II.54) and (II.55), i.e. we first observe that

$$K(z) + \int_{\infty-10i}^{-\infty-10i} dk \frac{e^{ikz}}{4\pi \cosh\left(\frac{\pi k}{10}\right)} = K(z)(1 + e^{10z}). \quad (\text{II.86})$$

The left-hand side of the previous equation is again a contour integral along the contour \mathcal{C} from Fig. 6

$$\lim_{R \rightarrow \infty} \oint_{\mathcal{C}} dk \frac{e^{ikz}}{4\pi \cosh\left(\frac{\pi k}{10}\right)} = \left(\int_{-\infty}^{\infty} + \int_{\infty-10i}^{-\infty-10i} \right) dk \frac{e^{ikz}}{4\pi \cosh\left(\frac{\pi k}{10}\right)}, \quad (\text{II.87})$$

where the left and right sides of the rectangle do not contribute for $R \rightarrow \infty$. Using the residue theorem we find

$$K(z) = \frac{5}{2\pi \sinh(5z)}. \quad (\text{II.88})$$

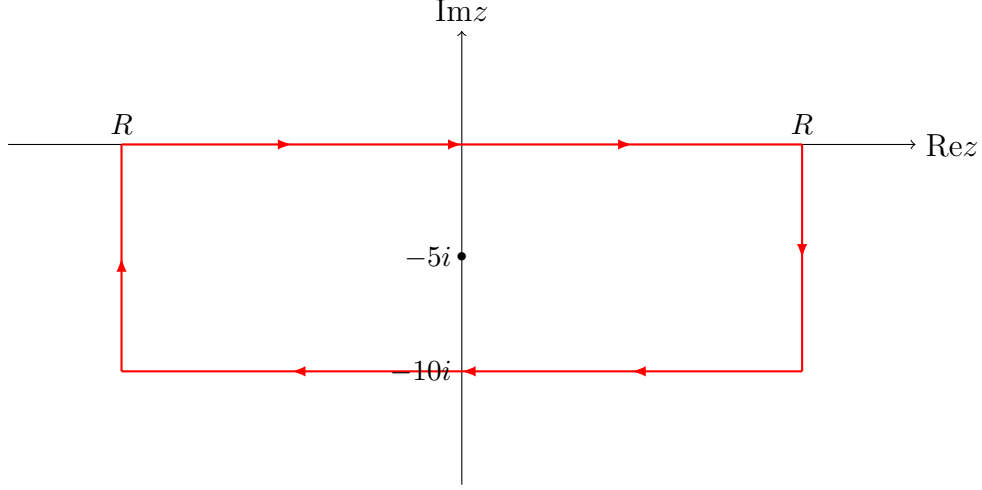


Figure 6: Graphical description of the contour \mathcal{C} .

By a similar trick we can solve the integral in (II.84) and find exact results for the correlation functions described above. Note that the integrand fulfils

$$b(u, y)K(z - y) = -b(u, y + i\pi)K(z - (y + i\pi)) \quad (\text{II.89})$$

and thus we choose an integration contour according in Fig. 6 but with $-10i$ replaced by $i\pi$. For small $x, u > 0$ the poles inside the contour are located at

$$\left\{ \frac{i\pi}{5} - ix, \frac{4i\pi}{5} - ix, i\pi - ix, \frac{2i\pi}{5} - ix, \frac{i\pi}{5} - iu, \frac{2i\pi}{5} - iu, \frac{3i\pi}{5} - iu, \frac{4i\pi}{5} - iu \right\}. \quad (\text{II.90})$$

Again, the left and right sides of the rectangle do not contribute in the limit $R \rightarrow \infty$. Hence, we can find an explicit expression for $a(u, z)$ using the residue theorem. Going back to the original function $\chi(\lambda_1, \lambda_2)$ we find after simplifications

$$\chi(\lambda_1, \lambda_2) = \frac{3 - \sqrt{5}}{4 \cos(2\lambda_{12}) + 4 \cos(4\lambda_{12}) + 2} \quad (\text{II.91})$$

and, hence, we obtain the two point function $f(\lambda_1, \lambda_2) = \chi(\lambda_1, \lambda_2) \varphi(\lambda_1, \lambda_2)$. As displayed in Fig. 7 we see a good convergence of the finite size correlation functions towards the exact result in the thermodynamic limit. However, the result is only valid for λ_2 from a small interval around 0. This can be seen by comparing the above results with finite size data. Even for $L = 6$ we already see an almost perfect matching around the origin but severe deviations in other areas (see Fig. 8).

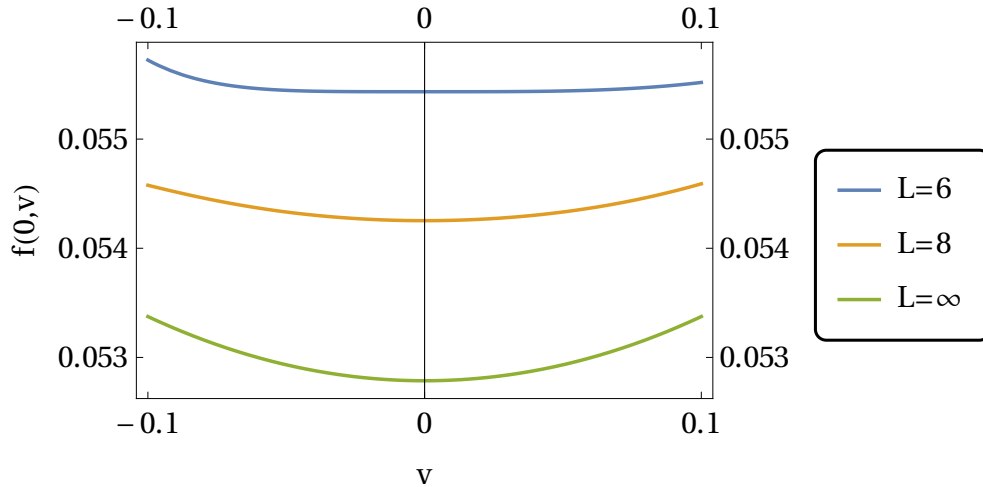


Figure 7: Comparison of the exact result (II.91) in the thermodynamic limit $L = \infty$ with the finite size correlation functions of system sizes $L = 6, 8$. In each case $f(0, v)$ is plotted for the homogeneous model.

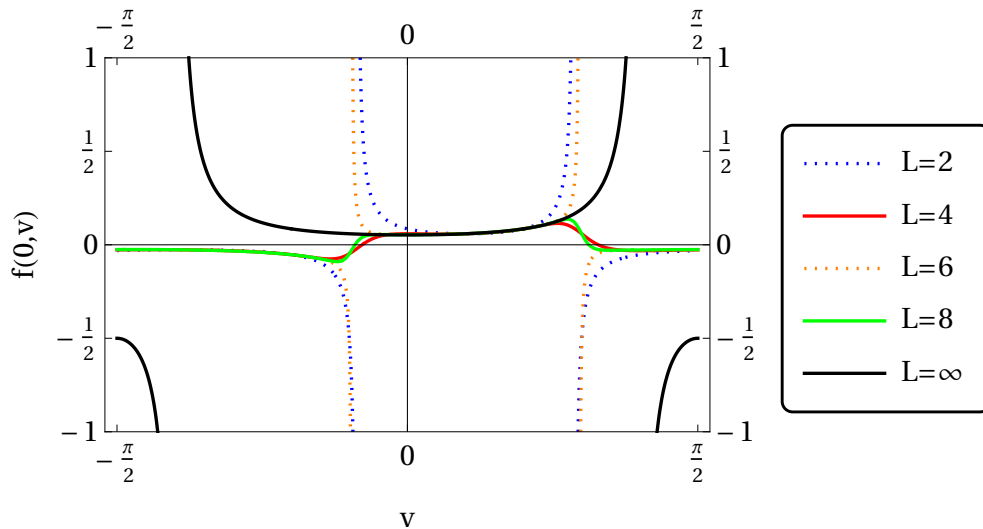


Figure 8: Comparison between the solution (II.91) of the functional equation (II.70) in the thermodynamic limit $L = \infty$ and the finite size function for different chain lengths L . One can see that further away from the origin both functions behave quite differently. It is also observed, that for $L \bmod 3 = 0$ (dashed lines) poles appear.

Luckily, this still suffices for the calculation of correlation functions in the thermodynamic limit. We find $(0, 0) = \frac{1}{2} - \frac{1}{\sqrt{5}}$, $(2, 0) = \frac{14}{5} - \frac{6}{\sqrt{5}}$ and $(1, 1) = \frac{2}{5}(-7 + 3\sqrt{5})$. Using these results and (II.81) we find an exact expression for the three-anyon projector for eigenstates $|\Phi\rangle$ in ferromagnetic ground state of the $r = 5$ RSOS model:

$$\langle \Phi | P_1^{(\tau\tau\tau \rightarrow 1)} | \Phi \rangle = 14\sqrt{5} - 23. \quad (\text{II.92})$$

We conclude this section with some remarks. Comparing the result for the thermodynamic limit with the $r = 4$ model, we see some similarities. For $r = 4$ the right-hand side (II.44) of the continuous functional equation (II.39) is discontinuous in the thermodynamic limit and agrees with the discrete functional equation (II.26) only in a neighbourhood of the origin. We expect a similar behaviour for $r = 5$. For $L \rightarrow \infty$ the right-hand side of (II.71) is exact in some interval containing the origin but deviates from the ‘real’ function $r(u)$ periodically. To obtain the exact solution one needs to find the continuous version of (II.71). This, as well as the extension to arbitrary values of r , will be interesting topics for future research.

2 $SO(5)_2$ anyons

Having studied some models of RSOS type, let us transfer the results to different face models and related anyon chains. There exist many strategies to construct such models. Here we shall focus on anyon models where the anyon types are labelled by representations of some algebra (in this section $U_q(\mathfrak{so}(5))$) and the fusion rules are read off from the decomposition of tensor products of representations into irreducible ones. These anyon models have been shown to be exactly solvable upon a fine tuning of the coupling constants. For some values the Hamiltonian is generated by transfer matrices of related integrable face models [16]. In this chapter we will focus on the $SO(5)_2$ anyon model and in particular on its related face models. Therefore, we give a brief introduction to the model and continue with the examination of its reduced density matrices. We conclude this section with the derivation of the discrete functional equations and give an outlook on their potential usage in future work.

2.1 The $SO(5)_2$ model

Let us consider anyons satisfying the fusion rules of $SO(5)_2$ as given in Table 1. F -moves consistent with those fusion rules have been constructed in [75]. There are four sets of gauge inequivalent⁸ F -moves parameterised by pairs of numbers (l, κ) where $l = 1, 3$ and $\kappa = \pm 1$. Considering the projection operators (I.52) one finds that they are independent of the choice of κ . Therefore we will fix $\kappa = +1$ and denote the F -moves by $F(l)$ whenever we want to specify the choice for l .

\otimes	ψ_1	ψ_2	ψ_3	ψ_4	ψ_5	ψ_6
ψ_1	ψ_1	ψ_2	ψ_3	ψ_4	ψ_5	ψ_6
ψ_2	ψ_2	$\psi_1 \oplus \psi_5 \oplus \psi_6$	$\psi_3 \oplus \psi_4$	$\psi_3 \oplus \psi_4$	$\psi_2 \oplus \psi_5$	ψ_2
ψ_3	ψ_3	$\psi_3 \oplus \psi_4$	$\psi_1 \oplus \psi_2 \oplus \psi_5$	$\psi_2 \oplus \psi_5 \oplus \psi_6$	$\psi_3 \oplus \psi_4$	ψ_4
ψ_4	ψ_4	$\psi_3 \oplus \psi_4$	$\psi_2 \oplus \psi_5 \oplus \psi_6$	$\psi_1 \oplus \psi_2 \oplus \psi_5$	$\psi_3 \oplus \psi_4$	ψ_3
ψ_5	ψ_5	$\psi_2 \oplus \psi_5$	$\psi_3 \oplus \psi_4$	$\psi_3 \oplus \psi_4$	$\psi_1 \oplus \psi_2 \oplus \psi_6$	ψ_5
ψ_6	ψ_6	ψ_2	ψ_4	ψ_3	ψ_5	ψ_1

Table 1: The fusion rules for $SO(5)_2$ anyons.

Consider a chain of L ψ_3 anyons. As explained in Section I.2 we obtain the fusion path basis via Eq. (I.51). From the F -moves we get the projection operators $P_i^{(33 \rightarrow b)}$ (see Eq. (I.52)). The fusion rules lead to the adjacency graph depicted in Fig. 9.

The fusion rule $\psi_3 \otimes \psi_3 = \psi_1 \oplus \psi_2 \oplus \psi_5$ implies that the most general local nearest

⁸The solution of the pentagon equations (I.50) usually requires some gauge fixing.

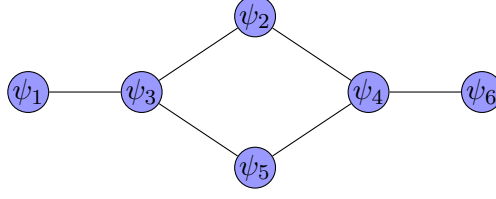


Figure 9: Adjacency graph for a chain of ψ_3 anyons.

neighbour Hamiltonian can be described by a single parameter θ

$$h_i(\theta) = \cos\left(\theta + \frac{\pi}{4}\right) P_i^{(33 \rightarrow 2)} + \sin\left(\theta + \frac{\pi}{4}\right) P_i^{(33 \rightarrow 5)} \quad (\text{II.93})$$

resulting in

$$H(\theta) = \sum_i h_i(\theta). \quad (\text{II.94})$$

Depending on the value of θ the model is described by different phases c.f. [76]. Here we will focus on some special values of θ where the Hamiltonian belongs to the set of conserved quantities of a face model.

Points of integrability have been found in [16] using the fact that the local projection operators yield a representation of the Birman-Murakami-Wenzl (BMW) algebra [77, 78] containing a copy of the Temperley-Lieb algebra (I.28) as a subalgebra. Using Baxterization techniques similar to those explained in Section I.1.3 IRF Boltzmann weights solving the Yang-Baxter equation have been found.

Their general form is given by

$$W^{\alpha\beta} \left(\begin{array}{cc|c} a & b & u \\ c & d & \end{array} \right) = \sum_{n=1}^6 w_n^{\alpha,\beta}(u) \left[\left(F_d^{a\beta\alpha} \right)_n^b \right]^* \left(F_d^{a\alpha\beta} \right)_n^c \quad (\text{II.95})$$

with $\alpha, \beta \in \{1, 2, \dots, 6\}$ and functions $w_n^{\alpha,\beta}(u)$. In our case of a chain of ψ_3 anyons only $\alpha = \beta = 3$ needs to be considered and we will use $w_n(u) \equiv w_n^{3,3}(u)$ and similarly $W^{3,3} \left(\begin{array}{cc|c} a & b & u \\ c & d & \end{array} \right) \equiv W \left(\begin{array}{cc|c} a & b & u \\ c & d & \end{array} \right)$.

Using only the Temperley-Lieb representation one obtains the non-zero functions

$$\begin{aligned} w_1(u) &= \sinh(\gamma - u) \\ w_2(u) &= \sinh(\gamma + u) \\ w_3(u) &= w_2(u) \end{aligned} \quad (\text{II.96})$$

with $\cosh(\gamma) = \sqrt{5}/2$. Notice that the anisotropy parameter corresponds to the massive phase of the XXZ model.

Another set of Boltzmann weights can be obtained using the full BMW algebra

$$\begin{aligned} w_1(u) &= \sinh\left(u + \frac{\pi i l_{FZ}}{10}\right) \sinh\left(u + \frac{3\pi i l_{FZ}}{10}\right) \\ w_2(u) &= \sinh\left(u - \frac{\pi i l_{FZ}}{10}\right) \sinh\left(u - \frac{3\pi i l_{FZ}}{10}\right) \\ w_3(u) &= \sinh\left(u + \frac{9\pi i l_{FZ}}{10}\right) \sinh\left(u + \frac{3\pi i l_{FZ}}{10}\right) \end{aligned} \quad (\text{II.97})$$

where $l_{FZ} = 3^9$ for $l = 1$ and $l_{FZ} = 1$ for $l = 3$ such that the weights explicitly depend on the choice of $F(l)$. Although we use the same notation for the Boltzmann weights of Temperley-Lieb and the BMW type, it should always be clear from context which one is meant

After the construction of the Boltzmann weights all definitions from the previous chapter can be applied to this model. In particular we can define the transfer matrix $t(u)$ via (I.11).

Taking the Hamiltonian limit as explained in Section I.1.2 we find that for certain values of θ the anyonic Hamiltonian (II.94) is obtained. To be definite, we set

$$H(\alpha', \alpha'') = \alpha' \frac{d}{du} \ln t(u) + \alpha'' L. \quad (\text{II.98})$$

The Temperley-Lieb representation then yields (II.94) for $\theta = 0$ and $\theta = \pi$ where $(\alpha', \alpha'') = \pm(\frac{1}{2\sqrt{2}}, \frac{1}{2\sqrt{10}})$. Using the BMW representation one finds two additional integrable points at $\theta = \eta$ and $\theta = \eta + \pi$ where $\eta = \arctan \frac{1+\sqrt{5}}{4} - \frac{\pi}{4}$.

In the following section we will examine the reduced density matrices for the $SO(5)_2$ model. Note that we are now actually considering three IRF models: one corresponding to the Temperley-Lieb solution for the Boltzmann weights and two corresponding to the BMW solution for $l = 1$ and $l = 3$. Before studying the density operators it is, however, useful to examine the symmetries of the model.

According to Section I.2 the Hilbert space can be decomposed into topological sectors i.e. into the eigenspaces of the operators Y_ℓ defined in Eq. (I.54). The transfer matrices commute with these operators and thus its eigenstates can be labelled by their eigenvalues. We will see that similar to the RSOS models we can use the Y_3 eigenvalues to characterise the ‘good’ sectors for which simplifications in the structure of the density matrices occur.

⁹The index of l_{FZ} stands for Fateev–Zamolodchikov. The $SO(5)_2$ IRF model is related to the \mathbf{Z}_2 Fateev–Zamolodchikov models where l_{FZ} characterises the R -matrices which are related to the IRF Boltzmann weights and vice versa.

2.2 The Temperley-Lieb model

Following the same strategy as in the previous Section II.1 on SOS models, we consider the reduced density operators $D_N(\lambda_{n_1}, \dots, \lambda_{n_2})$. Note that the Boltzmann weights and therefore also the (generalised) transfer matrices depend on the choice of the integrable point. Let us first consider the Temperley-Lieb point for which the model is Temperley-Lieb equivalent to the XXZ Heisenberg chain. In this case similar results as for the SOS models, which can be related to the 6-vertex model by face-vertex-correspondence, are expected.

As discussed earlier the transfer matrix commutes with the topological operator Y_3 and thus there exists a common basis of eigenstates. The eigenvalues of the operators Y_ℓ are known to be quotients of the modular S -matrix associated to each choice of F -moves which diagonalises the fusion rules [50]. In our case one finds $y_3 \in \{0, \pm 1, \pm\sqrt{5}\}$. In addition, the (generalised) transfer matrices do not depend on the choice of $F(l)$ for the Temperley-Lieb model.

Numerically calculating $D_1(\lambda_1)$ for small chain lengths we observe that it is always independent of the spectral parameter *and* the inhomogeneities for states in the $y_3 = \pm\sqrt{5}$ sectors and we will from now on restrict our studies to these sectors. In those sectors $D_1(\lambda_1)$ is particularly simple:

$$D_1^{[\alpha, \beta]}(\lambda_1) = \begin{cases} \frac{1}{20} & \text{for } (\alpha\beta) \in \{(13), (31), (64), (46)\} \\ \frac{1}{10} & \text{for all other allowed } (\alpha, \beta) \end{cases}. \quad (\text{II.99})$$

To find an exact expression for D_2 in the considered sectors we proceed similar to the algorithm from the previous Section II.1.2. Inspired by the structure of D_2 for the $r = 4, r = 5$ RSOS models, we assume that we can express the two-site density operator in terms of one off-diagonal element, i.e. we make the ansatz

$$f_0 + f_1 f(\lambda_1, \lambda_2) \quad (\text{II.100})$$

for any matrix element of $D_2(\lambda_1, \lambda_2)$ with constants f_0, f_1 being independent of the spectral parameter, inhomogeneities and system size. Specifically, choosing $f(\lambda_1, \lambda_2) \equiv \langle 232 | D_2(\lambda_1, \lambda_2) | 242 \rangle$ the constants f_0 and f_1 can be easily obtained from the exact finite size values of D_2 . Since the dimension of the auxiliary space $\dim(\mathcal{V}_2) = 28$ is quite large we only present the one-dimensional $[1, 1]$ block of the density operator as an example:

$$D_2^{[1,1]}(\lambda_1, \lambda_2) = \frac{1}{100} + \frac{2}{5} f(\lambda_1, \lambda_2). \quad (\text{II.101})$$

To study the functional equation (I.98) we first need to establish the unitarity and crossing relations of the $SO(5)_2$ face model at the Temperley-Lieb point. Regarding

unitarity we find that (I.6) holds with

$$\rho(u) = \sinh(u - \gamma). \quad (\text{II.102})$$

Note that for our choice of Boltzmann weights we have $\rho(0) = -1/2$. Furthermore, the initial condition (I.8) acquires a factor of $1/2$

$$\begin{array}{c} d \quad c \\ \boxed{0} \\ a \quad b \end{array} = \frac{1}{2} \delta_{a,c}. \quad (\text{II.103})$$

The crossing relation for this model is more complicated compared to RSOS models. We find that Eq. (II.15) needs to be modified to

$$W \left(\begin{array}{cc|c} a & b & u \\ c & d & \end{array} \right) = \frac{g_{ad}}{g_{bc}} W \left(\begin{array}{cc|c} b & d & -\gamma - u \\ a & c & \end{array} \right), \quad (\text{II.104})$$

where the gauge factors g_{ab} are given by

$$\begin{aligned} g_{13} &= -g_{64} = 1, \\ g_{23} &= g_{24} = g_{53} = g_{54} = \sqrt{2}, \\ g_{32} &= g_{35} = g_{42} = g_{45} = \sqrt{\frac{5}{2}}, \\ g_{31} &= -g_{46} = \sqrt{5}. \end{aligned} \quad (\text{II.105})$$

Taking into account these differences in comparison with the SOS models, we need to reconsider the P_- operator which we define as

$$\langle \alpha_0 \alpha_1 \alpha_2 | P_- | \beta_0 \beta_1 \beta_2 \rangle = \alpha_1 \begin{array}{c} \alpha_0 = \beta_0 \\ \diamond \\ P_- \\ \alpha_2 = \beta_2 \end{array} \beta_1 \equiv 2 \delta_{\alpha_0 \beta_0} \delta_{\alpha_2 \beta_2} \frac{g_{\alpha_0 \beta_1}}{g_{\alpha_1 \alpha_2}} \alpha_1 \begin{array}{c} \alpha_0 \\ \diamond \\ -\gamma \\ \alpha_2 \end{array} \beta_1. \quad (\text{II.106})$$

With this choice and keeping track of the gauge factors the A -operator must be multiplied by an additional factor of $g_{\beta_{N-1} \alpha_N} / g_{\alpha_{N-1} \alpha_N}$ (and $\lambda \rightarrow -\gamma$).

After simplifications the functional equation yields

$$\rho(u - v) f(u, v - \gamma) + \rho(u - (v - \gamma)) f(u, v) = \frac{1}{40}. \quad (\text{II.107})$$

2 $SO(5)_2$ anyons

Setting $g(u, v) := f(u, v)/\rho(u, v)$ we finally obtain

$$g(u, v) + g(u, v - \gamma) = \frac{1}{40 \rho(u - v) \rho(u - v + \gamma)}. \quad (\text{II.108})$$

Note that this equation is quite similar to those obtained for the $r = 5$ RSOS model (II.70). However, this model is massive and the solution will need some adaptations compared to those found in Section II.1.

2.3 The BMW models

In order to have (generalised) transfer matrices with real valued matrix elements we rescale their arguments by a factor i , i.e. we work with

$$\left(\langle \underline{\mathbf{a}} | \hat{\otimes} \langle \underline{\boldsymbol{\alpha}} | T(u) \left(| \underline{\boldsymbol{\beta}} \rangle \hat{\otimes} | \underline{\mathbf{b}} \rangle \right) \right) = \prod_{i=1}^L W \left(\begin{array}{c|c} a_{i-1} & a_i \\ b_{i-1} & b_i \end{array} \middle| i(u - u_i) \right) \delta_{a_0, \alpha_0} \delta_{a_L, \beta_0} \delta_{b_0, \alpha_1} \delta_{b_L, \beta_1}. \quad (\text{II.109})$$

In contrast to the Temperley-Lieb case the (generalised) transfer matrices now depend explicitly on the choice of F -moves. Recall that there are two inequivalent sets $F(l)$ with $l = 1$ and $l = 3$ which must be studied separately. Nonetheless, the unitarity relation is identical for both of them. One finds $\rho(u) = \sin\left(\frac{\pi}{10} + iu\right) \cos\left(\frac{1}{5}(\pi + 5iu)\right)$. The crossing relation is the same as for the Temperley-Lieb case (see (II.104) and (II.105)).

The $l = 1$ case

Restricting ourselves to the $y_3 = \pm\sqrt{5}$ sector one observes that $D_1(\lambda_1)$ is independent of u and the inhomogeneities and coincides with the result found for the Temperley-Lieb model (II.99).

The computation of $D_2(\lambda_1, \lambda_2)$ becomes more complicated even in the $y_3 = \pm\sqrt{5}$ sectors. Now two independent functions are needed to completely characterise the density operator. It turns out that the ansatz

$$a_0 + a_1 f(\lambda_1, \lambda_2) + a_2 g(\lambda_1, \lambda_2) \quad (\text{II.110})$$

with $f(\lambda_1, \lambda_2) \equiv \langle 232 | D_2(\lambda_1, \lambda_2) | 242 \rangle$ and $g(\lambda_1, \lambda_2) \equiv \langle 313 | D_2(\lambda_1, \lambda_2) | 323 \rangle$ is sufficient to decompose any matrix element of the density operator, where a_0 , a_1 and a_2 are constants independent of the spectral and system parameters.

As an example we compute the $[1, 1]$ block:

$$D_2^{[1,1]}(\lambda_1, \lambda_2) = \frac{1}{100} + \frac{1}{10} (5 - \sqrt{5}) f(\lambda_1, \lambda_2) + \frac{\sqrt{3 - \sqrt{5}}}{5} g(\lambda_1, \lambda_2). \quad (\text{II.111})$$

All other matrix elements are easily computed from the exact finite size D_2 operators.

Having found the general shape of D_2 we can insert it into the functional equation (I.98). Note that due to the additional i in the definition of the generalised transfer matrices the Boltzmann weights appearing in the A -operator have to be changed accordingly.

Using the decomposed D_2 operator, the functional equation (I.98) simplifies to a set of two coupled equations. For the sake of readability we use the notation $sk := \sin(k(u-v))$ and $ck := \cos(k(u-v))$ resulting into

$$\begin{aligned} \rho(u-v)\rho(v-u)f(u, v-i\lambda) &= \alpha_0(u, v) + \alpha_1(u, v)f(u, v) + \alpha_2(u, v)g(u, v) \\ \rho(u-v)\rho(v-u)g(u, v-i\lambda) &= \beta_0(u, v) + \beta_1(u, v)f(u, v) + \beta_2(u, v)g(u, v) \end{aligned} \quad (\text{II.112})$$

with coefficient functions

$$\begin{aligned} \alpha_0(u, v) &= \frac{1}{32} \left(-\frac{1}{5\sqrt{5}} \frac{1}{25} (\sqrt{5}+5) c2 \right), \\ \alpha_1(u, v) &= \frac{1}{32} \left(-\sqrt{5}+3 + 2\sqrt{5(5-2\sqrt{5})} s2 - \sqrt{2(\sqrt{5}+5)} s4 - 2c2 + (\sqrt{5}-1) c4 \right), \\ \alpha_2(u, v) &= \frac{1}{16} \left(-\sqrt{\frac{7}{5} + \frac{3}{\sqrt{5}}} + \sqrt{5 - \frac{11}{\sqrt{5}}} s2 + \frac{4}{\sqrt{\sqrt{5}+5}} s4 + \sqrt{\frac{7}{5} + \frac{3}{\sqrt{5}}} c2 \right), \\ \beta_0(u, v) &= \frac{1}{160\sqrt{2}}, \\ \beta_1(u, v) &= \frac{1}{32} \left(\sqrt{15-5\sqrt{5}} - \sqrt{125-55\sqrt{5}} s2 - \sqrt{15-5\sqrt{5}} c2 \right), \\ \beta_2(u, v) &= \frac{1}{16} \left(\frac{1}{2} \sqrt{50-22\sqrt{5}} s2 + \sqrt{\frac{1}{2}(\sqrt{5}+5)} s4 - \frac{1}{2}(\sqrt{5}-1) c2 + \frac{1}{2}(\sqrt{5}-1) c4 \right). \end{aligned}$$

We will now examine the model $F(l=3)$.

The $l=3$ case

Choosing $l=3$ does not affect the unitarity and crossing relations. Furthermore, $D_1(\lambda_1)$ is unchanged compared to the previous cases, while the decomposition of $D_2(\lambda_1, \lambda_2)$ differs. We can still choose $f(\lambda_1, \lambda_2) \equiv \langle 232|D_2(\lambda_1, \lambda_2)|242 \rangle$ and $g(\lambda_1, \lambda_2) \equiv \langle 313|D_2(\lambda_1, \lambda_2)|323 \rangle$ and write any matrix element according to (II.110). However, the constants do not agree, e.g. we find

$$D_2^{[1,1]}(\lambda_1, \lambda_2) = \frac{1}{100} + \frac{1}{10} (5 + \sqrt{5}) f(\lambda_1, \lambda_2) - \frac{\sqrt{\sqrt{5}+3}}{5} g(\lambda_1, \lambda_2). \quad (\text{II.113})$$

Plugging the above result into the functional equation (I.98) results again into two

2 $SO(5)_2$ anyons

equations given by

$$\begin{aligned} \rho(u-v)\rho(v-u)f(u, v-i\lambda) &= \alpha_0(u, v) + \alpha_1(u, v)f(u, v) + \alpha_2(u, v)g(u, v) \\ \rho(u-v)\rho(v-u)g(u, v-i\lambda) &= \beta_0(u, v) + \beta_1(u, v)f(u, v) + \beta_2(u, v)g(u, v) \end{aligned} \quad (\text{II.114})$$

where the coefficient functions are given by

$$\begin{aligned} \alpha_0(u, v) &= \frac{1}{32} \left(\frac{1}{5\sqrt{5}} - \frac{1}{25} (\sqrt{5}-5) c2 \right), \\ \alpha_1(u, v) &= \frac{1}{32} \left((\sqrt{5}+3) - \sqrt{40\sqrt{5}+100} s2 - \sqrt{10-2\sqrt{5}} s4 - 2c2 - (\sqrt{5}+1) c4 \right), \\ \alpha_2(u, v) &= \frac{1}{16} \left(\sqrt{\frac{7}{5} - \frac{3}{\sqrt{5}}} + \sqrt{5 + \frac{11}{\sqrt{5}}} s2 + 2\sqrt{\frac{1}{5}(\sqrt{5}+5)} s4 - \sqrt{\frac{7}{5} - \frac{3}{\sqrt{5}}} c2 \right), \\ \beta_0(u, v) &= \frac{1}{160\sqrt{2}}, \\ \beta_1(u, v) &= \frac{1}{32} \left(\sqrt{5(\sqrt{5}+3)} - \sqrt{\sqrt{5}+5} (3\sqrt{5}+5) s2 - \frac{(\sqrt{5}+5)}{\sqrt{2}} c2 \right), \\ \beta_2(u, v) &= \frac{1}{16} \left(\frac{1}{2}\sqrt{50+22\sqrt{5}} s2 + \sqrt{\frac{1}{2}(5-\sqrt{5})} s4 + \frac{1}{2}(\sqrt{5}+1) c2 - \frac{1}{2}(\sqrt{5}+1) c4 \right), \end{aligned}$$

using again the notation $sk := \sin(k(u-v))$ and $ck := \cos(k(u-v))$. One observes apart from some signs huge similarities between the functional equations for the $l=1$ and the $l=3$ model.

To conclude this section we emphasise that the structure of the functional equations resembles those found for the RSOS model. For the Temperley-Lieb model we were able to express D_2 by one single function similar to what has been discussed for the RSOS $r=4, 5$ models in the sectors with quantum dimension 1. However, the BMW models turned out to be more complicated even in the ‘good’ topological sectors. Here the structure of D_2 and the functional equations are similar to the RSOS models in the topological sectors with quantum dimension > 1 . Similar coupled equations have also been found for higher rank vertex models, e.g. in [79, 80]. It will be interesting to see if some of the methods can be adapted to the RSOS and $SO(5)_2$ models.

Conclusions

Correlation functions in integrable face models are still not as well understood as their vertex relatives. Corner transfer matrix [81] and functional methods [38, 82] have been used to calculate local height probabilities but in general the literature on this subject is rather scarce. In this thesis new functional methods have been developed and applied to several critical solid-on-solid models and the $SO(5)_2$ model.

To achieve this goal, we solved the ‘inverse problem’ for generic face models and thus were able to relate correlation functions to reduced density matrices. Instead of directly calculating these matrices, we derived a set of functional equations for inhomogeneous face models, a discrete one (I.98), which is only valid at a discrete set of points and a reduction relation (I.100) relating N - to $(N - 2)$ -point functions.

For instance, we have obtained explicit expressions for the reduced density matrices of the $r = 3$ CSOS model for a particularly simple reference state. They were expressed in terms of the one-point function which depends on the spectral parameter and the inhomogeneities. By contrast, the one-point functions in the RSOS models are independent of the spectral parameter. For the $r = 4, 5$ RSOS models we have been able to express the two-site density matrices in terms of two unknown functions similar to the spin-1/2 Heisenberg chains [29, 31]. These functions are uniquely determined by the derived functional equations for any transfer matrix eigenstate, given the analytical properties inherited from the Boltzmann weights.

Additional properties of the density matrices are found in topological sectors with quantum dimension $d_q = 1$ (containing the ground states of the RSOS model): here we have observed a reduction relating D_N to D_{N-1} when one of the spectral parameters approaches infinity. This resembles the asymptotic condition on the density matrices complementing the discrete qKZ equation for the Heisenberg spin chain guaranteeing the uniqueness of its solution [30, 31]. Moreover, we have found that the reduced density operators of the $r = 4$ and 5 RSOS models in these topological sectors can be further simplified. Here, the two-site density operator D_2 is completely characterised by one single function. Preliminary results support the conjecture that this holds true for any $r > 5$ in these sectors.

Restricting ourselves to these sectors, we were able to solve the functional equations for the ferromagnetic ground state of the $r = 4$ model. A key role was played by the reduction relation (I.100) which allowed us to find a continuous functional equation for the density operator. For finite chain lengths the solution is given by a single integral while in the thermodynamic limit an explicit expression can be derived. For the $r = 5$ model we were able to find an explicit solution of the functional equation in the thermodynamic limit again corresponding to the ferromagnetic ground state.

To efficiently find finite size correlation functions in the $r = 5$ (and possibly also $r > 5$ RSOS models), one needs to find a continuous version of the discrete functional equations. However, the reduction relation does not fulfil the task in this case. Inspecting the $r = 4$ case may give a hint how such an equation may look like. It will be interesting to examine this topic in future research.

Once the two-point functions are calculated these results can be used to obtain explicit expressions for the N -point reduced density matrices with $N > 2$. Motivated by similar results for the spin-1/2 Heisenberg chain [23], we assumed a factorisation of long-range correlators into an *algebraic part*, which is independent of system parameters, and a *physical part*, which is described in terms of the two-point functions (see Eq. (II.30)). Moreover, we proposed an efficient algorithm to calculate the algebraic part and used it for the calculation of the three-sites density operator of the $r = 4, 5$ RSOS models. Combined with the explicit results for the two-sites density operator we were able to exactly determine the three-point functions for these models and for the corresponding chain of Fibonacci anyons.

Since the functional methods developed in Part I. are quite general, one can apply them to the $SO(5)_2$ -model and any other face model which possesses crossing and unitarity symmetries. This IRF/anyon model belongs to solutions of the Yang-Baxter equation which are in part not of Temperley-Lieb type in contrast to the SOS models studied before. The $SO(5)_2$ anyon model can be mapped to the corresponding face model for some values of the coupling constants (integrable points). For certain topological sectors we were able to unveil the structure of the two-site reduced density matrix and derived functional equations for the functions which characterise them.

Methods from this thesis may be used to answer long-standing questions: first of all, in the context of RSOS models a comparison of the density matrices with the corresponding quantities for the related anisotropic Heisenberg chains at roots of unity can provide insights into the boundary contributions to correlation functions resulting from the particular fusion path nature of the RSOS Hilbert space.

Secondly we want to emphasise that the discrete functional equations (I.98) for the density operators hold for generic integrable IRF models (such equations are also known for vertex models and spin chains related to quantum groups [83]). Together with the algorithm used here for the computation of the structure functions in factorised expressions (II.29) and (II.30) this may well allow to shed some light on the question whether the factorisation of correlation functions is a general property of integrable models which extends beyond RSOS models and spin-1/2 chains. Therefore, it is desirable to extend the studies of the $SO(5)_2$ model to three-point functions and analyse their factorisation properties.

Other possible extensions are fused or higher rank face models. Their vertex coun-

terparts, i.e. spin chains with spin $> \frac{1}{2}$ have been addressed using similar techniques and explicit results for two- and three-point functions have been found [84, 85]. Since fused models obey crossing and unitarity symmetries it is expected that they can be tackled by methods developed in this thesis. Higher rank vertex models have also been studied but there are fewer results (see e.g. [66, 80] for explicit expressions for correlation functions of the $SU(3)$ spin chain). The functional equations for higher rank models differ from those found in the rank one case due to the absence of crossing relations. It is expected that similar methods can also be applied to higher rank face models to study their correlation functions.

To conclude, in this thesis quite general functional methods have been developed and applied to correlation functions of various face and anyon models. The open questions arising from it may be a starting point for further research in this context.

A Proof of Theorem 1.

Having shown the proof of Theorem 1. only for a chain length $L = 2$ we now present the general (graphical) proof. We use double arrows to indicate periodic boundary conditions in horizontal direction. For arbitrary L and $1 \leq n < L$ and $|\mathbf{a}\rangle, |\mathbf{b}\rangle \in \mathcal{H}_{\text{per}}^L$ we need to calculate the matrix element:

$$\langle \mathbf{a} | \left(\prod_{k=1}^{n-1} t(u_k) \right) T_{\alpha\beta}(u_n) T^{\alpha\beta}(u_{n+1}) \left(\prod_{k=n+2}^L t(u_k) \right) | \mathbf{b} \rangle =$$

	a_0	a_1	a_2	a_{L-2}	a_{L-1}	a_L	
\gg	0	$u_{1,2}$	\dots	$u_{1,L-1}$	$u_{1,L}$	\gg	
•	$u_{2,1}$	0	\dots	$u_{2,L-1}$	$u_{2,L}$	\gg	
\gg	\vdots	\vdots	\vdots	\vdots	\vdots	\gg	
•	$u_{n,1}$	$u_{n,2}$	\dots	$u_{n,L-1}$	$u_{n,L}$	\gg	
\gg	$u_{n+1,1}$	$u_{n+1,2}$	\dots	$u_{n+1,L-1}$	$u_{n+1,L}$	\gg	
•	\vdots	\vdots	\vdots	\vdots	\vdots	\gg	
\gg	$u_{L-1,1}$	$u_{L-1,2}$	\dots	0	$u_{L-1,L}$	\gg	
•	$u_{L,1}$	$u_{L,2}$	\dots	$u_{L,L-1}$	0	\gg	
\gg	b_0	b_1	b_2	b_{L-2}	b_{L-1}	b_L	

$= \alpha$

\cdot

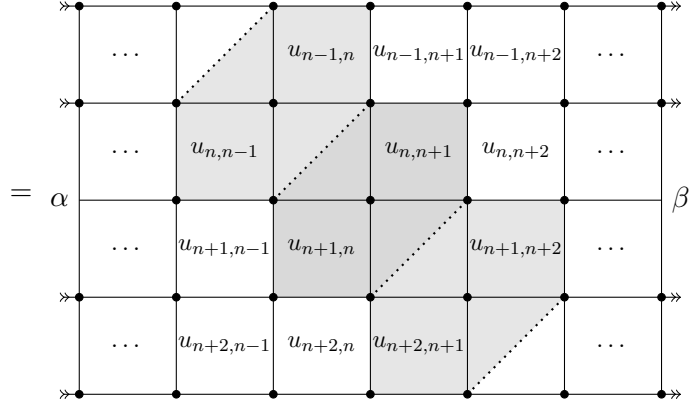
β

(A.1)

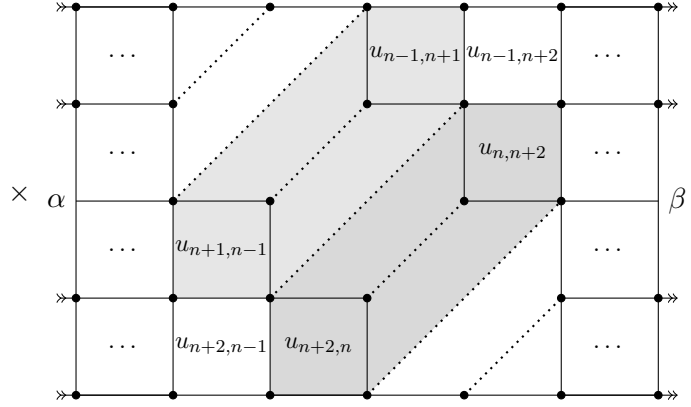
Let us have a closer look on the four central rows and illustrate the procedure. Having used the initial condition (I.8), we can repeatedly use unitarity (I.6) turning all Boltzmann weights into Kronecker δ 's. To guide the eye, each usage of unitarity is indicated

by shading the involved weights. One finds:

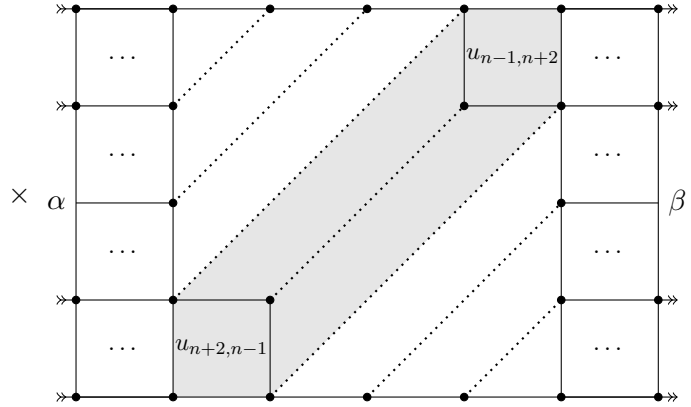
$$\cdots t(u_{n-1})T_{\alpha\beta}(u_n)T^{\alpha\beta}(u_{n+1})t(u_{n+2})\cdots =$$



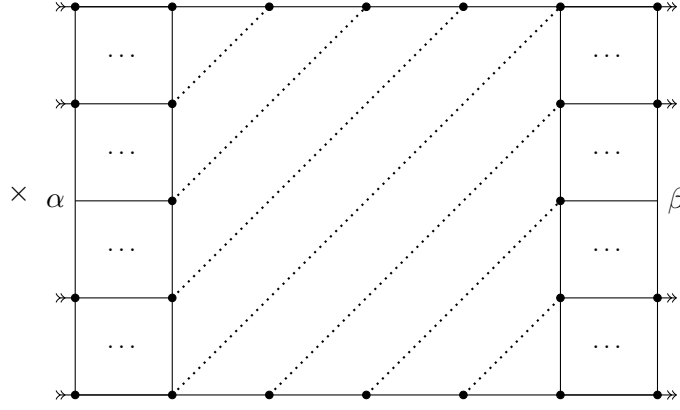
$$= \rho_{n-1,n}\rho_{n,n+1}\rho_{n+1,n+2} \times$$



$$= \rho_{n-1,n}\rho_{n,n+1}\rho_{n+1,n+2}\rho_{n-1,n+1}\rho_{n,n+2} \times$$



$$= \rho_{n-1,n}\rho_{n,n+1}\rho_{n+1,n+2}\rho_{n-1,n+1}\rho_{n,n+2}\rho_{n-1,n+2} \times$$



where $u_{i,j} \equiv u_i - u_j$ and $\rho_{i,j} \equiv \rho(u_i - u_j)\rho(u_j - u_i)$ has been used. Iterating the procedure in every row, we find

$$\langle \mathbf{a} | \left(\prod_{k=1}^{n-1} t(u_k) \right) T_{\alpha\beta}(u_n) T^{\alpha\beta}(u_{n+1}) \left(\prod_{k=n+2}^L t(u_k) \right) | \mathbf{b} \rangle =$$

$$= \prod_{k,\ell=1}^L \rho(u_k - u_\ell) \alpha \beta$$

$$= \prod_{k,\ell=1}^L \rho(u_k - u_\ell) \delta_{a_n, \alpha} \delta_{b_n, \beta} \prod_{j \neq n} \delta_{a_j b_j}$$

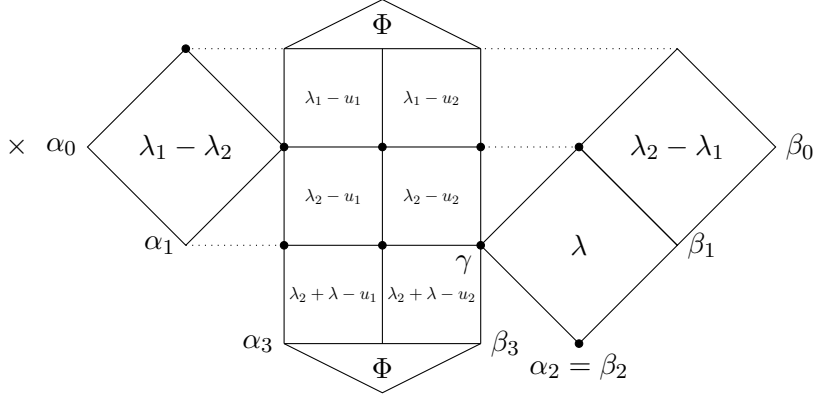
$$= \prod_{k,\ell=1}^L \rho(u_k - u_\ell) \langle \mathbf{a} | (E_\beta^\alpha)_n | \mathbf{b} \rangle$$

which ends the proof.

B Proof of Theorem 2.

Here we will provide the proof for the functional equation (I.98). It consists of three steps. The idea is, to consider the action of A_N on a density operator with one row added, i.e. $D_{N+1}(\lambda_1, \dots, \lambda_N, \lambda_N + \lambda)$. Recall, that for every $n \in \mathbb{N}$ $D_n(\lambda_1, \dots, \lambda_n)^{\{\underline{\alpha}\}\{\underline{\beta}\}} = 0$ if $\alpha_0 \neq \beta_0$ or $\alpha_n \neq \beta_n$. In those cases the functional equation holds trivially, so we may assume $\alpha_0 = \beta_0$. Also note that $(A_N(\lambda_1, \dots, \lambda_N) [D_{N+1}(\lambda_1, \dots, \lambda_N, \lambda_N + \lambda)])^{\{\underline{\alpha}\}\{\underline{\beta}\}}$ is a matrix element of an operator $\mathcal{V}^{N+1} \rightarrow \mathcal{V}^{N+1}$. To keep the presentation legible, the following steps will be shown graphically for $N = L = 2$, e.g.

$$A_2(\lambda_1, \lambda_2) [D_3(\lambda_1, \lambda_2, \lambda_2 + \lambda)]^{\{\underline{\alpha}\}\{\underline{\beta}\}} = \frac{\delta_{\alpha_0\beta_0} \delta_{\alpha_2\beta_2}}{\rho(\lambda_1 - \lambda_2) \rho(\lambda_2 - \lambda_1) \Lambda(\lambda_1) \Lambda(\lambda_2) \Lambda(\lambda_2 + \lambda)} \times$$



Now, writing $\mathcal{V}^{N+1} = \mathcal{V}^N \hat{\otimes} \mathcal{V}^1$ (see II.3 for the definition of the symbol $\hat{\otimes}$) we perform two ‘(constrained) partial traces’ over the factor \mathcal{V}^1 each leading to one side of the functional equation, i.e. operators on \mathcal{V}^N . In a final step we show that for the special choice of λ_N being one of the inhomogeneities $\{u_i\}$ the constraint can be dropped and both summations lead to the same result.

In a first step we note that from the definition (I.91) of the density operators

$$\sum_{\alpha_{N+1}} D_{N+1}(\lambda_1, \dots, \lambda_N, \lambda_N + \lambda)^{\{\underline{\alpha}\}\{\underline{\beta}\}} = D_N(\lambda_1, \dots, \lambda_N)^{\{\underline{\alpha}'\}\{\underline{\beta}'\}}, \quad (\text{B.2})$$

where $\underline{\alpha}' = (\alpha_0, \dots, \alpha_N)$ and $\underline{\beta}' = (\beta_0, \dots, \beta_N)$ with $\alpha_0 = \beta_0$ and $\alpha_N = \beta_N$. This gives immediately

$$\sum_{\alpha_{N+1}} A_N(\lambda_1, \dots, \lambda_N) [D_{N+1}(\lambda_1, \dots, \lambda_N, \lambda_N + \lambda)]^{\underline{\alpha}\underline{\beta}} = A_N(\lambda_1, \dots, \lambda_N) [D_N(\lambda_1, \dots, \lambda_N)]^{\underline{\alpha}'\underline{\beta}'}. \quad (\text{B.3})$$

Note that this fixes the spin γ to be equal to α_1 in the graphical representation above (or α_{N-1} for general N). Therefore we have obtained the left-hand side of the functional equation (I.98).

For the second step we sum over $\alpha = \alpha_N = \beta_N$ and fix the spin γ to be equal to β_{N-1} . For $N = L = 2$ this becomes (thick dotted lines indicate where the constraint $\delta_{\gamma\beta_1}$ is used)

$$\begin{aligned}
& \delta_{\gamma\beta_1} \sum_{\alpha_2} A_2(\lambda_1, \lambda_2) [D_3(\lambda_1, \lambda_2, \lambda_2 + \lambda)]^{\{\underline{\alpha}\}\{\underline{\beta}\}} = \\
& = \frac{\delta_{\alpha_0\beta_0}}{\rho(\lambda_1 - \lambda_2)\rho(\lambda_2 - \lambda_1)\Lambda(\lambda_1)\Lambda(\lambda_2)\Lambda(\lambda_2 + \lambda)} \times \\
& \quad \times \sum_{\alpha} \alpha_0 \times \text{Diagram 1} \\
& = \frac{\delta_{\alpha_0\beta_0}}{\rho(\lambda_1 - \lambda_2)\rho(\lambda_2 - \lambda_1)\Lambda(\lambda_1)\Lambda(\lambda_2)\Lambda(\lambda_2 + \lambda)} \times \\
& \quad \times \alpha_0 \times \text{Diagram 2} \\
& = \frac{\delta_{\alpha_0\beta_0}}{\Lambda(\lambda_1)\Lambda(\lambda_2)\Lambda(\lambda_2 + \lambda)} \times \text{Diagram 3}
\end{aligned}$$

$$= \frac{1}{\Lambda(\lambda_1)\Lambda(\lambda_2 + \lambda)} \begin{array}{c} \text{\textcircled{\scriptsize Φ}} \\ \alpha_0 \quad \beta_0 \\ \lambda_1 - u_1 \quad \lambda_1 - u_2 \\ \alpha_1 \quad \beta_1 \\ \lambda_2 + \lambda - u_1 \quad \lambda_2 + \lambda - u_2 \\ \alpha_3 \quad \beta_3 \\ \text{\textcircled{\scriptsize Φ}} \end{array} = D_2(\lambda_1, \lambda_2 + \lambda) \underline{\tilde{\alpha}} \underline{\tilde{\beta}}$$

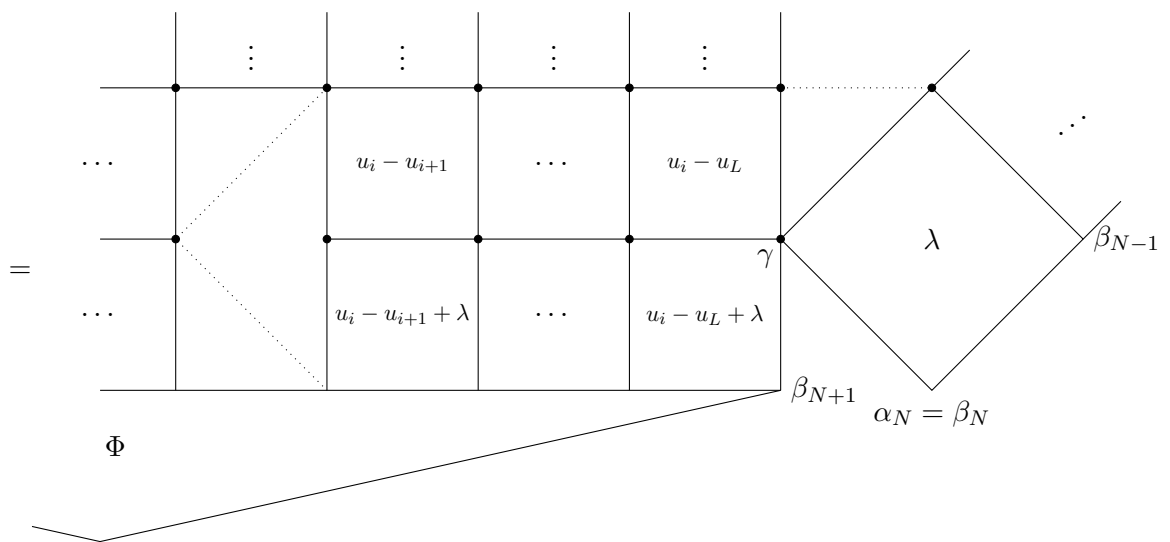
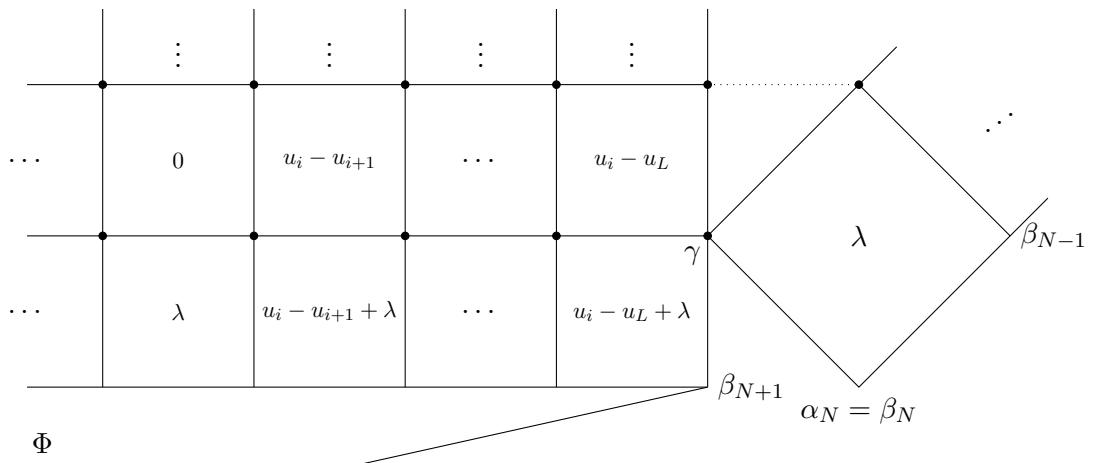
with $\underline{\tilde{\alpha}} = (\alpha_0, \alpha_1, \alpha_3)$ and $\underline{\tilde{\beta}}$ accordingly. Here we have used the initial and crossing conditions to evaluate the Boltzmann weight at λ , the Yang-Baxter equation to pull the rotated weight from the right to the left and finally $\langle \Phi | T_{\alpha_0 \alpha_0}(\lambda_2) = \Lambda(\lambda_2) \langle \Phi | P_{\alpha_0 \alpha_0}$ with the projection operator $P_{\alpha\alpha} : \mathcal{H}_{\text{per}} \rightarrow \mathcal{H}_{\alpha\alpha}$. For general $N > 2$ these operations have to be iterated to move the row $T(\lambda_N)$ to the top yielding the right-hand side of Eq. (I.98).

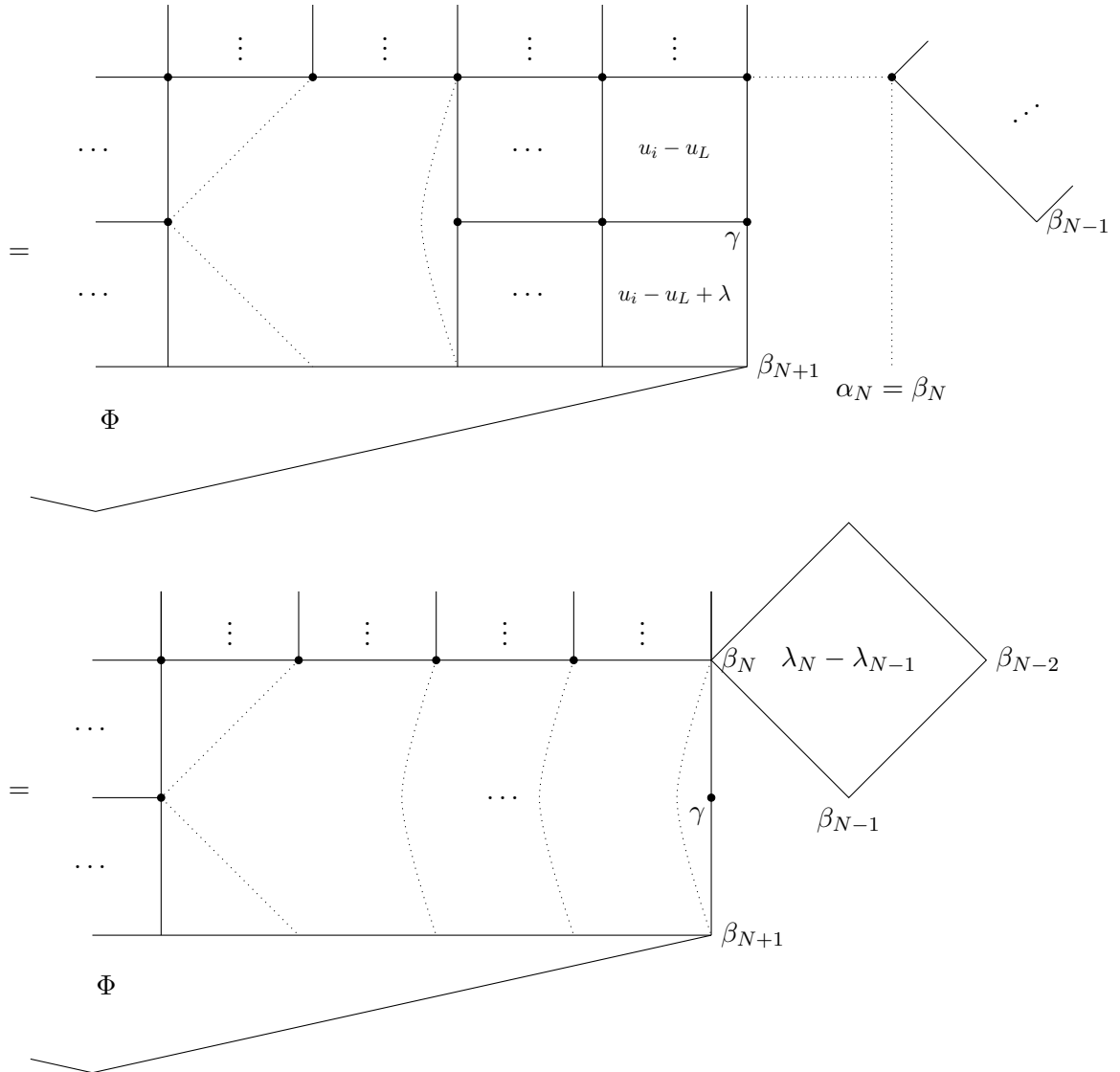
The final step consists of showing that for the special choice of λ_N the two operations shown above yield the same result. Recall Eq. (I.12) which for convenience reads:

$$\begin{array}{c} a \quad b \\ \text{\textcircled{\scriptsize u}} \\ c \quad d \\ \text{\textcircled{\scriptsize $u + \lambda$}} \\ a \quad e \end{array} = \rho(u)\rho(-u) \delta_{be}. \tag{B.4}$$

This relation can be iterated which was used to find inversion relations for the transfer matrices of inhomogeneous face models [39]. Here it is the key ingredient to complete the proof. To this end we focus on the last two lines of $A_N[D_{N+1}](\lambda_1, \dots, u_i, u_i + \lambda)$. The scalar prefactors appearing in (I.97) and in the following operations are suppressed as they do not depend on the spins in the auxiliary spaces and are irrelevant for the proof. Now we use the initial condition in the i -th column and (I.12) in the following

ones until the rightmost line of spins is reached:





Using the initial condition for the rotated weight with spectral parameter λ we obtain that $\beta_N = \beta_{N+1}$. By definition of the operator A_N and periodic boundary conditions in quantum space \mathcal{H}_{per} we also have $\alpha_N = \alpha_{N+1}$. The spin γ is not connected to one of the Boltzmann weights any more and therefore the partial traces considered above yield the same result. This proves the theorem.

Note that the restriction of $\lambda_N \in \{u_i\}$ in the functional equation (I.98) can be dropped for matrix elements where α_{N-1} is a leaf node of the adjacency graph \mathfrak{G} : in this case all neighbouring spins are necessarily equal and therefore the lowest two rows can be removed using (I.12) for arbitrary values of λ_N .

Finally one should remark that, depending on the definition of the Boltzmann weights for a particular model, the crossing relation may be modified by height dependent gauge factors, see e.g. (II.15) for the RSOS model. While these factors cancel in calculations

where periodic boundary conditions can be imposed they have to be taken care of in the functional equation (I.98) – either by rescaling the operators A and D or by adding constant (i.e. not spectral parameter dependent) prefactors.

C Proof of Theorem 3.

The proof consists of a repeated usage of (I.12) and is shown in a graphical manner. Note that we are rescaled the right-hand side by its denominator.

$$\prod_{i=1}^N \Lambda(\lambda_i) \langle \alpha | W_N(\lambda) \cdot D_N(\lambda_1, \dots, u, u + \lambda) | \beta \rangle =$$

ϕ

ϕ

ϕ

$= \rho(u - u_1)\rho(u_1 - u)$

$$= \prod_{i=1}^L \rho(u - u_i) \rho(u_i - u)$$

In the first step we used that a Boltzmann weight evaluated at λ degenerates to a Kronecker- δ . Then repeatedly using (I.12) the two last rows disappear while producing a product of ρ functions. Dividing the resulting equation by $\prod_{i=1}^{N-2} \Lambda(\lambda_i)$ gives (I.100) and thus proves the theorem.

D Factorisation of D_3 for the $r = 5$ RSOS model

Similar as in the $r = 4$ case, Eq. (II.30), the matrix elements of the three-site density operator $D_3(\lambda_1, \lambda_2, \lambda_3)$ in transfer matrix eigenstates from the $j = 0$ sector of the $r = 5$ RSOS model can be decomposed in terms factorizing into the two-point function $f(\lambda_i, \lambda_j)$, $1 \leq i < j \leq 3$, as defined in (II.65) and a set of structure functions $f_{i,j}(\lambda_1, \lambda_2, \lambda_3)$, i.e.

$$f_0 + f_{1,2}(\lambda_1, \lambda_2, \lambda_3) f(\lambda_1, \lambda_2) + f_{2,3}(\lambda_1, \lambda_2, \lambda_3) f(\lambda_2, \lambda_3) + f_{1,3}(\lambda_1, \lambda_2, \lambda_3) f(\lambda_1, \lambda_3).$$

Furthermore we find that all structure functions can be written as

$$\begin{aligned} f_{1,2}(\lambda_1, \lambda_2, \lambda_3) &= \frac{1}{4} \left(f_{1,2}^1 + f_{1,2}^2 \cot(\lambda_{13}) + f_{1,2}^3 \cot(\lambda_{23}) + f_{1,2}^4 \cot(\lambda_{13}) \cot(\lambda_{23}) \right) \\ f_{1,3}(\lambda_1, \lambda_2, \lambda_3) &= \frac{1}{4} \left(f_{1,3}^1 + f_{1,3}^2 \cot(\lambda_{12}) + f_{1,3}^3 \cot(\lambda_{23}) + f_{1,3}^4 \cot(\lambda_{12}) \cot(\lambda_{23}) \right) \\ f_{2,3}(\lambda_1, \lambda_2, \lambda_3) &= \frac{1}{4} \left(f_{2,3}^1 + f_{2,3}^2 \cot(\lambda_{12}) + f_{2,3}^3 \cot(\lambda_{13}) + f_{2,3}^4 \cot(\lambda_{12}) \cot(\lambda_{13}) \right) \end{aligned} \quad (\text{D.5})$$

where f_0 and $\{f_{i,j}^1, f_{i,j}^2, f_{i,j}^3, f_{i,j}^4\}$ are constants depending on the considered matrix element. Hence, we can uniquely describe any matrix element by in total 13 constants. In Table 2 we list these constants for the non-zero matrix elements $\langle \underline{\alpha} | D_3(\lambda_1, \lambda_2, \lambda_3) | \underline{\beta} \rangle$ in the sector with odd α_0 . All other matrix elements can be obtained by using reflection symmetry.

Table 2: Coefficients of the structure functions (D.5) appearing in the three site density operator for the $r = 5$ RSOS model.

$\underline{\alpha}$	$\underline{\beta}$	f_0	$f_{1,2}^1$	$f_{1,2}^2$	$f_{1,2}^3$	$f_{1,2}^4$	$f_{1,3}^1$	$f_{1,3}^2$	$f_{1,3}^3$	$f_{1,3}^4$	$f_{2,3}^1$	$f_{2,3}^2$	$f_{2,3}^3$	$f_{2,3}^4$
(1212)	(1212)	$\frac{1}{2} - \frac{1}{\sqrt{5}}$	4	0	0	0	0	0	0	0	0	0	0	0
(1212)	(1232)	0	$-\sqrt{5(\sqrt{5}-2)}$	$\sqrt[4]{5}$	$-\sqrt[4]{5}$	$-\sqrt[4]{5}$	$-\sqrt{5(\sqrt{5}-2)}$	$-\sqrt[4]{5}$	$\sqrt[4]{5}$	$-\sqrt[4]{5}$	$-\sqrt[4]{5}$	$-\sqrt[4]{5}$	$-\sqrt[4]{5}$	$-\sqrt{5(\sqrt{5}-2)}$
(1232)	(1212)	0	$-\sqrt{5(\sqrt{5}-2)}$	$-\sqrt[4]{5}$	$-\sqrt[4]{5}$	$-\sqrt[4]{5}$	$-\sqrt{5(\sqrt{5}-2)}$	$-\sqrt[4]{5}$	$\sqrt[4]{5}$	$-\sqrt[4]{5}$	$-\sqrt[4]{5}$	$-\sqrt[4]{5}$	$-\sqrt[4]{5}$	$-\sqrt{5(\sqrt{5}-2)}$
(1232)	(1232)	$\frac{1}{2} - \frac{1}{\sqrt{5}}$	$\sqrt{5}-3$	0	0	0	$3\sqrt{5}-5$	0	0	0	0	0	0	$3\sqrt{5}-5$
(1234)	(1234)	$\frac{7}{4\sqrt{5}} - \frac{3}{4}$	$-(\sqrt{5}+1)$	0	0	0	$3\sqrt{5}-5$	0	0	0	0	0	0	$-(3\sqrt{5}-5)$

Table 2: continued

α	$\underline{\beta}$	f_0	$f_{1,2}^1$ $f_{1,3}^1$ $f_{2,3}^1$	$f_{1,2}^2$ $f_{1,3}^2$ $f_{2,3}^2$	$f_{1,2}^3$ $f_{1,3}^3$ $f_{2,3}^3$	$f_{1,2}^4$ $f_{1,3}^4$ $f_{2,3}^4$
(3212)	(3212)	$\frac{3}{4\sqrt{5}} - \frac{1}{4}$	-4 0 0	0 0 0	0 0 0	0 0 0
(3212)	(3232)	0	$\sqrt{5(\sqrt{5}-2)}$ $\sqrt{\sqrt{5}+2}$ $3\sqrt{\sqrt{5}+2}$	$-\sqrt[4]{5}$ $\sqrt[4]{5}$ $-\sqrt[4]{5}$	$\sqrt[4]{5}$ $-\sqrt[4]{5}$ $\sqrt[4]{5}$	$\sqrt{5(\sqrt{5}-2)}$ $-\sqrt{5(\sqrt{5}-2)}$ $\sqrt{5(\sqrt{5}-2)}$
(3212)	(3432)	0	$-\frac{1}{2}(\sqrt{5}+5)$ $\frac{1}{2}(-3\sqrt{5}-7)$ $-\frac{1}{2}(\sqrt{5}+5)$	$-\sqrt{\frac{1}{2}(5-\sqrt{5})}$ $\sqrt{\frac{1}{2}(5-\sqrt{5})}$ $-\sqrt{\frac{1}{2}(5-\sqrt{5})}$	$\sqrt{\frac{1}{2}(5-\sqrt{5})}$ $-\sqrt{\frac{1}{2}(5-\sqrt{5})}$ $\sqrt{\frac{1}{2}(5-\sqrt{5})}$	$-\frac{1}{2}(\sqrt{5}+5)$ $\frac{1}{2}(\sqrt{5}+5)$ $-\frac{1}{2}(\sqrt{5}+5)$
(3232)	(3212)	0	$\sqrt{5(\sqrt{5}-2)}$ $\sqrt{\sqrt{5}+2}$ $3\sqrt{\sqrt{5}+2}$	$\sqrt[4]{5}$ $-\sqrt[4]{5}$ $\sqrt[4]{5}$	$-\sqrt[4]{5}$ $\sqrt[4]{5}$ $-\sqrt[4]{5}$	$\sqrt{5(\sqrt{5}-2)}$ $-\sqrt{5(\sqrt{5}-2)}$ $\sqrt{5(\sqrt{5}-2)}$
(3232)	(3232)	$\frac{3}{4\sqrt{5}} - \frac{1}{4}$	$3-\sqrt{5}$ $-\sqrt{5}-1$ $3-\sqrt{5}$	0 0 0	0 0 0	$5-3\sqrt{5}$ $3\sqrt{5}-5$ $5-3\sqrt{5}$

Table 2: continued

$\underline{\alpha}$	$\underline{\beta}$	f_0	$f_{1,2}^1$ $f_{1,3}^1$ $f_{2,3}^1$	$f_{1,2}^2$ $f_{1,3}^2$ $f_{2,3}^2$	$f_{1,2}^3$ $f_{1,3}^3$ $f_{2,3}^3$	$f_{1,2}^4$ $f_{1,3}^4$ $f_{2,3}^4$
(3232)	(3432)	0	$3\sqrt{\sqrt{5}+2}$ $\sqrt{\sqrt{5}+2}$ $\sqrt{5(\sqrt{5}-2)}$	$-\sqrt[4]{5}$ $\sqrt[4]{5}$ $-\sqrt[4]{5}$	$\sqrt[4]{5}$ $-\sqrt[4]{5}$ $\sqrt[4]{5}$	$\sqrt{5(\sqrt{5}-2)}$ $-\sqrt{5(\sqrt{5}-2)}$ $\sqrt{5(\sqrt{5}-2)}$
(3432)	(3212)	0	$-\frac{1}{2}(\sqrt{5}+5)$ $\frac{1}{2}(-3\sqrt{5}-7)$ $-\frac{1}{2}(\sqrt{5}+5)$	$\sqrt{\frac{1}{2}(5-\sqrt{5})}$ $-\sqrt{\frac{1}{2}(5-\sqrt{5})}$ $\sqrt{\frac{1}{2}(5-\sqrt{5})}$	$-\sqrt{\frac{1}{2}(5-\sqrt{5})}$ $\sqrt{\frac{1}{2}(5-\sqrt{5})}$ $-\sqrt{\frac{1}{2}(5-\sqrt{5})}$	$-\frac{1}{2}(\sqrt{5}+5)$ $\frac{1}{2}(\sqrt{5}+5)$ $-\frac{1}{2}(\sqrt{5}+5)$
(3432)	(3232)	0	$3\sqrt{\sqrt{5}+2}$ $\sqrt{\sqrt{5}+2}$ $\sqrt{5(\sqrt{5}-2)}$	$\sqrt[4]{5}$ $-\sqrt[4]{5}$ $\sqrt[4]{5}$	$-\sqrt[4]{5}$ $\sqrt[4]{5}$ $-\sqrt[4]{5}$	$\sqrt{5(\sqrt{5}-2)}$ $-\sqrt{5(\sqrt{5}-2)}$ $\sqrt{5(\sqrt{5}-2)}$
(3432)	(3432)	$\frac{3}{4\sqrt{5}} - \frac{1}{4}$	0 0 -4	0 0 0	0 0 0	0 0 0

Table 2: continued

α	$\underline{\beta}$	f_0	$f_{1,2}^1$ $f_{1,3}^1$ $f_{2,3}^1$	$f_{1,2}^2$ $f_{1,3}^2$ $f_{2,3}^2$	$f_{1,2}^3$ $f_{1,3}^3$ $f_{2,3}^3$	$f_{1,2}^4$ $f_{1,3}^4$ $f_{2,3}^4$
(3234)	(3234)	$\frac{1}{2} - \frac{1}{\sqrt{5}}$	$\sqrt{5} + 1$ $\sqrt{5} + 1$ $\sqrt{5} - 3$	0 0 0	0 0 0	$3\sqrt{5} - 5$ $-(3\sqrt{5} - 5)$ $3\sqrt{5} - 5$
(3234)	(3434)	0	$\sqrt{\sqrt{5} + 2}$ $-\sqrt{\sqrt{5} + 2}$ $-\sqrt{5(\sqrt{5} - 2)}$	$\sqrt[4]{5}$ $-\sqrt[4]{5}$ $\sqrt[4]{5}$	$-\sqrt[4]{5}$ $\sqrt[4]{5}$ $-\sqrt[4]{5}$	$-\sqrt{5(\sqrt{5} - 2)}$ $\sqrt{5(\sqrt{5} - 2)}$ $-\sqrt{5(\sqrt{5} - 2)}$
(3434)	(3234)	0	$\sqrt{\sqrt{5} + 2}$ $-\sqrt{\sqrt{5} + 2}$ $-\sqrt{5(\sqrt{5} - 2)}$	$-\sqrt[4]{5}$ $\sqrt[4]{5}$ $-\sqrt[4]{5}$	$\sqrt[4]{5}$ $-\sqrt[4]{5}$ $\sqrt[4]{5}$	$-\sqrt{5(\sqrt{5} - 2)}$ $\sqrt{5(\sqrt{5} - 2)}$ $-\sqrt{5(\sqrt{5} - 2)}$
(3434)	(3434)	$\frac{1}{2} - \frac{1}{\sqrt{5}}$	0 0 4	0 0 0	0 0 0	0 0 0

References

- [1] W. Heisenberg. „Zur Theorie des Ferromagnetismus.“ In: *Original Scientific Papers Wissenschaftliche Originalarbeiten*. Springer, 1985, pp. 580–597.
- [2] P. A. M. Dirac. „On the theory of quantum mechanics.“ In: *Proceedings of the Royal Society of London. Series A, Containing Papers of a Mathematical and Physical Character* 112.762 (1926), pp. 661–677.
- [3] H. Bethe. „Zur Theorie der Metalle.“ In: *Zeitschrift für Physik* 71.3-4 (1931), pp. 205–226.
- [4] R. Baxter. *Exactly solved models in statistical mechanics*. Academic Press, 1982.
- [5] R. Baxter. „Eight-vertex model in lattice statistics and one-dimensional anisotropic Heisenberg chain. I. Some fundamental eigenvectors.“ In: *Annals of Physics* 76.1 (1973), pp. 1–24.
- [6] R. Baxter. „Eight-vertex model in lattice statistics and one-dimensional anisotropic Heisenberg chain. II. Equivalence to a generalized ice-type lattice model.“ In: *Annals of Physics* 76.1 (1973), pp. 25–47.
- [7] R. Baxter. „Eight-vertex model in lattice statistics and one-dimensional anisotropic Heisenberg chain. III. Eigenvectors of the transfer matrix and Hamiltonian.“ In: *Annals of Physics* 76.1 (1973), pp. 48–71.
- [8] J. M. Leinaas and J. Myrheim. „On the theory of identical particles.“ In: *Il Nuovo Cimento B (1971-1996)* 37.1 (1977), pp. 1–23.
- [9] F. Wilczek. „Quantum mechanics of fractional-spin particles.“ In: *Physical review letters* 49.14 (1982), p. 957.
- [10] K. v. Klitzing, G. Dorda, and M. Pepper. „New method for high-accuracy determination of the fine-structure constant based on quantized Hall resistance.“ In: *Physical Review Letters* 45.6 (1980), p. 494.
- [11] D. C. Tsui, H. L. Stormer, and A. C. Gossard. „Two-dimensional magnetotransport in the extreme quantum limit.“ In: *Physical Review Letters* 48.22 (1982), p. 1559.
- [12] R. B. Laughlin. „Anomalous quantum Hall effect: an incompressible quantum fluid with fractionally charged excitations.“ In: *Physical Review Letters* 50.18 (1983), p. 1395.
- [13] A. Y. Kitaev. „Fault-tolerant quantum computation by anyons.“ In: *Annals of Physics* 303.1 (2003), pp. 2–30.
- [14] A. Feiguin et al. „Interacting anyons in topological quantum liquids: The golden chain.“ In: *Physical review letters* 98.16 (2007), p. 160409.

- [15] P. E. Finch. „From spin to anyon notation: the XXZ Heisenberg model as a D_3 (or $su(2)_4$) anyon chain.“ In: *Journal of Physics A: Mathematical and Theoretical* 46.5 (2013), p. 055305.
- [16] P. E. Finch, M. Flohr, and H. Frahm. „Integrable anyon chains: From fusion rules to face models to effective field theories.“ In: *Nuclear Physics B* 889 (2014), pp. 299–332.
- [17] M. Jimbo et al. „Correlation function for the XXZ model for $\Delta < -1$.“ In: *Phys. Lett. A* 168 (1992), pp. 256–263. eprint: [hep-th/9205055](#).
- [18] M. Jimbo and T. Miwa. „Quantum KZ equation with $|q| = 1$ and correlation functions of the XXZ model in the gapless regime.“ In: *J. Phys. A: Math. Gen.* 29 (1996), p. 2923. eprint: [hep-th/9601135](#).
- [19] N. Kitanine, J. M. Maillet, and V. Terras. „Correlation functions of the XXZ Heisenberg spin-1/2 chain in a magnetic field.“ In: *Nucl. Phys. B* 567 (2000), pp. 554–582. eprint: [math-ph/9907019](#).
- [20] N. Kitanine et al. „Spin-spin correlation functions of the XXZ-1/2 Heisenberg chain in a magnetic field.“ In: *Nucl. Phys. B* 641 (2002), pp. 487–518. eprint: [hep-th/0201045](#).
- [21] F. Göhmann, A. Klümper, and A. Seel. „Integral representations for correlation functions of the XXZ chain at finite temperature.“ In: *J. Phys. A: Math. Theor* 37 (2004), pp. 7625–7652. arXiv: [hep-th/0405089](#) [[hep-th](#)].
- [22] H. E. Boos, V. E. Korepin, and F. A. Smirnov. „Emptiness Formation Probability and Quantum Knizhnik-Zamolodchikov Equation.“ In: *Nucl. Phys. B* 658 (2003), pp. 417–439. arXiv: [hep-th/0209246](#) [[hep-th](#)].
- [23] H. Boos et al. „A recursion formula for the correlation functions of an inhomogeneous XXX model.“ In: *St. Petersburg Math. J.* 17 (2006), pp. 85–117. eprint: [hep-th/0405044](#).
- [24] H. Boos et al. „Reduced qKZ equation and correlation functions of the XXZ model.“ In: *Comm. Math. Phys.* 261 (2006), pp. 245–276. eprint: [hep-th/0412191](#).
- [25] H. E. Boos et al. „Factorization of multiple integrals representing the density matrix of a finite segment of the Heisenberg spin chain.“ In: *J. Stat. Mech.* (2006), P04001. arXiv: [hep-th/0603064](#) [[hep-th](#)].
- [26] J. Damerou et al. „Density matrices for finite segments of Heisenberg chains of arbitrary length.“ In: *J. Phys. A: Math. Theor* 40 (2007), pp. 4439–4453. eprint: [cond-mat/0701463](#).
- [27] H. Boos et al. „Hidden Grassmann structure in the XXZ model.“ In: *Comm. Math. Phys.* 272 (2007), pp. 263–281. arXiv: [hep-th/0606280](#) [[hep-th](#)].

- [28] H. Boos et al. „Hidden Grassmann Structure in the XXZ Model II: Creation Operators.“ In: *Comm. Math. Phys.* 286 (2009), pp. 875–932. arXiv: 0801.1176 [hep-th].
- [29] M. Jimbo, T. Miwa, and F. Smirnov. „Hidden Grassmann Structure in the XXZ Model III: Introducing Matsubara direction.“ In: *J. Phys. A: Math. Theor* 42 (2009), p. 304018. arXiv: 0811.0439 [math-ph].
- [30] J. Sato et al. „Computation of static Heisenberg-chain correlators: Control over length and temperature dependence.“ In: *Phys. Rev. Lett.* 106 (2011), p. 257201. arXiv: 1105.4447.
- [31] B. Aufgebauer and A. Klümper. „Finite temperature correlation functions from discrete functional equations.“ In: *J. Phys. A: Math. Theor* 45(34) (2012), p. 345203. eprint: 1205.5702.
- [32] A. J. Coleman and V. I. Yukalov. *Reduced density matrices: Coulson’s challenge*. Vol. 72. Springer Science & Business Media, 2000.
- [33] D. A. Mazziotti. „Two-electron reduced density matrix as the basic variable in many-electron quantum chemistry and physics.“ In: *Chemical reviews* 112.1 (2012), pp. 244–262.
- [34] C. S. Gardner et al. „Method for solving the Korteweg-deVries equation.“ In: *Physical review letters* 19.19 (1967), p. 1095.
- [35] J.-S. Caux and J. Mossel. „Remarks on the notion of quantum integrability.“ In: *Journal of Statistical Mechanics: Theory and Experiment* 2011.02 (2011), P02023.
- [36] L. Faddeev. *Integrable models in 1 + 1 dimensional quantum field theory*. Tech. rep. CEA Centre d’Etudes Nucleaires de Saclay, 1982.
- [37] A. Izergin and V. Korepin. „The most general \mathcal{L} -operator for the \mathcal{R} -matrix of the XXX model.“ In: *Letters in Mathematical Physics* 8.4 (1984), pp. 259–265.
- [38] G. E. Andrews, R. J. Baxter, and P. J. Forrester. „Eight-vertex SOS model and generalized Rogers-Ramanujan-type identities.“ In: *Journal of Statistical Physics* 35.3-4 (1984), pp. 193–266.
- [39] H. Frahm and N. Karaiskos. „Inversion identities for inhomogeneous face models.“ In: *Nuclear Physics B* 887 (2014), pp. 423–440.
- [40] H. Frahm and N. Karaiskos. „Non-Abelian anyons: inversion identities for higher rank face models.“ In: *Journal of Physics A: Mathematical and Theoretical* 48.48 (2015), p. 484001.
- [41] N. Braylovskaya, P. E. Finch, and H. Frahm. „Exact solution of the D_3 non-Abelian anyon chain.“ In: *Physical Review B* 94.8 (2016), p. 085138.

- [42] C. Gómez, M. Ruiz-Altaba, and G. Sierra. *Quantum groups in two-dimensional physics*. Cambridge University Press, 2005.
- [43] S. Trebst et al. „A short introduction to Fibonacci anyon models.“ In: *Progress of Theoretical Physics Supplement* 176 (2008), pp. 384–407.
- [44] E. Ardonne et al. „Microscopic models of interacting Yang–Lee anyons.“ In: *New Journal of Physics* 13.4 (2011), p. 045006.
- [45] A. A. Belavin, A. M. Polyakov, and A. B. Zamolodchikov. „Infinite conformal symmetry in two-dimensional quantum field theory.“ In: *Nuclear Physics B* 241 (1984), pp. 333–380.
- [46] D. Friedan, Z. Qiu, and S. Shenker. „Conformal invariance, unitarity, and critical exponents in two dimensions.“ In: *Physical Review Letters* 52.18 (1984), p. 1575.
- [47] J. Lepowsky, S. Mandelstam, and I. M. Singer. *Vertex Operators in Mathematics and Physics: Proceedings of a Conference November 10–17, 1983*. Vol. 3. Springer Science & Business Media, 2013.
- [48] A. Klümper and P. A. Pearce. „Conformal weights of RSOS lattice models and their fusion hierarchies.“ In: *Physica A: Statistical Mechanics and its Applications* 183.3 (1992), pp. 304–350.
- [49] C. Nayak et al. „Non-Abelian anyons and topological quantum computation.“ In: *Reviews of Modern Physics* 80.3 (2008), p. 1083.
- [50] A. Kitaev. „Anyons in an exactly solved model and beyond.“ In: *Annals of Physics* 321.1 (2006), pp. 2–111.
- [51] P. H. Bonderson. „Non-Abelian anyons and interferometry.“ PhD thesis. California Institute of Technology, 2007.
- [52] K. Beer et al. „From categories to anyons: a travelogue.“ In: *arXiv preprint arXiv:1811.06670* (2018).
- [53] N. Kitanine, J. M. Maillet, and V. Terras. „Form factors of the XXZ Heisenberg spin-1/2 finite chain.“ In: *Nucl. Phys. B* 554 (1999), pp. 647–678. eprint: [math-ph/9807020](https://arxiv.org/abs/math-ph/9807020).
- [54] L. Faddeev. „How Algebraic Bethe Ansatz works for integrable model.“ In: *arXiv preprint hep-th/9605187* (1996).
- [55] J. M. Maillet and V. Terras. „On the quantum inverse scattering problem.“ In: *Nuclear Physics B* 575.3 (2000), pp. 627–644.
- [56] D. Levy-Bencheton and V. Terras. „An algebraic Bethe ansatz approach to form factors and correlation functions of the cyclic eight-vertex solid-on-solid model.“ In: *J. Stat. Mech.* 2013 (2013), P04015. eprint: [1212.0246](https://arxiv.org/abs/1212.0246).

- [57] P. A. Pearce and K. A. Seaton. „Solvable hierarchy of cyclic solid-on-solid lattice models.“ In: *Physical review letters* 60.14 (1988), p. 1347.
- [58] G. Felder. „Elliptic quantum groups.“ In: *Proc. XI-th International Congress of Mathematical Physics*. 1995.
- [59] G. Felder and A. Varchenko. „Algebraic Bethe ansatz for the elliptic quantum group $E_{\tau,\eta}(sl_2)$.“ In: *Nucl. Phys. B* 480 (1996), pp. 485–503. eprint: [q-alg/9605024](https://arxiv.org/abs/q-alg/9605024).
- [60] B. Enriquez and G. Felder. „Elliptic Quantum Groups $E_{\tau,\eta}(\mathfrak{sl}(2))$ and Quasi-Hopf Algebras.“ In: *Communications in mathematical physics* 195.3 (1998), pp. 651–689.
- [61] V. G. Drinfeld. „Quantum groups.“ In: *Proceedings of the International Congress of Mathematicians, Berkeley*. 1986, pp. 798–820.
- [62] H. Frahm and D. Westerfeld. „Density matrices in integrable face models.“ In: *SciPost Phys.* 11 (3 2021), p. 57.
- [63] N. A. Slavnov. „Calculation of scalar products of wave functions and form factors in the framework of the algebraic Bethe ansatz.“ In: *Teoreticheskaya i Matematicheskaya Fizika* 79.2 (1989), pp. 232–240.
- [64] H. Boos, V. Korepin, and F. Smirnov. „New formulae for solutions of quantum Knizhnik-Zamolod-chikov equations on level-4.“ In: *Journal of Physics A: Mathematical and General* 37.2 (2003), p. 323.
- [65] H. E. Boos et al. „Factorization of the finite temperature correlation functions of the XXZ chain in a magnetic field.“ In: *Journal of Physics A: Mathematical and Theoretical* 40.35 (2007), p. 10699.
- [66] H. Boos, A. Hutsalyuk, and K. S. Nirov. „On the calculation of the correlation functions of the \mathfrak{sl}_3 -model by means of the reduced qKZ equation.“ In: *Journal of Physics A: Mathematical and Theoretical* 51.44 (2018), p. 445202.
- [67] A. Morin-Duchesne, C. Hagendorf, and L. Cantini. „Boundary emptiness formation probabilities in the six-vertex model at $\Delta = -\frac{1}{2}$.“ In: *Journal of Physics A: Mathematical and Theoretical* 53.25 (2020), p. 255202.
- [68] V. Pasquier. „Etiology of IRF models.“ In: *Yang-Baxter Equation In Integrable Systems*. World Scientific, 1990, pp. 482–491.
- [69] D. Kim and P. Pearce. „Operator content of the cyclic solid-on-solid models.“ In: *J. Phys. A: Math. Gen.* 22 (1989), pp. 1439–1450.
- [70] P. Di Francesco and F. Smirnov. „OPE for XXX.“ In: *Rev. Math. Phys.* 30 (2018), p. 1840006. arXiv: [1711.04123](https://arxiv.org/abs/1711.04123) [[hep-th](https://arxiv.org/abs/1711.04123)].

- [71] F. Smirnov. „Exact density matrix for quantum group invariant sector of XXZ model.“ In: *preprint* (2018). arXiv: 1804.08974 [math-ph].
- [72] T. Miwa and F. Smirnov. „New exact results on density matrix for XXX spin chain.“ In: *Lett. Math. Phys.* 109 (2019), pp. 675–698. arXiv: 1802.08491 [math-ph].
- [73] V. V. Bazhanov and N. Reshetikhin. „Critical RSOS models and conformal field theory.“ In: *Int. J. Mod. Phys. A* 4 (1989), pp. 115–142.
- [74] D. L. O’Brien, P. A. Pearce, and S. O. Warnaar. „Finitized conformal spectrum of the Ising model on the cylinder and torus.“ In: *Physica A: Statistical Mechanics and its Applications* 228.1-4 (1996), pp. 63–77.
- [75] E. Ardonne, P. E. Finch, and M. Titsworth. „Classification of metaplectic fusion categories.“ In: *arXiv preprint arXiv:1608.03762* (2016).
- [76] P. E. Finch et al. „Quantum phases of a chain of strongly interacting anyons.“ In: *Physical Review B* 90.8 (2014), p. 081111.
- [77] J. S. Birman and H. Wenzl. „Braids, link polynomials and a new algebra.“ In: *Transactions of the American Mathematical Society* 313.1 (1989), pp. 249–273.
- [78] J. Murakami. „The Kauffman polynomial of links and representation theory.“ In: *Osaka Journal of Mathematics* 24.4 (1987), pp. 745–758.
- [79] G. Ribeiro. „Correlation functions of integrable $O(n)$ spin chains.“ In: *Nuclear Physics B* 957 (2020), p. 115106.
- [80] G. A. Ribeiro and A. Klümper. „Correlation functions of the integrable $SU(N)$ spin chain.“ In: *Journal of Statistical Mechanics: Theory and Experiment* 2019.1 (2019), p. 013103.
- [81] R. J. Baxter. „Corner Transfer Matrices of the Eight-Vertex Model. I. Low-Temperature Expansions and Conjectured Properties.“ In: *J. Stat. Phys.* 15 (1976), pp. 485–503.
- [82] O. Foda et al. „Vertex operators in solvable lattice models.“ In: *J. Math. Phys.* 35(1) (1994), pp. 13–46. eprint: hep-th/9305100.
- [83] A. Klümper, K. S. Nirov, and A. V. Razumov. „Reduced qKZ equation: general case.“ In: *J. Phys. A: Math. Theor* 53 (2020), p. 015202. arXiv: 1905.06014 [math-ph].
- [84] F. Göhmann, A. Seel, and J. Suzuki. „Correlation functions of the integrable isotropic spin-1 chain at finite temperature.“ In: *Journal of Statistical Mechanics: Theory and Experiment* 2010.11 (2010), P11011.

- [85] A. Klümper, D. Nawrath, and J. Suzuki. „Correlation functions of the integrable isotropic spin-1 chain: algebraic expressions for arbitrary temperature.“ In: *Journal of Statistical Mechanics: Theory and Experiment* 2013.08 (2013), P08009.

Acknowledgements

At first I want to express my deep gratitude to Prof. Dr. Holger Frahm for his great effort to help me with any problems during the time as a PhD candidate. Likewise, I would like to thank all former members of our research group, in particular Daniel Borcharding and Konstantin Hobuß, for their support, discussions and good conversations in and outside the ITP. Besides, I am happy that Sascha Gehrman joined our group and proved to be always ready to help. I'm also grateful to Alexi Morin-Duchesne for very helpful discussions and providing valuable tips.

I want to thank Prof. Dr. Frank Göhmann and Prof. Dr. Eric Jeckelmann for their agreement to act as second reviewers of this thesis as well as Prof. Dr. Rolf Haug for chairing the PhD examination committee.

I am thankful for all the people who read parts of the thesis and corrected typos: Deniz Stiegemann, Merlin Füllgraf, Althea Capelli, Hannes Kakuschke, Magdalena Misslisch, Nele-Marie Knoop, Sascha Gehrman, Philipp Baasch, Jannik Mielke, Johanna Fette and Daniel Borcharding.

I am very grateful to the Deutsche Forschungsgemeinschaft for partially providing the funding for this work as part of the research unit *Correlations in Integrable Quantum Many-Body Systems* (FOR2316) under grant No. Fr 737/9-1. I really enjoyed being part of this group. In this context I especially want to thank the people in Wuppertal for organising interesting workshops and for their hospitality during my stays over there.

Finally, I thank my family and my friends for supporting me all the time. Thank you for everything!

Daniel Westerfeld

Selbstständigkeitserklärung

Hiermit erkläre ich, diese Arbeit selbständig und nur mit den angegebenen Hilfsmitteln angefertigt zu haben. Alle Stellen der Arbeit, die wörtlich oder sinngemäß aus anderen Werken übernommen wurden, sind als solche kenntlich gemacht. Diese Arbeit lag weder in dieser, noch in ähnlicher Form bereits einer Prüfungsbehörde vor.

Hannover, 12. Mai 2022

Curriculum Vitae

Personal

Name Daniel Westerfeld

Date of birth 26.06.1990

Place of birth Uelzen

Education

02/2016 - 04/2022 Research associate, Leibniz University Hannover,
Dissertation: Functional methods for correlation functions
of integrable face and anyon models

01/2014 - 01/2016 M.Sc. Physics, Leibniz University Hannover,
Master's thesis: Analytische Eigenschaften von
Eigenwerten und -zuständen des RSOS-Modells

10/2010 - 12/2013 B.Sc. Physics, Leibniz University Hannover,
Bachelor's thesis: Quantisierung des Toda-Gitters

06/2010 Allgemeine Hochschulreife, Herzog-Ernst-Gymnasium Uelzen